ALMA MATER STUDIORUM - UNIVERSITÀ DI BOLOGNA

CAMPUS DI CESENA

SCUOLA DI INGEGNERIA E ARCHITETTURA

CORSO DI LAUREA MAGISTRALE IN INGEGNERIA BIOMEDICA

TITOLO DELLA TESI

IN VITRO ASSESSMENT OF THE PRIMARY STABILITY OF THE ACETABULAR COMPONENT IN HIP ARTHROPLASTY

(Valutazione sperimentale della stabilità primaria della componente acetabolare nell'artroplastica dell'anca)

Tesi in MECCANICA DEI TESSUTI BIOLOGICI

Relatore	Presentata da
Chiar.mo Prof. Luca Cristofolini	Mariateresa Linsalata

Co-Relatore

Ing. Federico Morosato

Sessione III
Anno accademico 2016-2017

CONTENTS

ABSTRACT

In Europe, more than 700,000 hip arthroplasties are performed annually. The failure rate of hip implants is 2-8% (at 10 years). Of this, more than 50% is due to the aseptic mobilization of the acetabular component (more than to the femoral component). Some follow-up clinical studies demonstrate a correspondence between the loss of the primary stability and the late aseptic loosening of the prosthesis, hence, the need to investigate more thoroughly the primary stability of the acetabular component. Despite the presence in literature of *in vivo* evaluations carried out through radiographic criteria, there are no exhaustive pre-clinical studies conducted *in vitro* with respect to primary stability.

The central aim of this project is to create a pilot-test for the in vitro evaluation of the primary stability of a commercial acetabular component, implanted in a synthetic hemipelvis (implanted by *press-fit* surgical procedure). The micromovement evaluation includes a multi-faceted approach, consisting in using the Digital Image Correlation (DIC) and linear displacement sensors. To adapt and improve the performance of the two measuring instruments, the study aims to: (1.a) optimize the measurements obtained from image correlation, (1.b) create and perform the internal calibration procedure of the displacement sensors and optimize the measurements obtained from the sensors themselves (used as spot-check of the entire pilot-test). The second part of the work is to implement a reliable methodology for calculating the relative roto-translations between cup and bone, applying a physiological critical load on the specimen. The creation of a dedicated algorithm provides, therefore, to evaluate: (2.a) permanent migration and (2.b) inducible micromotion.

The use of image correlation was a focal point for the study. Thanks to the power of the DIC in analysing displacement motion and strain in full-field, in contact-less and relying on stereophotogrammetry, for the first time it was possible to obtain 3D information of the migration vector of the cup. Furthermore, by creating an optimized procedure for the calibration of the DIC, it was possible to report all the measurements obtained from the pilot-test, to the Anterior Pelvic Plane (reference frame with clinical relevance).

The results obtained from the pilot-test highlight the reliability of the procedure, proposing it as *modus-operandi* for a test campaign on composite and cadaveric hemipelvises.

RIASSUNTO

In Europa, più di 700'000 interventi di artroplastica d'anca vengono effettuati annualmente. Il tasso di fallimento della chirurgia è del 2-8 % (a 10 anni). Di questo, più del 50% è dovuto alla mobilizzazione asettica della componente acetabolare (più che ad un fallimento legato alla componente femorale). Alcuni studi clinici di follow-up, dimostrano esserci una corrispondenza tra la perdita della stabilità primaria e la mobilizzazione asettica tardiva della protesi. Da ciò nasce l'esigenza di investigare più a fondo sulla stabilità primaria della componente acetabolare. Nonostante la presenza in letteratura di valutazioni condotte *in vivo*, specialmente attraverso criteri radiografici, mancano studi esaustivi di carattere pre-clinico condotti *in vitro* rispetto alla stabilità primaria.

Lo scopo centrale di questo progetto di tesi è quello di creare un pilot-test per la valutazione *in vitro* della stabilità primaria di una componente acetabolare commerciale, impiantata in una emipelvi sintetica (senza cemento, attraverso la procedura chirurgica *press-fit*). La valutazione dei micromovimenti prevede un approccio multiplo, costituito dall'utilizzo della Digital Image Correlation (DIC) e di sensori lineari di spostamento. Per adeguare e migliorare le prestazioni dei due strumenti di misura, lo studio prevede: (1.a) l'ottimizzazione delle misure ottenute dalla correlazione di immagini, (1.b) creare ed effettuare la procedura di calibrazione interna dei sensori di spostamento e l'ottimizzazione delle misure ottenute dai sensori stessi come monitor dell'intero pilot-test. La seconda parte del lavoro si prone di implementare una metodologia affidabile per il calcolo delle roto-traslazioni relative tra coppa e osso. La creazione di un algoritmo dedicato, prevede, quindi, di valutare: (2.a) la migrazione permanente e (2.b) i micromovimenti inducibili dai picchi di carico.

L'utilizzo della correlazione di immagini è risultato un gran punto di forza dello studio. Grazie al potere della DIC nell'elaborare spostamenti e deformazioni a tutto campo, senza contatto e in stereofotogrammetria, per la prima volta è stato possibile ottenere informazioni 3D del vettore migrazione della coppa. Inoltre, creando una procedura ottimizzata dell'allineamento del provino sotto la macchina, si sono potute riferire tutte le misure ottenute dal pilot-test, all'Aneterior Pelvic Plane (sistema di riferimento di rilevanza clinica).

I risultati ottenuti dall'esecuzione del pilot-test mettono in luce l'efficacia della procedura creata, proponendola come *modus-operandi* per una campagna di test su emipelvi in composito e biologici.

1. INTRODUCTION

The aim of the introduction is to provide some information about the anatomy and the biomechanics of the pelvis, about the total hip arthroplasty and its failure risks. In addition, for a proper knowledge of the work, the primary stability definition is given, with a synthetize state of the art about its assessment. Finally, an overview about the sensors used for this study is presented.

1.1 ANATOMY OF THE PELVIS

1.1.1 Bone tissue

Bone tissue is a specialized form of the connective tissue. It is characterized by a mineralized extracellular matrix which lend stiffness and mechanical strength[1].
The bone is the major structural and supportive tissue of the body, constituting the skeleton[2].
The bone exerts important functions in the body, such as locomotion, support and protection of soft tissues, calcium and phosphate storage, and hosting of bone marrow[3, 4]
It is composed by the 25% of water, the 32% of organic matrix and the 43% of apatite mineral[1].
Bone exhibits four types of cells: osteoblasts, bone lining cells, osteocytes, and osteoclasts. Osteoblasts and osteocytes are involved in the formation and mineralization of bone; osteoclasts are involved in the resorption of bone tissue: despite its inert appearance, bone is a highly dynamic tissue that is continuously resorbed by osteoclasts and reconstituted by osteoblasts. There are evidences that osteocytes act as mechanosensors and orchestrators of this bone remodelling process[5], necessary for fracture healing, skeleton adaptation to mechanical use and for calcium homeostasis. Finally, flat-shaped osteoblasts become the lining cells that form a protective layer on the bone surface. Precisely, the lining cells are set in the inner surface of bones, which separates the bone from the marrow, called *endosteum*. The external surface of bones is composed by a high-vascularized soft tissue called *periosteum*[6].
Bone tissue is a mineralized tissue of two types: cortical bone and trabecular bone.
The cortical bone represents the outer shell of bones and is composed by several closely packed osteons or *harvesian* systems. The osteon is a 150-250 micrometers cylinder in diameter, consisting of a central canal (*harvesian* canal) through which blood and lymphatics vessels and nerve run, surrounded by 4-20 concentric layers of *lamellae*[7].
The trabecular bone consists in a network of about 0.2 mm-thick *trabeculae*, composed by packages of parallel *lamellae*, up to 1 mm long and 50-60 microns in section and linked by cemented lines. Here, the nutrients are directly taken from the mellow in the interstitial space between *trabeculae*. Trabecular bone density and orientation may widely vary within different anatomical sites depending on the mechanical role which locally cover; trabecular structure, in fact, results to be mainly oriented along the primary load direction[8]. Because of its structure, trabecular bone does not significantly contribute to the bone stiffness alone; however, due to the

cheaper metabolic cost (rather than the cortical) and in combination with the cortical bone, it covers an important role in terms of:

- stiffen the structure connecting the outer shell of cortical bone;
- support the layer of the cortex and distribute the loads in the case of lateral impacts;
- support the articular cartilage and act as shock-absorber during load
- transfer and distribute the load to the surrounding cortical bone;
- protect the cave bones from phenomena of instability (buckling)[1].

Due to their shape, bones can be classified in:

- Long: characterized by a shaft, the diaphysis, that is much longer than its width, and by an epiphysis, a rounded head at each end of the shaft. They are made mostly of compact bone, with lesser amounts of marrow, located within the medullary cavity, and areas of spongy, cancellous bone at the ends of the bones;
- Short: they mostly withstand compressive loads and transfer loads between articular surfaces;
- Flat: these kind of bones (i.e. the pelvis) are made by a typical sandwich structure, with the thin layers of cortical bone carrying most of the load[9]. The thin layers are separated by the trabecular bone (Fig.1).
  This structure is optimized for being characterized both by stiffness (high inertia) and tenacity, thus with high deformability and strength[1].
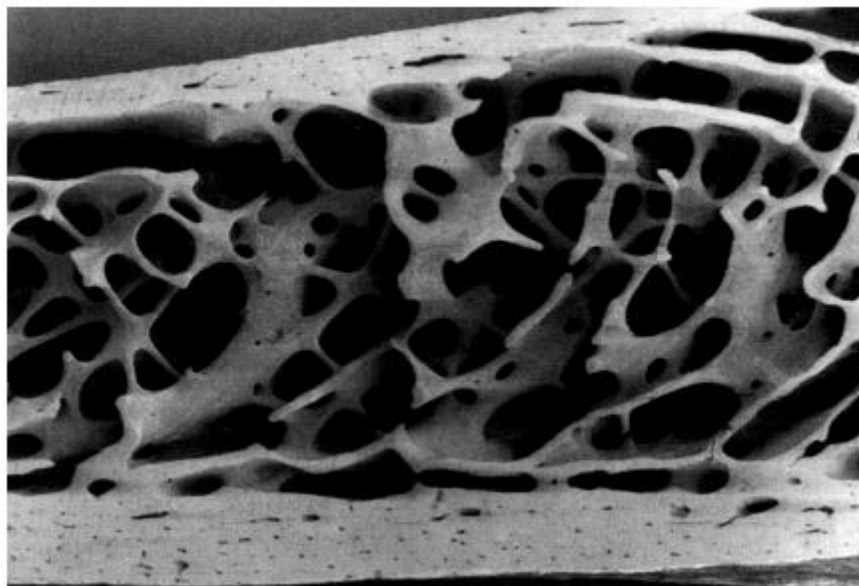
Fig.1: Detail of the iliac crest flat bone.

- Irregular: all the bones that do not fit the categories above

1.1.2 Optimized hip structure is functional to the load distribution

The concept that bone adapts to stress, or a lack of it, is known as Wolff's law. It's the reason why astronauts return with reduced bone density after floating in microgravity![10]

The adaptive nature of bone lies in its ability to respond to the environment by conforming and reshaping itself constantly to accommodate life-time stresses experienced throughout daily activities[11]. Wolff's law states that bone has the ability to adapt to mechanical loads: it means that the external and internal structure of bone changes depending on the load occurring in the bone. Especially with regard to implant technology and arthroplasty, bone adaptation (bone remodelling) plays an important role: if the biomechanical distribution of forces in and around the treated joint is reconstructed inappropriately during surgery, or if the design of the implant is improper, many complications can occur[20].

This ongoing turnover of bone is a process of resorption followed by replacement of bone, with little changes in shape accomplished through osteoblasts and osteoclasts. Cells are stimulated by a variety of signals, maybe as the result of bone's piezoelectric properties, which cause bone to generate small electrical potentials under stress[12]. Approximately 10% of the skeletal mass of an adult is remodelled each year[13].

1.1.3 The pelvic girdle

The pelvic girdle is composed by two symmetrical flat bones that constitute the pelvic girdle, the bony structure that links the axial skeleton to the lower limbs. The hip bone presents three articulations:

- Sacroiliac joint: articulation with the *sacrum* (Fig.2.A).
- Pubic symphysis: articulation with the contro-lateral hip bone (Fig.2.B).
- Hip joint: articulation with the head of the femur (Fig.2.C)[14].

A   B   C

The hip bone is formed by three parts: the *ilium*, the *ischium*, and the *pubis*, fused together in the acetabulum, the socket in which the femoral head is inserted (Fig.3.A). The complete fusion of *ilium*, *ischium* and *pubis* occurs at the end of the teenage years (14–16), with the calcification of the triradiate cartilage (Fig.3.B).

A   B
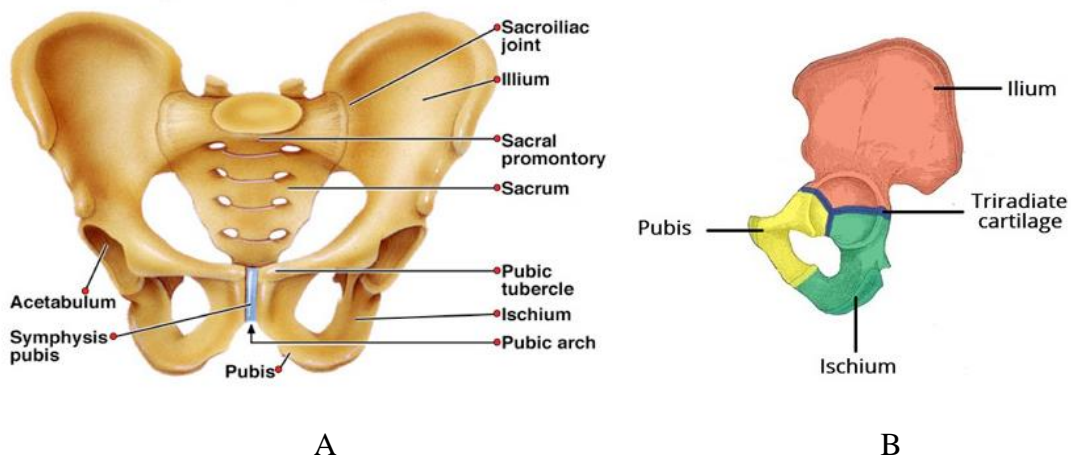
Fig.3: A. Anterior view of the pelvic girdle;
B. The hip bone of a 5 years old, with triradiate cartilage still present.

The *acetabulum* is supported by the anterior and the posterior columns (Fig.4.A). Because of their architecture, these columns act as struts, adding stability and transferring the forces exerted by the femoral head[15]. The two columns join superiorly to the *acetabulum*, forming a radiolucent triangle, which gives flexibility to the *acetabulum*. The acetabular rim is inferiorly interrupted with the acetabular notch. Here the *legamentum teres* is originated and it directly links the acetabulum with the femoral head, allowing more stability to the joint. The *legamentum teres* is a somewhat flattened band inserted by its apex into the antero-superior part of the *fovea capitis femoris*. Under the notch there is the oval *foramen*, through which nutrient vessels and nerves reach the joint (Fig.4.B)[16].

A B
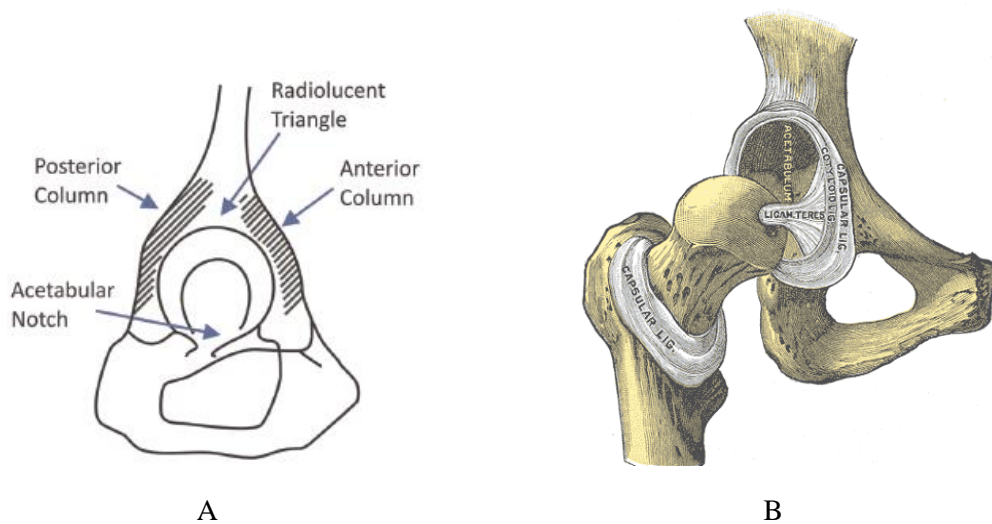
Fig.4: A. Acetabular columns, acetabular notch and the radiolucent triangle labelled on figure; B. Legamentum teres;

The *legamentum teres* is the intracapsular ligament of the hip joint. The extracapsular ligaments are:

- the ileofemoral ligament (Fig.5.A),
- the ischiofemoral ligament (Fig.5.B),
- the pubofemoral ligament (Fig.5.A),

All three strengthen the capsule and prevent an excessive range of movement and dislocation in the joint [17].

A B
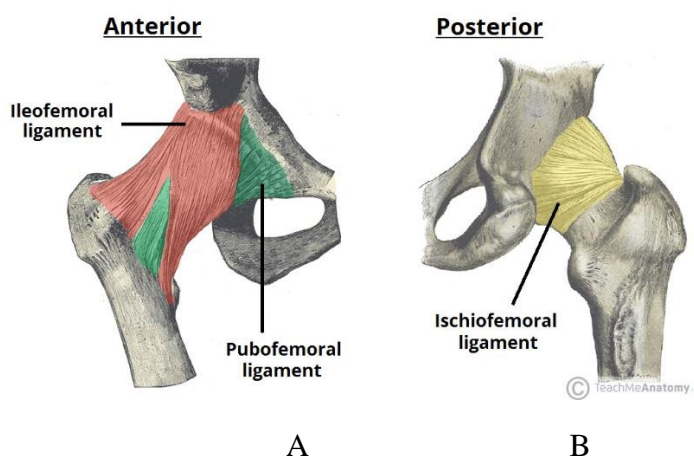
Fig.5: A. Pubofemoral ligament and ileofemoral ligament in anterior view; B. Ischiofemoral ligament in posterior view

1.1.3.4 The hip joint

A joint, or articulation, is a connection between two bones, which allows their relative movement. The hip joint, or acetabulo-femoral joint (*art. coxae*), is one of the largest among the synovial joints of the body, which are characterized by bones joined each other with a fibrous joint capsule that is continuous with the periosteum of the joined bones. The joint capsule is made up of an outer layer, the articular capsule, which keeps the bones together structurally, and an inner layer, the synovial membrane, which seals in the synovial fluid. The hip joint is formed by the femur and the *acetabulum* and its primary function is to support the weight of the body in both static and dynamic tasks ensuring relative movement between thighs and pelvis. It is a ball-and-socket joint, where the ball is the femoral head and the socket is the *acetabulum*.

As a ball-and-socket joint, the allowable movements at the hip joint are three components of rotation:

- flexion and extension (in the sagittal plane of the body);
- abduction and adduction (in the frontal plane of the body);
- intra and extra rotation (in the transverse plane of the body)[10,18] (Fig.6).
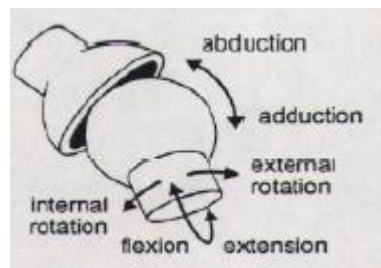
Fig.6: ball- and -socket simplified representation with allowed movements labelled.

These movements are limited both by the morphology of the hip bone and by the soft tissues, ligaments and muscular structures. In addition, the presence of osteophytes (referred to bone irregularities that form in joints margin to give more contact surface between articular bodies), along the acetabular rim (i.e. *labrum*), may constrain the joint mobility.

1.2 BIOMECHANICS OF THE HIP

Biomechanics is the science that studies the forces acting in the living body. Under gravity and other loads, controlled by the nervous system, human movement is achieved through a complex and highly coordinated mechanical interaction between bones, muscles, ligaments and joints within the musculoskeletal system. If any of these individual elements is injured or lesioned, the mechanical interaction will change, causing degradation, instability or disability of movement[19].

Thus, it's necessary to study and to understand the body biomechanics to prevent injury, correct abnormality, and improve healing and rehabilitation.

Tab.1 shows the movements at the hip joint (with their own range of motion) and the muscles involved (Fig.7).

Tab.1: List of the kind of rotation (first column), the range of motion of the related rotation in human pelvis (degrees (°)) and the main muscles involved in the related rotation.[20]

Rotation	Range of Motion	Muscles involved
external rotation	30° with the hip extended 50° with the hip flexed	gluteus maximus; quadratus femoris; obturator internus; dorsal fibers of gluteus medius and minimus; iliopsoas (including psoas major)
internal rotation	40°	anterior fibers of gluteus medius and minimus; tensor fasciae latae; the part of adductor magnus inserted into the adductor tubercle; and, with the leg abducted also the pectineus.
Extension	20°	gluteus maximus; tensor fasciae latae: pectineus; adductor longus; adductor brevis; gracilis.
Flexion	140°	iliopsoas; tensor fasciae latae; pectineus; adductor longus; adductor brevis; gracilis; rectus femoris; sartorius.
Abduction	50° with hip extended, 80° with hip flexed	gluteus medius; tensor fasciae latae; gluteus maximus with its attachment at the fascia lata; gluteus minimus; piriformis; obturator internus.
Adduction	30° with hip extended, 20° with hip flexed	adductor magnus with adductor minimus; adductor longus, adductor brevis, gluteus maximus with its attachment at the gluteal

		tuberosity; gracilis (extends to the tibia); pectineus, quadratus femoris; and obturator externus
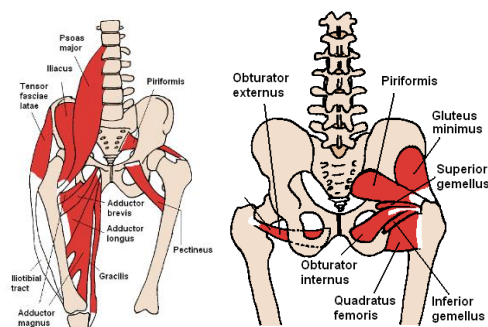
Fig.7: Main muscles involved in hip movements.

All the knowledge about the biomechanics is due to experimental investigations, conducted through different methods, generally classified as: *in vitro, in vivo* and *in silico.*

1.2.1 In *vivo*, *in vitro*, *in silico* tests in biomechanics

- *In vivo* (latin for "within the living") refers to those observations in which the effects of various biological entities are tested on whole, living organisms or cells, usually animals, including humans, and plants, as opposed to a tissue extract or dead organism[21].

  In biomechanics one of the most common *in vivo* study performed, is the gait analysis. This is the study of human motion through specific tools able to measure body movements, body mechanics and the activity of the muscles. Nowadays this kind of test is largely used to support clinical decision-making, for example in case of gait dysfunction[22]. Another approach for *in vivo* assessment is given by follow-up studies, performed thanks to Roentgen Stereophotogrammetric Analysis (RSA) (see Par.).

- *in vitro* (latin for "within the glass") refers to the technique of performing a given procedure in a controlled environment outside of a living organism[25].

  In biomechanics, the *in vitro* studies are often used to assess the behaviour of human cadaveric or synthetic (even subjected, or not, to prosthetic implants) specimens, under controlled loading conditions. When a structure is loaded, this can induce deformations. As the load-deformation plot is function of the material properties and the geometry structure[26], it is possible to characterize the specimen (stiffness, ductility, elasticity, toughness and so on) in a controlled condition.

- *In silico* means "performed on computer or via computer simulation". *In silico* it is possible to test virtually any kind of specimen realized as numerical model. Computational biomechanical modelling is a very useful tool in bioengineering research as cheaper and practical alternative of physical tests. Computational analysis allows many variables to be tested quickly and provides full-field data predictions, such as strains within a tissue structure. This is particularly useful in orthopaedics where finite element (FE) models are commonly used to predict the structural behaviour of joint prostheses and the mechanical response of the supporting bone[23,24]. However, the main limit is that the outcomes are strictly affected by the approximation of the input data, for example isotropic versus anisotropic, homogeneous versus inhomogeneous, etc.

Anyway, in each case of study, a reference frame is essential for biomechanical assessment.

1.2.2 Reference frames of the pelvis

Anatomical reference frames are based on reliable landmarks that should be identified on the bone [27]. Dealing with the pelvis or the hemipelvis, the most experimentally used anatomical landmarks are (Fig.8):

- Anterior Superior Iliac Spine (ASIS) defined as the most prominent point on the iliac surface;

- Posterior Superior Iliac Spine (PSIS) defined as the upper and most posterior point of the iliac crest;

- Pubic Tubercle (PT) defined as a prominent forward-projecting tubercle on the upper border of the medial portion of the superior ramus of the pubis[28].
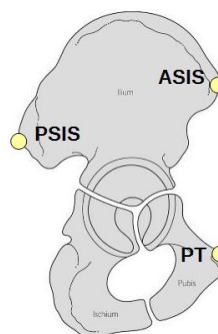
Fig.8: ASIS, PSIS and PT position on the hemipelvis.

By the definitions of these landmarks it is possible to define different anatomical reference frames such as:

- The ISB Plane: the plane recommended by the Standardization and Terminology Committee of the International Society of Biomechanics (ISB) (Fig.9.A). The ISB plane is used in gait analysis. In fact, it is suitable for *in vivo* application because it relies on anatomical landmarks that can be accessed non-invasively in living subjects and that can be palpable on them[29,30];

- The Anterior Pelvic Plane (APP): it is defined by the ASISs and the PTs (Fig.9.B) (described by several, such as Robinson and Lewinnek[31]) and it is the most used in clinical applications; in example it is commonly used for the assessment of acetabular cup orientation after total hip replacement.

A   B
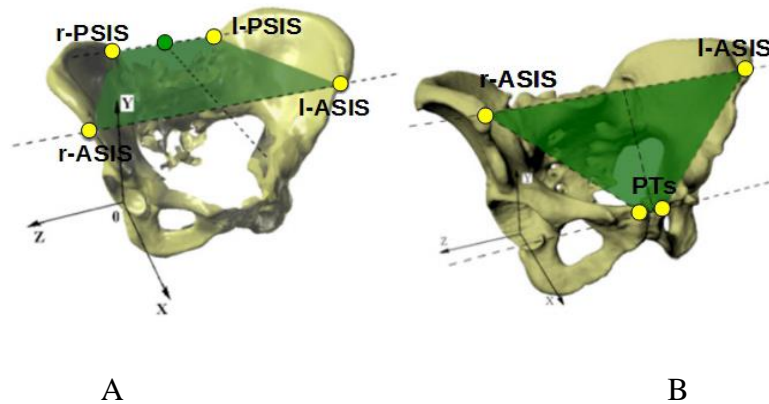
Fig.9: Planes of reference for measurement and pelvic XYZ coordinate system. A. Reccomanded by ISB, this is the typical gait analysis sdr because it relies on anathomic reference frames more palpable than B; B. The Anterior Pelvic Plane (APP);

1.2.3 The hemipelvis stress distribution

The hemipelvis stress distribution results different with respect to:

- the cortical bone, which become thick at the points of major stress;
- the trabecular bone, which is more stressed in thin cortical bone regions;
- the bone density, that increases in response to mechanical loading;

Because of these evidences, the highest stresses are commonly located near the superior acetabular rim, the incisura ischiadaca region (Fig.10) and, to a lesser extent, the pubic bone[32].

Hence, the structure of bones may contain direct information about the forces they may have undergone.
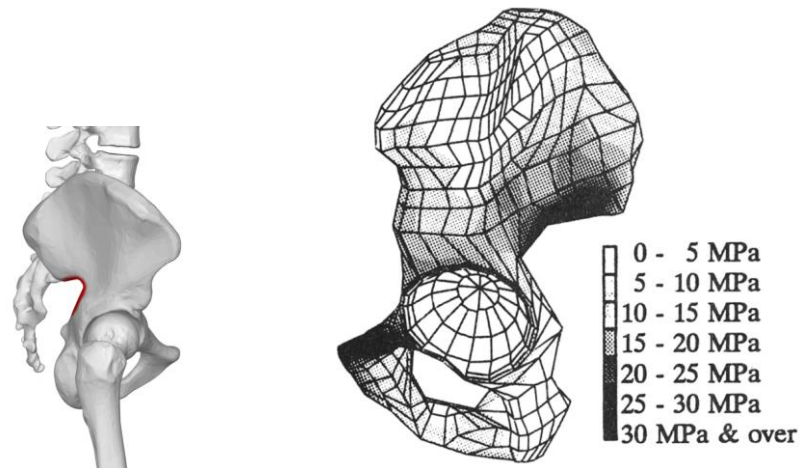
Fig.10: left: focus on the incisura ischiadica; right: Lateral view of the von Mises stress distribution during one-legged stance in the cortical shell if only the hip joint force is applied. The iliac bone remains largely unloaded, while loading of the pubic bone is high.

1.2.4 Forces across the Hip Joint

Hip joint force (or joint reaction force) is the most important force acting in the body-pelvis. It's the resultant mainly of the muscles and ligaments action and of the body weight[33]. Generally, the concept of *equilibrium* is used in the static analysis of joint loading. In this case, the joint of interest is considered in isolation from the rest of the body, and all forces and moments acting on it are identified, establishing the free body diagram for the joint. The *equilibrium* condition is then applied to find the resulting joint reaction force[34].

In first approximation, basic analytical approaches to the balance of forces and moments about the hip joint has been frequently approximated with a simplified, two-dimensional analysis performed in the frontal plane[35]. The involved forces are:

- the body weight;
- the abductors muscles, which can counter the torques produced by the body weight by their pulling action;
- for some tasks the ligaments transferred tension (these are not represented in figures because negligible);

- the joint reaction force, the resultant force of the aforementioned forces.

1.2.4.1 Both leg stance

When the weight of the body is hold up on both legs in static conditions, the centre of gravity is centred between the two hips and its force is exerted equally on both hips. Under these loading conditions, the join reaction force vector is vertical[42]. In this case the joint reaction force is approximately twice the body weight[36].

1.2.4.2 Single leg stance

In a single leg stance, the effective centre of mass moves distally and away from the supporting leg since the non-supporting leg is now calculated as part of the body mass acting upon the weight-bearing hip (Fig.11). This downward force exerts a turning motion around the centre of the femoral head, the moment is created by the 5/6 of the body weight[34] (**5W/6:** the magnitude of the bodyweight equals the bodyweight minus the weightbearing leg[37]), and its moment arm, **c** (distance from femur to the centre of mass). The muscles that resist this movement are offset by the combined abductor muscles, **M**. This group of muscles includes the upper fibres of the gluteus maximus, the tensor *fascia lata*, the *gluteus medius* and *minimus*, and the *piriformis* and *obturator internus*. The force of the abductor muscles also creates a moment around the centre of the femoral head; however, this moment arm is considerably shorter than the effective lever arm of body weight. Therefore, the combined force of the abductors must be a multiple of body weight.
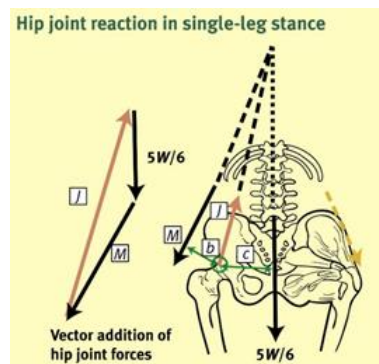
Fig.11: J, hip joint reaction force, M, abductor muscle force; W, body weight component. Moments about joint centre, Mb=(5W/6)c.

Typical joint reaction force levels for single leg stance are three times bodyweight. Thus, anything that increases the lever arm ratio also increases the abductor muscle force required for gait and consequently the force on the head of the femur as well [38].

1.2.4.3 Walking task

Earlier Rydell *et al.*[39], later Bergmann *et al.*[36], measured in *vivo* the hip joint forces finding out that the walking cycles are characterized of two pick forces of the joint reaction force: the first just after heel strike and the second just before toeing off .

The highest peak load measured by Bergmann was in average 238% of the body weight. Hence, during a walking task, the hip contact force can reach more than twice the body weight.

1.2.4.4 Telemetric measurements
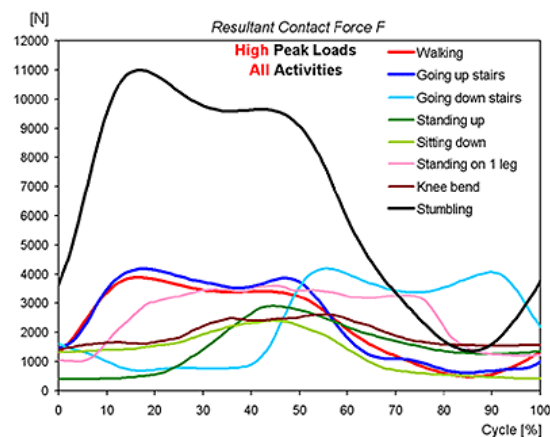
Fig.12: Plot of Bergmann's in vivo study, about several motor tasks, of the resultant contact force (joint reaction force): in x-axis the cycle in percentage (%), in y-axis the force (N).

Bregmann *et al.* conducted his study by means ten volunteers, which were operated by instrumented hip implants. Throughout these ingenious devices, the real patient-specific loads were acquired and telemetrically transmitted. The data were stored in a database containing load information across the hip bone for several motor tasks (Fig.12). After processing data, it was possible to document all the forces applied on the joint of every patient, and to plot them, both as single trials and as average values. Finally, the peak load was highlighted (Fig.13).

This database of hip contact forces is turned out to be so convenient in *in vitro* and *in silico* studies to align the prosthetic components as better as possible to maximize the support of the implant[40] and to apply the physiological load direction through mechanical tests, in several motor tasks (walking, going up stairs, going down stairs, standing up, sitting down, etc…).

In addition, because of it is a free accessible database, the telemetric forces are becoming an important landmark both in research field and in clinical assessments.
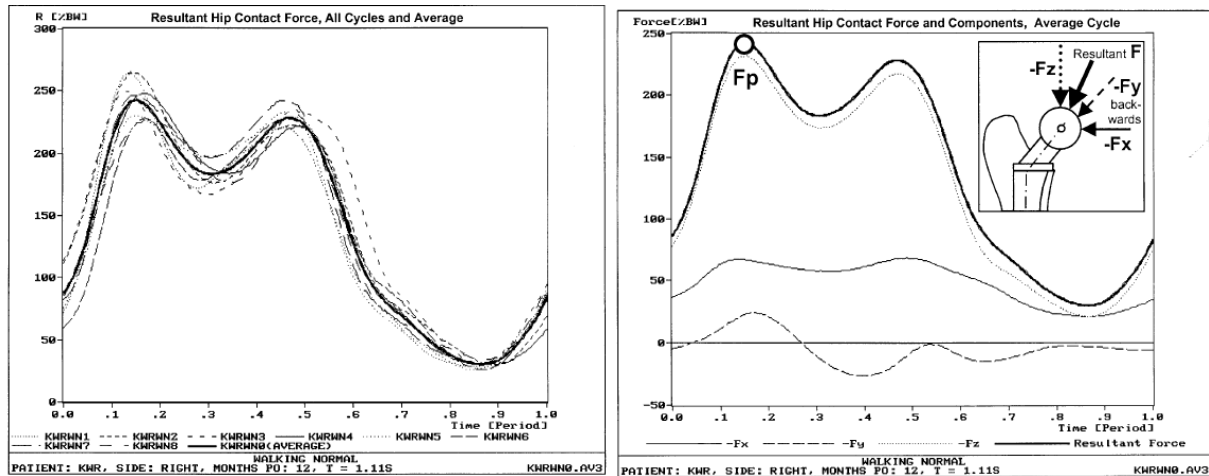
Fig.13: Eexample of contact force F (the action reaction JRF vector at the head of the femur) on the femoral head during normal walking. Left: Hip contact force Fin % BW: thin lines represent single trials; thick line represents the average value. Right: Individual average of force F from left diagram and its components -Fx, -Fy, -Fz, where the x-axis of the femur system is parallel to the dorsal contour of the femoral condyles in the transverse plane, the z-axis is parallel to an idealized midline of the femur. The highest value is the peak force Fp.

1.3 TOTAL HIP ARTHROPLASTY

The total hip arthroplasty is an orthopaedic procedure that aims to restore the physiological motion of the hip joint, to reduce pain and return patients to "better function"[41].

The total hip arthroplasty (THA) procedure was further developed in the 1950s by pioneers such as McKee and Farrar. This early work gave the groundwork for the innovative studies of Sir John Charnley who, in the late 1960s, approached the problem of artificial hip joint design by using the biomechanical principles of human hip joint function[40].

This procedure involves the surgical excision of the head and the proximal neck of the femur and the removal of the acetabular cartilage and subchondral bone. An artificial canal is created in the proximal medullary region of the femur, and a metal femoral prosthesis, composed of a stem and small-diameter head, is inserted into the femoral medullary canal. An acetabular component is inserted proximally into the enlarged acetabular space. The acetabular component is a modular prosthesis formed by a metal black that constrains the acetabular element with the bony hip tissue and an insert as articulating surface (Fig.14). The insert can be made of high-molecular-weight polyethylene (more common nowadays) or of ceramic. The first case (metal on polyethylene) represents the most commonly implanted bearing surface (also called: liner), but this kind of coupling could be associated to the formation of wear particles that may lead to failure for osteolysis. So, ceramic liners are also used for THA and good mid to long term outcomes have been reported[42] .

24

To conclude, the mission of the THA is to restore the physiological biomechanics of the hip joint and so, to give back the autonomy of the hip movements that will lead to a significant improvement in the quality of life.
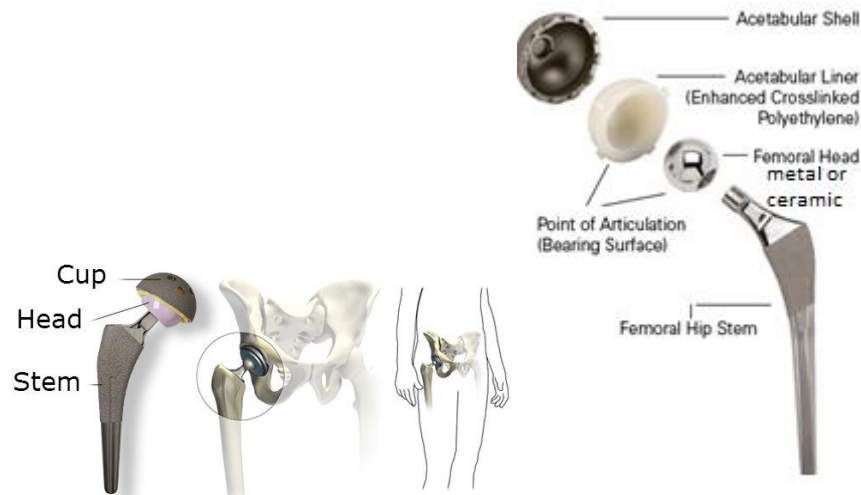
Fig.14: Left: the total hip implant in the human body; right: the implant components.

1.3.1 Causes for Total Hip Arthroplasty

Despite its efficient structure, the pelvis can be damaged from altered loading derived from several disease, pathologies or traumas. The most common cause of chronic hip pain and disability is arthritis (70% of cases[40]): osteoarthritis, rheumatoid arthritis, and traumatic arthritis are the most common forms of this disease.

- Osteoarthritis: an age-related "wear and tear" type of arthritis. The cartilage cushioning the bones of the hip wears away. The bones then rub against each other, causing hip pain and stiffness.

- Rheumatoid arthritis: it is an autoimmune disease in which the synovial membrane becomes inflamed and thickened.

- Post-traumatic arthritis: this can follow a serious hip injury or fracture. The cartilage may become damaged and lead to hip pain and stiffness over time.

- Avascular necrosis: this is a disease in which an injury to the hip, such as a dislocation or fracture, may limit the blood supply to the femoral head. The lack of

blood may cause the surface of the bone to collapse, and arthritis will result. Some diseases can also cause avascular necrosis.

- Childhood hip disease. Some infants and children have hip problems. Even though the problems are successfully treated during childhood, they may still cause arthritis later in life. This happens because the hip may not grow normally, and the joint surfaces are affected[43].

These are the major causes that lead to the THA and in such as a background, the total hip arthroplasty becomes vital[9].

1.3.2 The incidence of the Total Hip Arthroplasty

In Europe every year 700 000 hip implants are performed[44]; 285 000 interventions are carried out each year in the United States according to the Agency for Healthcare Research and Quality.
In Italy the 60% of the arthroplasty surgeries involve the hip and this number is expected to increase during the next 2 decades of 5% every year[45]. Even if the arthroplasty is characterized by a low rate of failure (approximately 5%[46]), follow-up studies report higher incidence of failure for the acetabular cup than for the femoral stem[47].
In Fig.15 are shown data about prosthetic replacements in, from the Hip and Knee Arthroplasty Annual Report- National Joint Registry, Australian Orthopaedic Association (2003-2010)[48].

Hip Category	Number	Percent
Primary Partial Hip	47835	16.3
Primary Total Hip	211114	71.7
Revision Hip	35380	12.0
TOTAL	294329	100.0
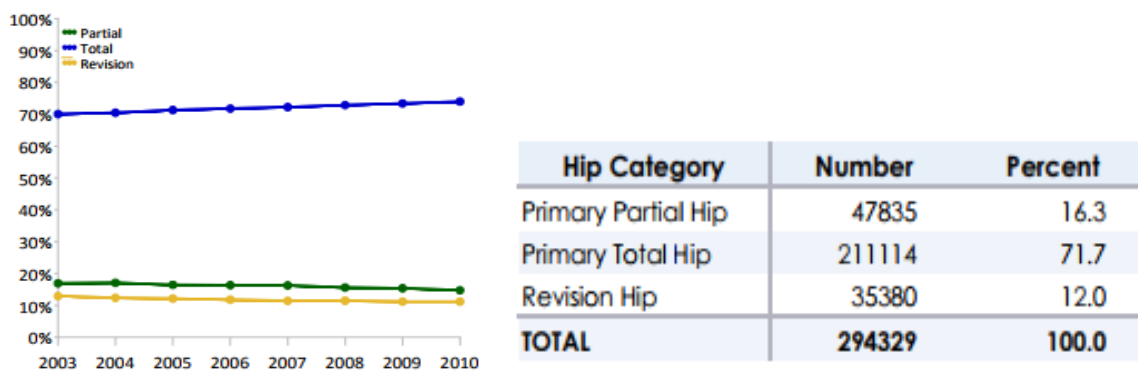
Fig.15: Left: Proportion of Hip Replacements; right: number and percent of hip replacements reported to the National Joint Registry by the Australian Orthopaedic Association, with a procedure date up to and including 31 December 2010.

As shown in Fig.15, the hip arthroplasty can consist of a total or a partial replacement (the surgical procedure used to replace half of the hip joint, involving the replacement of the head of the femur only). Another distinction can be done between primary and revision hip arthroplasty. The second one is a consequence of the failure of the primary THA and it is characterized by many risk factors

which are patient-related (e.g., gender, neuromuscular disorder status, and bone quality) or surgery-related (e.g., surgical approach of primary THA, orientation of the cup, component malpositioning, femoral head size, neck head offset, and surgeon experience)[49].

To yield successful results, the prosthetic components must be fixed firmly to the bone: this can be done with or without surgical cement.

1.3.3 Press-fit fixation (cementless)

Cementless THA was developed in response to evidence that cement debris plays an important role in promoting bone lysis and loosening[50] (as explained in 1.3.4). Nowadays, cementless devices are most frequently used in young patients with high physical demands where a revision surgical procedure in the future will be more likely[45]. Preliminary data suggest that cementless THA have a relatively low revision rate and excellent prosthetic durability for as long as more than 10 years[47, 59]

In the 2016 Norwegian Arthroplasty Register[51], the Norwegian survival percentage of total hip prostheses from 2005 to 2015 in function of years of failure, has been reported (Fig.17), showing a clear sign of good performance of cementless implants after 10 years and sometimes even better than the cemented implant (i.e. for patients younger than 55 years old ones).

The aim of *cementless* fixation is to obtain osteointegration of the implant, generally referred to as biological fixation [52]. The use of the cement for the cup implant is decreasing because of the problems linked to cement: fatigue failure and wear and debris.

So prosthetic devices have been developed without cement, but with a method which rely on biological bone ingrowth: the *press-fit* technique. Today this is the most used procedure of implant for the cup (usually combined with the femoral component implanted with cement).

The *press-fit* fixation involves the implant of the cup forcing it in the bone. The diameter of the cup is usually bigger then the reaming diameter of the acetabular bone, to ensure the best fit and adhesion of the cup with the bone surface (under-reaming *press-fit)*. If the acetabular bone is very sclerotic and hard, or if the hemispherical dome created by reaming is small, sometimes it is difficult for the acetabular cup to contact the whole acetabular roof, since its pole cannot reach the predeterminate depth. Under these conditions a gap will be created. Some authors in literature[15], encourage the presence of the small gap at the dome. In this way, the contact area between the bone and the cup should be limited to the equatorial rim of the acetabulum. This fact is translated into a strong equatorial fit which produces compressive stress at the periphery of the acetabulum that stabilize the cup. Despite the great clinical results, a standard criterion for press-fit fixation lacks. For example, Tabata *et al.*[53] stated that the optimal fixation of the acetabular component needs a press-fit that involves the complete adaptation to the component seat (without any gap at the dome) for optimizing the available surface for the bone ingrowth and the transfer of stress between the implant and the bone. Additionally, if the hemispherical dome created by reaming is larger than necessary, initial press-fit fixation cannot be expected to gain sufficient cup stability. In order to promote the biological fixation of the press-fit implants, all the cups are coated by a porous structure (Fig.16). A study by Bobyn *et al.*[54] suggests the use of porous tantalum material

for coating the cup thank to its remarkable outcomes: more bone occupied the porous tantalum than other porous materials. The reason can be found in the high porosity of tantalum (75% to 85%), greater than in either fibre metal (45% to 50%) or sintered beaded (30% to 35%) coatings. Another controversial issue is related to the use of screws to enhance the fixation: a press-fit implant combined with screws may lead to obtain a better stability of the implant. Kwong *et al.*[55] suggest that the optimum fixation might be performed through an under-reaming *press fit* of 1 mm of the cup with the use of screws (only if not dangerous for close vascular structures). Other studies[53, 56] suggest that the screws fixation doesn't influence the longevity of the implant; in example, Wilson-McDonald *et al.* [57] stated that "the screw fixation makes no difference to failure rate" of the implants. Furthermore, the problems related to screw fixation can be several, such as:

- screws and its holes can be conduit for migration of polyethylene debris that can cause osteolysis;
- a high number of screws holes decreases the treated surface area for stimulating bon ingrowth;
- a wrong insertion of the screws risks vascular injury.

Fig.16: Detail of a porous acetabular component coat.
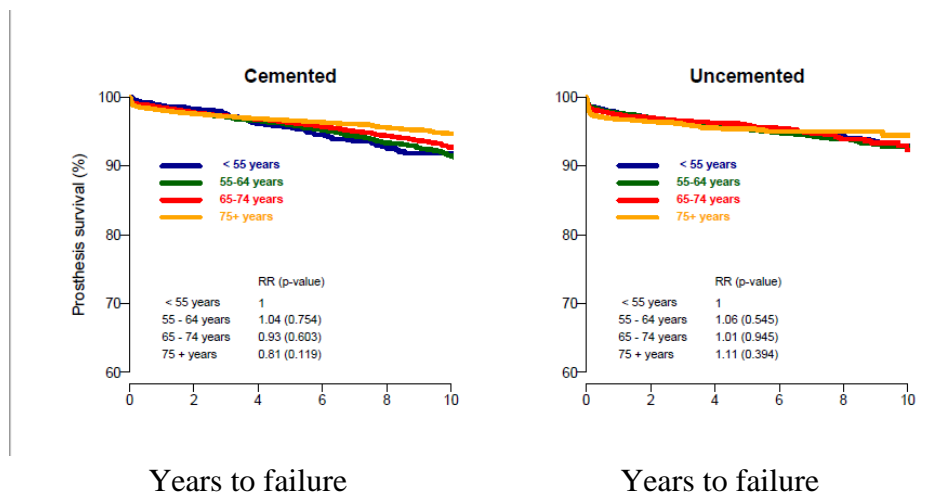
Years to failure   Years to failure

1.3.5 The acetabular orientation

In this paragraph, the practical aspect about the acetabular orientation is discussed. It is essential both to perform the right acetabular component settlement during the operation by surgeons and to monitor it by mean of radiographs. In addition, the acetabular orientation needs to be known to reproduce *in vitro* the correct implanted (or not) pelvis positioning and to test it under physiological condition.

According to Murray[61], the acetabular orientation in the space can be defined with an anatomical approach, radiographically and by the direct observation during the operation. The work of Murray has been essential for switching from one spatial alignment to another, comparing and finding differences among each one. The most common description of the acetabular orientation is due to the combination of two tilts, called inclination and anteversion.

- In the anatomical definition, the angle between the face of the *acetabulum* and the transverse plane is considered to be the anatomical inclination. The anteversion is the angle defined between the transverse axis and acetabular axis when it is projected onto the transversal plane (so the angle between the acetabular axis and the coronal plane).

- Due to the importance of clinical assessment, the orientation of the *acetabulum* can be evaluated post-operatively on anteroposterior radiographs[29] especially for detecting the inclination angle, or on lateral radiographs and CT scans for assessing the anteversion angle (as this cannot be determined reliably on an AP radiograph[62]). So, in the radiograph definition (used for CT scans too[63]), the inclination is the angle between the longitudinal axis and the acetabular axis when projected onto the coronal plane (thus, the angle formed through the face of the acetabulum and the transverse axis) and the anteversion is the angle between the acetabular axis and the coronal plane (Fig.18);
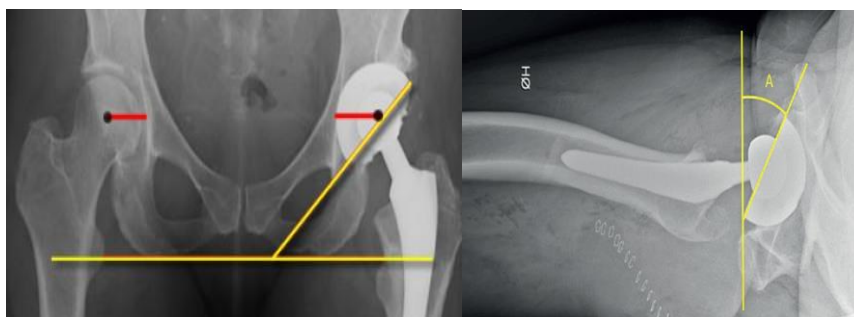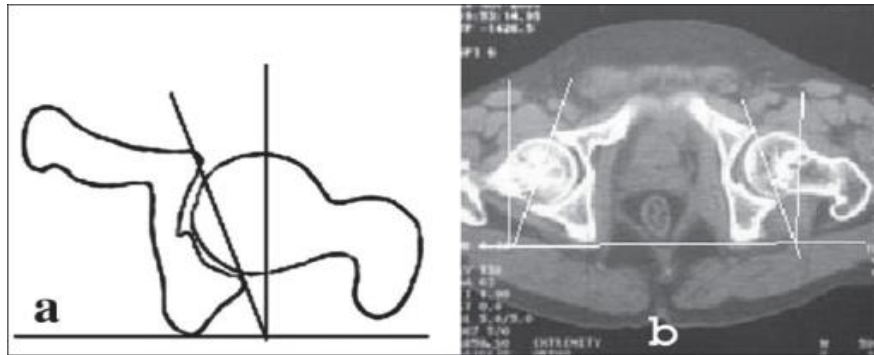
Fig.18: *The upper-left panel shows the inclination angle in a radiograph of an implanted pelvis; the upper-right panel shows a lateral shoot-through radiograph in which A is the anteversion angle; the down panel shows: a. sketched anteversion angle; b. anteversion angle in a CT scan.*

- in the operative approach, the inclination angle is defined as that between the acetabular axis and the sagittal plane, while the anteversion is the angle between the longitudinal axis of the patient and the acetabular axis as projected onto the sagittal plane.

The measured average value of the inclination and anteversion angle, conventionally used by clinicians for diagnosis and surgery, are respectively of 45° and 20°[29, 30, 31, 64, 65, 66].

1.3.5.1 The Standard Acetabular Plane

All the previous mentioned reference frames (paragraph 1.2.2) are suitable for an entire pelvis. As in *in vitro* application hemipelvis is frequently adopted, Morosato *et al.*[24] defined a reference frame suitable for a single hemipelvis, adapting the APP reference frame: this is called Standard Acetabular Plane (SAP) (Fig.10). Due to the link with the orientation of the acetabular plane, it can be potentially used to assess clinical problems[67]. In addition, the relative alignment of the proposed reference frame with respect to the ISB reference frame was measured. This reference frame born specially to overcome the problem related to the different orientation of the cup in cadaveric specimen. Measuring with respect to the SAP it was possible to standardize the actual alignment.
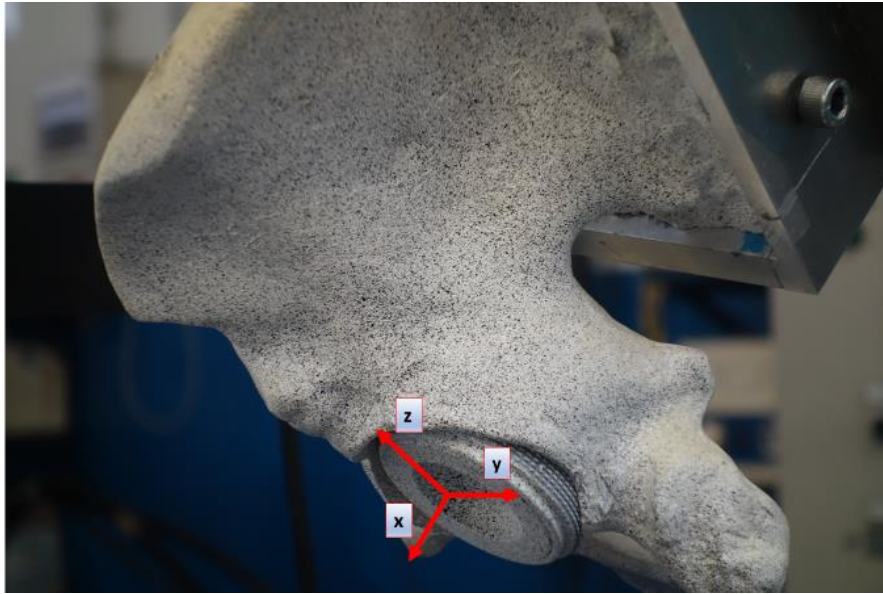
Fig.19: Visualization of the SAP reference frame
(the picture shows the acetabular component implanted on left hemipelvis, which
was potted and painted ad hoc for the Digital Image Correlation analysis).

1.3.6 Failure risks of the Total Hip Arthroplasty

In THA, the causes of failure of primary implant are several. It has been reported [68,69] that the prostheses may fail because of:

- implant fracture,
- surgical technique error,
- dislocation,
- wear/osteolysis,
- infection,
- periprosthetic fracture,

but especially because of the late aseptic loosening, leading to the revision surgery[70] (up in the figure Fig.20, the percentage of revisions, because of the failure of the THA, reported in some registers and studies from 2006 to 2011 are shown; down in the figure, the number and the percentage values of diagnosis in revision of primary THA are reported from the Regional Register of Orthopaedic Prosthetic Implantology (RIPO), which depends on all the orthopaedic units in the Emilia-Romagna region in 2013: the most common cause of revision is the cup aseptic loosening[71]).

Register/Study	Year	Percentage of revisions by cause					
		Aseptic loosening	Dislocation (Rank)	Infection	Periprosthetic fracture	Pain	Other*
Australian register	2011	29.9	27.6 (2)	16.7	14.7	2	9
National Joint Registry of Great Britain and Wales	2011	42	13 (3)	12	8	24	NA
New Zealand register	2010	41	30.6 (2)	13.2	9.5	10.7	NA
Bozic et al.	2005–2006	19.7	22.5 (1)	14.8	6.2	NA	36.8
Current study	2010–2011	41.5	10.4 (5)	11.2	11.8	1.3	23.8

* Other includes implant failure, implant fracture, wear, osteolysis, mechanical problems, surgical technique errors, and adverse reaction to metallic debris (aseptic lymphocytic vasculitis associated lesion); NA = not applicable; [†]in the New Zealand and Great Britain and Wales registries, there was often more than one reason listed on the data form and all are entered.

Diagnosis in revision of primary THA	Number	Percentage
Cup aseptic loosening	3.800	33,1
Total aseptic loosening	2.517	21,9
Stem aseptic loosening	1.472	12,8
Prosthesis dislocation	1.042	9,1
Bone fracture	633	5,5
Prosthesis breakage*	560	4,9
Two steps prosthesis removal	530	4,6
Poly wear	401	3,5
Pain without loosening	184	1,6
Septic loosening	132	1,1
Primary instability	92	0,8
Heterotopic bone	42	0,4
Metallosis	37	0,3
Trauma	27	0,2
Acetabulum fracture	12	0,1
Other	77	0,7
Total°	11.481	100,0

Fig.20 Up: the percentage of revision because of the failure risks of the THA reported in some registers/ studies from 2006 to 2011; "Current study" refers to Delaunay et. al. study[69]; Down: number and percentage values of diagnosis in revision of primary THA are reported from the Regional Register of Orthopaedic Prosthetic Implantology (RIPO).

In general, aseptic (not caused by infection) loosening refers to the failure of fixation at the bone/implant interface, with resultant micro- or macro-motion of the implant, relative to the adjacent bone. It may occur early, because of the failure of initial ingrowth of bone into the prosthesis or caused by poor cementing technique. Alternately, loosening of a fixed implant may occur months (or years) after implantation, potentially because of mechanical overload, physiologic bone resorption, or a combination of both at the bone–implant interface [Ref]. In addition, aseptic loosening is due to the presence of debris caused by the wearing of the prosthetic

components. The localization *in situ* of these particles can be the result of inadequate initial fixation, mechanical loss of fixation over time, or biologic loss of fixation caused by particle-induced osteolysis around the implant, oxidative reactions, minor pathogen contaminations [ref].

When the mobilization affects a significantly large area at the implant-bone interface, then the ingrowth process will result in formation of fibrous or fibro-cartilagineous tissue more than bony tissue: this is the initial anti-inflammatory response of the body. Later the macrophages absorb particles. The osteolysis process act and lead to the failure of the implant (Fig.21). Pain and functional limitation often represent the final phase of this process.
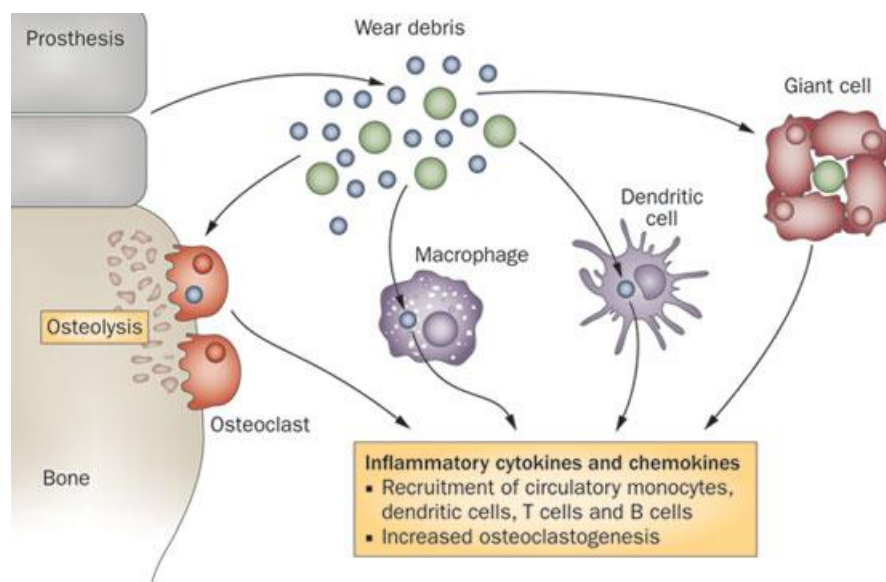
In cemented implant, from radiographic examination, bone resorption progressively enlarges lytic *foci* around the prosthetic components. Mechanical loosening of the device ultimately occurs, occasionally with further fragmentation of the cement surrounding the components[72].

Fig.21: Representation of the Osteolysis process

Similar lytic bone resorption may take place in cementless arthroplasties due to debris produced by wear of the femoral head against the polyethylene acetabular component as previously mentioned (2.6.3).

Thus, the nature of the implant technique (cemented or cementless) influence the rate of loosening: despite its initial stability, cemented implants demonstrate an unfavourable rate of late aseptic loosening. Charnley[73] reported a 25% overall incidence of aseptic loosening of cemented acetabular components at 12-15 years. Sutherland *et al.*[74] reported a 29% rate of loosening at 10 years and underlined that acetabular loosening increased exponentially after 8 years [50], causing more debris then the cementless implants. However, exact rates of aseptic loosening are difficult to define, since definitions and methods of diagnosing loosening vary considerably in the literature.

Recently the AAOS (American Academy of Orthopaedic Surgeons) developed a treatment algorithm for osteolysis as well as several "pearls" of surgery[75] as shown in figure. (Fig.22).
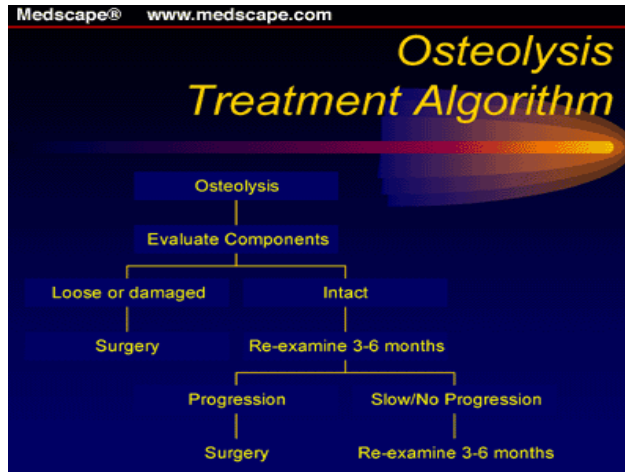
Fig.22 Treatment Algorithm developed by the American Academy of Orthopaedic Surgeons[75].

1.4 PRIMARY STABILITY

Primary stability is the essential prerequisite to achieve the osseointegration of prosthesis with bone[15]. The primary stability is the capacity of the prosthesis to not incur in loosening (below a low predetermined threshold) in a conventionally adopted period equal to the first 90 days right after the settlement of the acetabular component.

The stabilization of the cup after the surgical implant is of outstanding importance to create the right environment to favour the osteointegration at the bone-implant interface. There is still not consensus about an absolute definition of the primary stability. Either tested *in vivo*, *in vitro,* or detected by clinicians through diagnostic tests, the primary stability can be assessed by mean of different methods. For sure, this is the outcome of both a good osteointegration and of a well performed implant. If the osteointegration is not achieved, the formation of fibrous tissue may occur, in the cup-bone interface, leading to the aseptic loosening [76] (Fig.23).
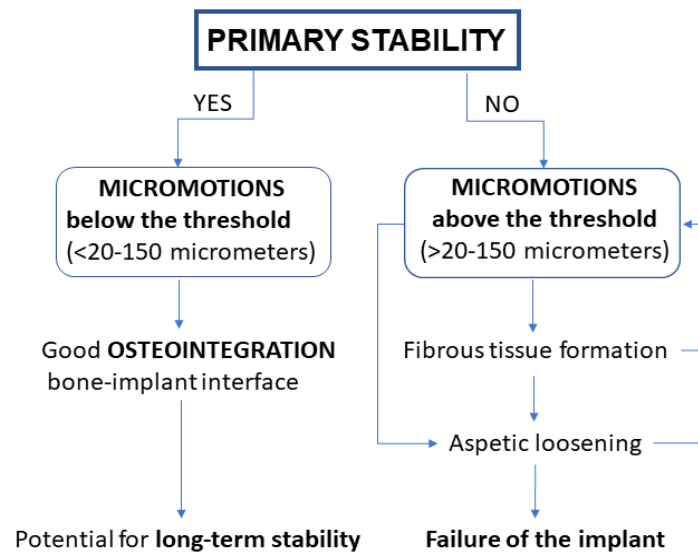
Fig.23: Flowchart about the influence of Primary Stability on the failure of the implant (if the primary stability is ensured, this yields a good osteointegration).

The osseointegration is the bone ingrowth, where new bone is laid down directly on the implant surface and the implant exhibits mechanical stability[77] .

1.4.1 *In vivo* assessment of tolerance to micromotion

As several definitions and not complete understanding of the mechanism of the osteointegration evolution at the implant surface still doesn't exist, some *in vivo* studies have been conducted to assess the primary stability from a biological point of view.

In Sennerby *et al.*'s work[78], titanium implants were inserted into the tibia of rabbits. The osteointegration was then assessed over 3-180 days through optical microscopy and transmission electron microscope:

- At 3 days red blood cells and scattered macrophages predominated at the implant surface after 3 days;
- At day 7 multinuclear giant cells were found at the implant surface protruding into the bone marrow and in areas with no bone-titanium contact;
- At days 14-28 gradually more frequently with longer time, apparently fully mineralized bone was seen close to the implant;
- At days 28-180 the bony tissue is born, and the mineralized bone continue to ingrowth and move to the implant;
- After 6 months the mineralized bone reached the titanium implant.

Similarly, Søballe's work[79], was focused on the influence of micromovements on bony ingrowth into titanium alloy (Ti) and Hydroxyapatite (HA)-coated devices, implanted into femoral condyles of seven mature dogs. A loaded unstable device producing movements of 500 micrometers during each gait cycle was developed while a stable device was kept as controls. Histological analysis after 4 weeks of implantation showed a fibrous tissue membrane surrounding both Ti and HA-coated implants subjected to micromovements, whereas variable amounts of bony ingrowth were obtained in mechanically stable implants. Unstable HA-coated implants were surrounded by a fibrous membrane containing islands of fibrocartilage with higher collagen concentration, whereas fibrous connective tissue with lower collagen concentration was predominant around unstable Ti implants. In conclusion, micromovements between bone and implant inhibited bony ingrowth and led to the development of a fibrous membrane.

Obsorn's and Newesley's studies showed that the bone ingrowth occurs because of two events. The first is focused on the osteoblasts deposition and the late mineralization which arise in a specific direction: from periphery to the implant; in other words, the bone goes to encircle the implant. The second event happens when the osteointegration is in the opposite direction (from implant to periphery). The apposition of new bone requires a continuous recall of cells from the bone and bloodstream to the implant, since the osteoblasts, after differentiation, are only able to produce bone by apposition. Once they are polarized, they produce extracellular matrix proteins, especially collagen, in order to give a precise structure to the bone-implant interface, which, after calcification, is transformed into an osteoid matrix and finally into bone tissue [80].

The *in vivo* most relevant result is that: if no micromotions are detected below 20 micrometers, there is not the evidence of fibrous tissue formation; above 150 micrometers, the fibrous tissue formation happens. Between 20 and 150 micrometers both events can occur[81, 82].

1.4.2 *In vivo* assessment of cup stability

A different *in vivo* approach consists in assess failure of the acetabular component by mean of the stereophotogrammetric analysis. An—interesting *in vivo* study has been conducted by Nieuwenhuijse *et al.*[83] with clinical and Roentgen Stereophotogrammetric Analysis (RSA) for ten years follow-up, establishing the existence of the relationship between the early migration and the late aseptic loosening of the acetabular cups. In fact, early migration, as **RSA** measured has good diagnostic capabilities for the detection of acetabular components at risk for future aseptic loosening and this method appears to be an appropriate means of assessing the performance of new implant-related changes. The *in vivo* follow-up showed that after two postoperative years, the loose acetabular components showed markedly greater and more rapid cranial (upper) translation and rotation about antero-posterior axis (change of inclination). Similarly, Kim *et al.* used the Ein-Build-Rontgen-Analyse (**EBRA-cup**) to prove that the absence of proximal translation within the first 60 months indicates a component is not likely to be loose. Both the EBRA-cup and the RSA are two technique which improves the accuracy of radiographic (clinical) criteria [84,85].

So, follow-up tests [83,86,31, 87], combined with clinical criteria assessments, indicate some thresholds values, such as (Tab.2):

	CRANIAL MIGRATION	VARIATION IN INCLINATION
Nieuwenhuijse *et al.*	1.76 mm	2.53°
Abrahams *et al.*	3 mm	5°
Kim Y.S *et al.*	1 mm	1.15°
Pijls *et al.*	1 mm	-

Tab.2: Thresholds values for cranial migration of the acetabular cup (mm) and variation in inclination (°) in literature.

about change of inclination and along cranial translation (Fig.24).
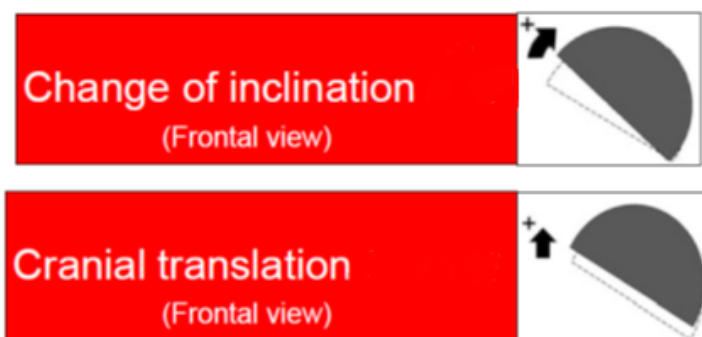
Fig.24 outline of the change of inclination and the cranial translation of the cup.

1.4.3 *In vitro* assessment of cup stability

In vitro tests are conducted to measure the motion of the acetabular component in different loading conditions and different models are used.

1.4.3.1 Simplified assessment methods

Some studies have been developed simulating the acetabular cavity by mean of a simplified way: in foam blocks with a controlled density[15,56]. Static load to failure may be applied (torsional, edge loading and pull out tests[88,87, 68,89]), for essentially investigating the design limits of the implant to extreme conditions[90].

1.4.3.2 Realistic assessment methods

To better simulate physiological conditions, other studies apply cycles of load until failure or for a fixed number of cycles and by using animal and cadaveric specimens [50,55, 91,58,26,]

Two representative *in vitro* studies are the ones by Perona *et al.* [50] and Kwong *et al.*[55]

Perona's study was designed to quantify initial micromotion at the cup-bone interface and to have a comparison between different fixation methods (cemented, cementelss, with screws and without). To measure the displacements, they used current transducers (Fig.25). Relative motions between the cup and the bone, perpendicular to the plane of the rim, were able to detect, during 5 cycles of axial loads of up 2534N, reaching 3 times the bodyweight (if 80 kg person).
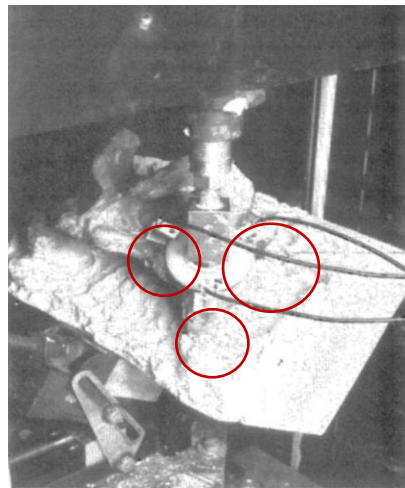
Fig. 25 Focus on Eddy current transducers on the cadaveric specimen.

The average micromotion at the maximum applied load were 162 micrometers at the ilium, 97 micrometers at the pubis, and 54 micrometers at the ischium, with the *press fit* fixation.

Kwong *et al.* conducted a similar study using exstensometers fixed to the specimen with a custom setup (Fig.26).

Fig.26: Sketch of Kwong's in vitro study setup[55].

They evaluated the performance of the *press fit* fixation, testing (with axially load) the acetabular cup implanted in cadaveric specimens simulating a critical physiological load (in a single leg stance) with or without the presence of screws (Fig.27).

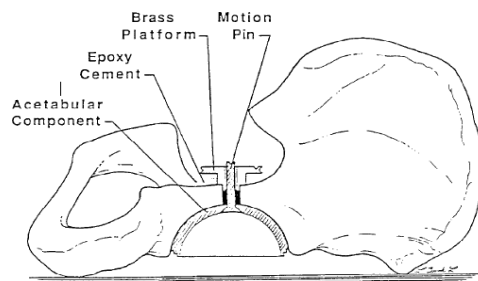|	Specimen	Dome Pin Site/Axial Motion (μm)					Lateral Pin Site/Lateral Tilt (μm)				
		Number of Screws					Number of Screws				
		4	3	2	1	0	4	3	2	1	0
2 mm press-fit	1L	15.1	14.8	18.3	26.5	25.8	16.6	17.4	8.8	6.5	9.8
	1R	13.1	15.7	15.6	31.1	32.6	13.6	17.4	12.8	22.0	22.9
	2L	34.2	30.4	34.5	58.6	64.3	39.0	33.9	62.4	64.2	88.4
	2R	38.6	32.8	30.8	43.8	45.8	34.6	32.2	56.2	58.9	66.8
	3L	23.8	24.3	31.4	31.4	28.3	26.0	19.7	40.0	63.0	2.7
	3R	20.8	17.2	20.0	22.4	31.4	10.5	8.1	11.5	11.8	20.9
	Average	24.3	22.5	25.1	35.6	38.0	23.4	21.5	32.0	37.7	35.3
	SD	10.2	7.8	8.0	13.4	14.6	11.7	9.8	24.1	27.1	34.3
1 mm press-fit	1L	17.4	18.1	24.0	32.8	30.8	1.2	0.5	5.8	7.0	10.2
	1R	19.7	24.0	26.0	31.0	37.5	6.4	6.2	4.7	6.5	11.2
	2L	32.5	38.4	41.6	66.4	50.9	39.3	35.6	60.2	68.4	84.0
	2R	52.4	52.4	52.8	55.4	63.8	28.7	29.3	32.4	26.3	24.3
	3L	29.6	29.3	25.5	27.0	34.6	5.8	4.0	9.6	4.2	1.0
	3R	19.8	19.0	24.0	22.6	23.8	6.5	5.1	6.9	6.1	3.8
	Average	28.6	30.2	32.3	39.2	40.2	14.7	13.5	19.9	19.8	22.4
	SD	13.2	13.2	12.1	17.5	14.6	15.5	15.0	22.3	25.2	31.2
Exact-fit	1L	16.3	16.9	18.3	41.4		3.8	6.2	8.2	11.6	
	1R	17.5	24.0	24.4	30.0		10.3	9.6	10.2	10.2	
	2L	31.6	30.2	37.8	104.4		42.3	48.1	78.6	121.8	
	2R	33.8	34.2	35.8	66.6		102.4	114.5	139.2	115.3	
	3L	38.1	35.9	39.1	148.0		45.4	51.0	70.0	83.2	
	3R	31.5	52.8	42.1	106.1		34.5	10.6	15.6	29.0	
	Average	28.1	32.3	32.9	82.8		39.8	40.0	53.6	61.9	
	SD	9.0	12.2	9.4	44.8		35.1	41.6	52.2	51.3	

Fig.27: Results in Kwong et al's work.

Thus, *in vivo* tests underline the importance of keeping micromotions at the bone-implant interface below a threshold (still not conventionally decreed), because it is a fibrous tissue formation index[52]. Thus, the *in vitro* tests on acetabular components are conducted for preclinical primary stability assessment, because it is extremely important to have an early performance on these kinds of implants to prevent mechanical failure or to investigate what is the best method of implant (with screws or not, with or without cement and so on) or eventually a design variation.

1.4.4 *In silico* assessment of cup stability

No studies about the assessment of the primary stability have been carried out *in silico* yet. Despite this, an explicative example about FE analysis has been conducted by Gosh (2012), who used the Digital Image Correlation technique to validate a FEM predicting strain distribution both for the intact and implanted hemi-pelvis (with the THA acetabular component).
FEM was a valid predictor of the strain distribution, advantageous for detecting full field data and to allow investigations of many variables quickly and relatively inexpensively[92].

1.4.5 How to measure the *primary stability* of acetabular cups: Clinical criteria

Clinicians usually assess the *primary stability* through the evaluation of the aseptic loosening. The diagnosis relies especially on clinical symptoms and on radiographic criteria.

The challenges in diagnosis arise from the difficulty in detecting the presence of implant motion, particularly when it is in the submillimeter range. Thus, qualitative measures, such as radiolucent lines adjacent to implants or increased absorption on radiographs, are typically used, together with the assessment of the pain.

Clinicians are used to act a differential diagnosis: firstly, they evaluate the origin and the localization of the pain. In a follow-up study (about the diagnosis of the dislocation)[93] , authors use the Postel Merle d'Aubigne scoring, showed in Fig.28, that in 1954 was published to give a rating scale both to the intensity of the pain and to the activity which leads the pain to raise.

Score	Pain	Mobility	Ability to walk
0	Pain is intense and permanent	Ankylosis with bad position of the hip	Impossible
1	Pain is severe even at night	No movement; pain or slight deformity	Only with crutches
2	Pain is severe when walking, prevents any activity	Flexion under 40 degrees	Only with two canes
3	Pain is tolerable with limited activity	Flexion between 40 and 60 degrees	With one cane, less than one hour. Very difficult without a cane
4	Pain is mild when walking; it disappears with rest	Flexion between 60 and 80° degrees; patient can reach his foot	A long time with a cane; short time without cane and with limp
5	Pain is mild and inconstant; normal activity	Flexion between 80 and 90 degrees; abduction of at least 15 degrees	Without cane but with slight limp
6	No pain at all	Flexion of more than 90 degrees; abduction to 30 degrees	Normal

Fig.28: Scoring Pain with respect to mobility and ability to walk.

By scoring the pain it is possible to speculate about the severity of the case, as a first approach during this phase of anamnesis and objective examination. Then a standard protocol is followed:

1. clinicians assess if there would have been a pain change due to extrinsic causes, not inherent with the surgery;
2. if it is found that there was an interval without pain after operation, it is necessary to consider prosthesis intrinsic causes instead of extrinsic causes:
3. RX, PCR (Protein C Reactive, index of inflammation if the test is positive) and ESR (Erythrocyte Sedimentation Rate, index of inflammation if the test is positive) investigations are necessary;
4. if PCR and VES are negative, the diagnosis must continue with the bone scan: if this is positive, clinical assessment suggest aseptic loosening. Conversely it suggests other causes;

5. if PCR and VES are positive it probably deals with infection (Fig.)[94].

Radiographic criteria include measuring acetabular component migration relative to surrounding bone, identifying radiolucent lines [95]. A radiolucent line is a dark line of demarcation between the acetabular component and the cancellous bone. According to DeLee and Charnley, in case of radiolucent lines with a thickness ≥ 2.0 mm, or in any zone with the presence of sclerotic border, the implant is considered loose. A sclerotic border is defined as a condensed bright light adjacent to the surrounding cancellous bone [83]. However, the accuracy and interobserver agreement of these measures are unknown [96].

Another clinical aseptic loosening parameter is the visual identification of the cup migration. This assessment relies on the observation of a series of radiographs or of scintigraphy too, which is generally used to detect inflammations or tumours.

With the presence of loosening, the scintigraphy shows areas of anomalous hyperconcentration of the radiopharmaceutical perfusion, in the bone around the prosthesis.[94].

	Sensitivity	Specificity
Scintigraphy	83% (confidence interval 95%, 69-92)	67% (confidence interval 95%, 46-84)
Radiography	85% (confidence interval 95%, 71-94)	85% (confidence interval 95%, 66-96)

Tab.3 Sensitivity and Specifity of scintigraphy and radiography developed by Temmerman OP *et al.'s follow-up study*[97].

Among the techniques above, as shown in Tab.3., the radiographic analysis has the higher accuracy (and the lowest risk) in detecting the loosening of the cup, hence in evaluating the presence (or not) of the primary stability.

All these methods are limited by the inter-observers' variation and the possibility of a loosening not detectable on radiographs of the diagnostic tests.

The pain parameter is such a controversial tool, too. It may range from no pain to persistent hip pain beginning immediately after THA or even later (many months or years after a previously nonsymptomatic THA).

These limits underline the importance of preclinical assessments of the implant stability, that are quantitative and reliable. To reach this goal many studies are conducted *in vivo, in silico and in vitro*.

1.5 DISPLACEMENT TOOLS FOR IN VITRO TESTING

1.5.1 Displacement sensors

Displacement transducers measure the position throughout an electrical signal variation. The Linear variable differential transformer (LVDT) is a type of electrical transformer used for measuring absolute linear displacement (position).

An LVDT consists of a coil assembly and a cylindrical ferromagnetic core with a probe at the apex which feel the displacement of a specimen (Fig.29). The coil assembly consists of three coils of wire wound around the hollow form. The core can slide freely inside the form. The centre coil is the primary coil, which is excited by an AC source as shown (Fig.29) (The frequency is usually in the range 1 to 10 kHz[98]). The magnetic flux produced by the primary is coupled to the two secondary coils, inducing an AC voltage in each coil. In fact, as the core moves, these mutual inductances change, causing the voltages induced in the secondaries to change. The coils are connected in reverse series, so that the output voltage is the difference (hence "differential") between the two secondary voltages. When the core is in its central position, equidistant between the two secondaries, equal but opposite voltages are induced in these two coils, so the output voltage is zero. Thus, the core displacement is transduced in voltage values.
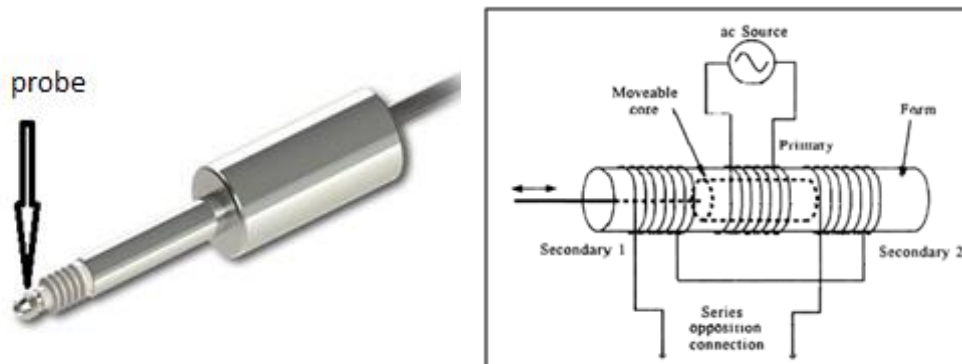
Fig.29: On left, LVDT design with focus on the probe; on right general LVDT assembly.

The magnitude of the output voltage is proportional to the linear displacement of the core (up to its limit of travel). The phase of the voltage indicates the direction of the displacement. When stated without a polarity, it is called LVDT's full range, full stroke, or total stroke.

By mean of wire connections, the LVDT is commonly connected to a signal conditioning circuit that translates the output of the LVDT to a measurable voltage.

The wire connection can be at 4-wire or 5-wire configuration (Fig.30) and the respectively equations that relate displacements with voltage, are:

- 4-wire configuration: displacement $= G \, (V_{CH+} - V_{CH-})$;

- 5-wire configuration: displacement = G [(V_{CH+} - V_{CH-})/ (V_{CH+} + V_{CH-})].

Where G is the sensor gain or sensitivity, defined by the ratio between voltage and displacement (V/mm).
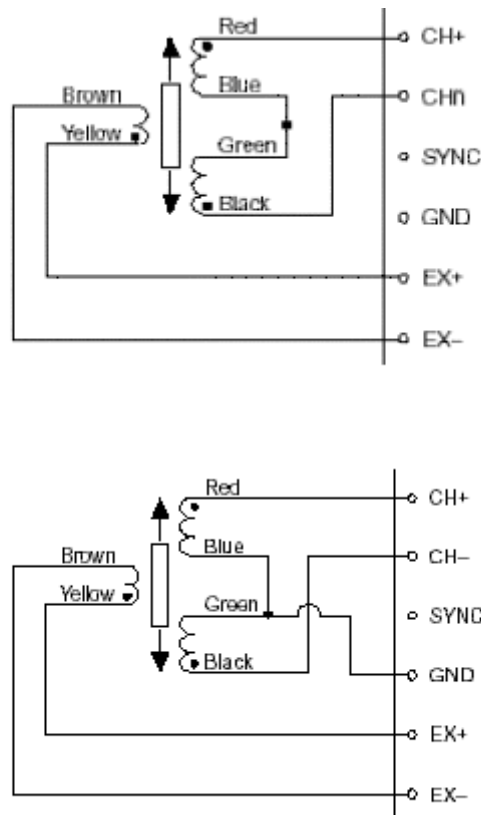
Fig. 30: Up, 4-wire connection of an LVDT to a signal conditioning circuit; Down, 5-wire connection of an LVDT to a signal Conditioning Circuit

The signal conditioning circuitry synchronously demodulates the secondary output signal with the same primary excitation source. The resulting DC voltage is proportional to core displacement [99].

1.5.1.1 Measurements Error

Typically, the LVDTs have a very high resolution: it can be better than a micron for those with the related full scale[100]. Resolution is defined as the smallest core position change that can be observed in LVDT output. They also have a high precision: LVDT is able to reproduce the same output, less than a few microns, for repeated trials of the same input under constant operating and environmental conditions. For these reasons, they are robust tool for small displacements

detection. However, as all the sensor, it can be affected by the systematic and random errors on the measurements[101]. Random errors are unpredictable deviations from the true value due to stochastic temporal variations. Random errors are also referred to as *noise* and it is usually due to environment causes such as temperature and humidity.

However, LVDTs can be designed to operate at cryogenic temperatures or up to 1200 °F (650 °C), in harsh environments, under high vibration and shock levels. So random errors are expected to be low.

As LVDT output is a nominally linear function of core displacement within its linear range of motion, a plot of output voltage magnitude versus core displacement (the input, x, is the displacement, the output, y, is voltage) is essentially a straight line. Beyond the nominal linear range, output begins to deviate from a straight line into a gentle curve. From a statistically best-fit straight line versus core displacement within an LVDT's nominal linear range, the maximum deviation of LVDT output is defined as the linearity error or the non-linearity of the LVDT (Fig.31). This represents a systematic error.

Fig. 31: Non -linearity error description.

Linearity error is typically expressed as a percentage of full-range output. The typical value for standard LVDT is of ±0.25% of full range output (depending on the budget, it can differ from 2% to 0.1% too). However, improvements to these specifications are possible with special construction techniques or using onboard signal processing. Linearity errors as low as ±0.05% of full range output can be obtained in this manner[102].

Other errors affecting the LVDT outcomes can be related to the quantization error due to the signal quantization (systematic error) and due to random for different causes (external contamination in the form of dirt over long term use also contributes to accelerated wear). Trends derived by performing *calibration* (i.e.Fig.32) can provide an indication of these changes over time.

In fact, the sensor calibration should be done periodically. This action establishes a historical relationship between the value indicated by a measuring instrument or measuring system and the corresponding calibration standard[103].
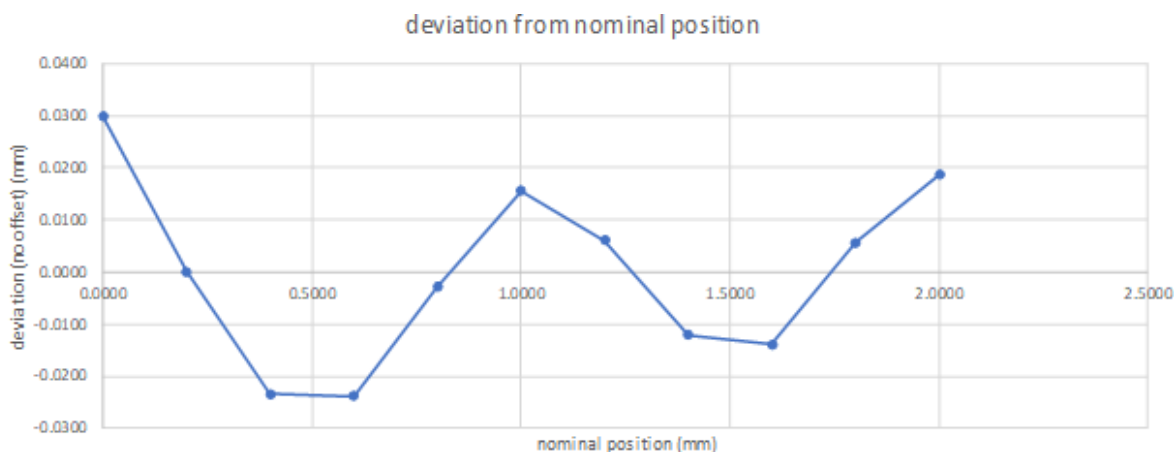
Fig.32: Plot of the calibration of an LVDT, developed in the Laboratory of Biomechanics, before a test campaign to quantify the measurement uncertainty: about x-axis is plotted the nominal position imposed (and known) by the operator on a first sample; about the y-axis is plotted the deviation from the nominal position which derives from the difference between the LVDT measure and the nominal position.

1.5.1.2 Use of Linear variable differential transformer for THA assessment

LVDTs are largely used in so many fields of applications such as power turbines, hydraulics, automation, aircraft, satellites, nuclear reactors, and many others.

Because of their strong performances in micro-technologies the LVDTs sensors are also used for detecting micromovements in biomechanical tests. With strain gauges, LVDTs are the most used sensors to detect micromotion of implants (i.e movements of the acetabular cup) or to evaluate point-wise deformation at the bone tissue level.

For example, Gonzalez *et al.* in 2014[104] used as many as eight LVDTs (with 20 micro meter of resolution) to measure *in vitro* the small displacements that a pelvis and acetabular cup experienced under loading conditions (e.g., during walking, jogging, squatting, etc.). Gonzalez devised an interesting set up to measure the acetabular cup migration under loading: a metal rod was used as the LVDT contact point to capture cup motion. A total of six LVDTs contacted the metal rod. Three were along the Z-axis and three were radially out from the centre of the metal cross (#4-6 in Fig.33). Lastly, two LVDTs contacted the bony rim of the acetabulum along the X and Y-axis to capture acetabular cup migration under loading (Fig.41). In this work it was assumed that no rotation around the Z-axis took place. The combination of LVDTs #1-5 allows a kinematic analysis of the five degree of freedom acetabular cup.
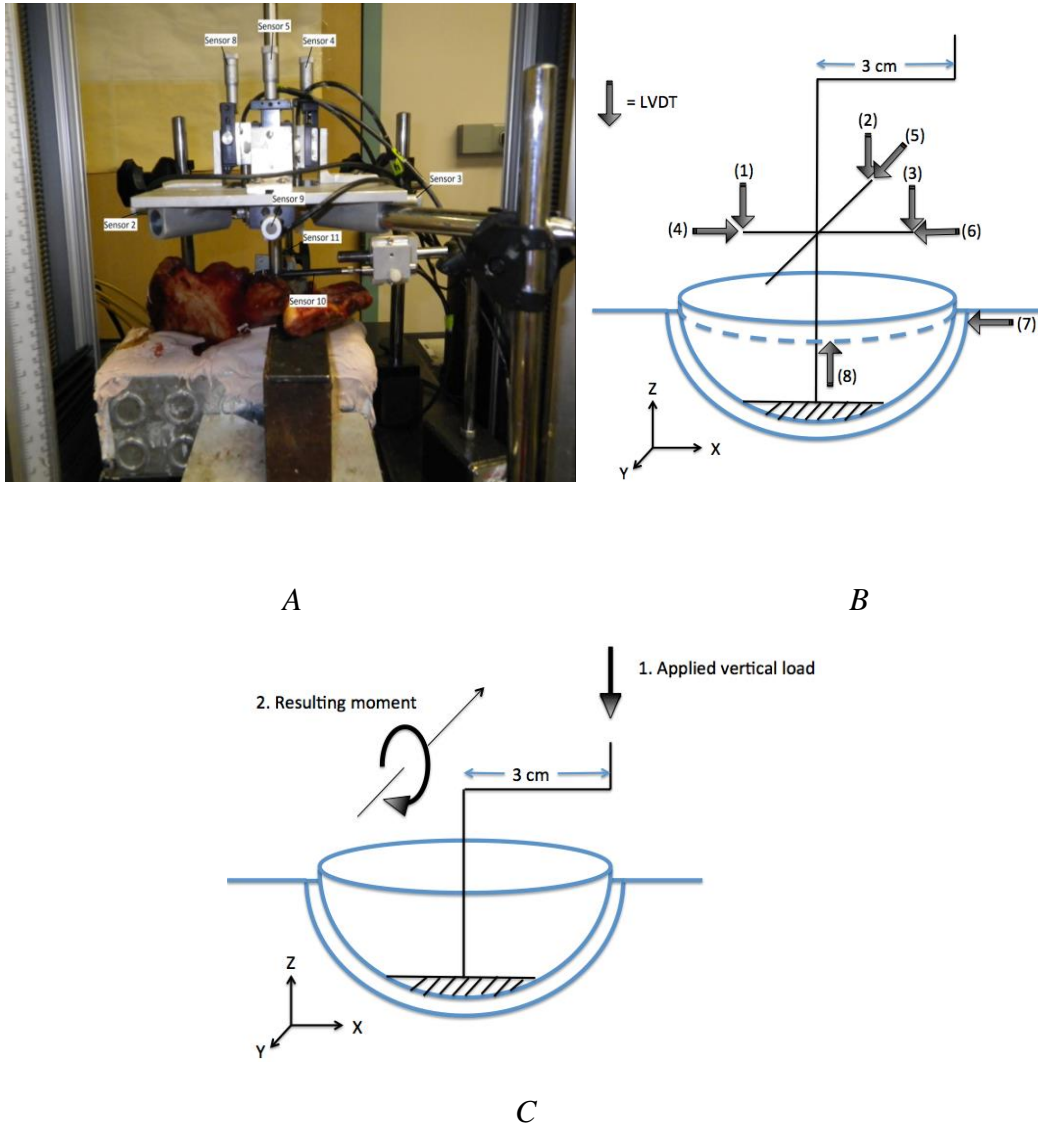
Fig.33: A. Gonzales et al.'s set up for the in vitro test; B and C. diagrams for the LVDTs position and the applied load and the resulting moment.

Despite the high accuracy and resolution of LVDTs, they show some limits for measuring the primary stability of the acetabular cup. By mean an LVDT it is possible to perform only a measure along an axis: one degree of freedom. Implanting several of them on a hemipelvis specimen, may be a hard, complicate and invasive method. A more versatile tool is necessary, which allow to measure all the rotation an all the translation in 3D (six degree of freedom).

1.5.2 Digital Image Correlation

The Digital Image Correlation (DIC) is a contact-less, non-invasive optical method for measuring surface displacements and strains of objects or materials, subjected to mechanical stress. Basically, the method compares two images of the same specimen before and after deformation, acquired by mean of one or two cameras (Fig.34). Through only one camera the technique is implemented for a two-dimensional outcome; through two cameras for a three-dimensional outcome. 3D results exploit the concept of stereovision, which presupposes a mechanism of depth perception by merging two projections of the same scene obtained from two different points of view. The specimen must be illuminated by white homogeneous lights throughout the test.   The DIC is used in a widespread field of applications as e.g. in automotive, aerospace, biomechanics and research fields [105].

1.5.2.1 Operating principles

The correlation of digital images is based on the acquisition of a set of frames of the specimen surface at various stages of deformation (from the unloaded body to the stressed body) and the consequent processing of the displacement and of the strain distribution. This is allowed by means of a dedicated software, which uses the cross-correlation to measure shifts in datasets.

After the acquisition, the DIC software recognizes, identifies and follows every single point on the specimen surface of all snapshots acquired during the process. This operation is possible thanks to a particular surface preparation; in fact, to uniquely identify each point of the specimen surface it is necessary to create a random pattern of colour with high contrast[106]. This is feasible by painting the specimen surface, firstly creating a homogeneous white background, secondly realising a speckle random black pattern on the homogeneous background. It is possible to invert the colour choice, because it is relevant to preserve the high contrast, that allows the correlation algorithm to work properly.
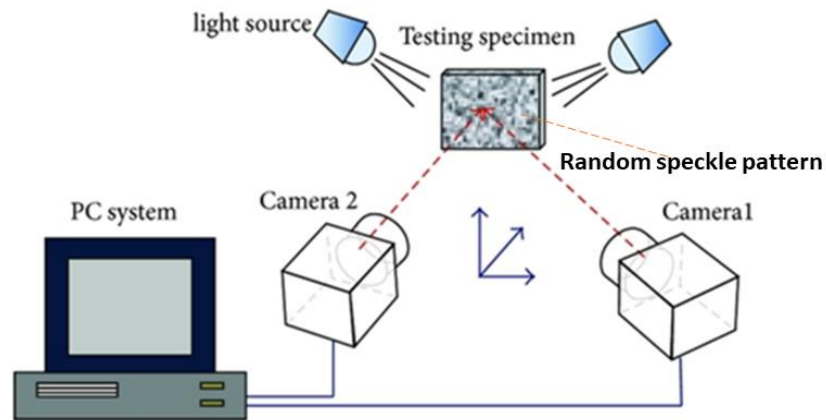
Fig.34 Diagram of the complete DIC set-up.

1.5.2.2 A brief history of the DIC

The concept of using cross-correlation to measure shifts in datasets has been known for a long time, and it has been applied to digital images since at least the early 1970s.Today the applications are almost innumerable and include image analysis, image compression, velocimetry, and strain estimation. Many early works with the DIC in the field of mechanics were led by researchers at the University of South Carolina in the early 1980s[107,108]. More details are shown in Tab.4:

Tab.4 History of DIC born from 1980 to 2000[97,98].

1980	**William F. Ranson and Walter H. Peters III**	Proposed approach for conversion of digitized ultra-sound images into estimates for local surface displacements by employing continuum-based matching principles (2D).
1982	**Cheng and Sutton; Sutton and Wolters**	Developed non-linear least squares approaches using first-order gradients in a matching function to obtain local displacements.
1985	**Chu TC. *et al.***	Used a camera to record images of a speckle pattern, demonstrating conclusively that the method could be used to measure deformations: -Translations, large or small; -Rotations, large or small; -Strains, large and relatively small

1989	**Bruck** *et al.*	Developed and demonstrated order of magnitude speed improvement using Hessian-based methodology for computing iterative improvements in optimal matching positions of each group of pixels.
1993	**Luo, Chao** *et al.*	Developed a stereo-vision system and verified the ability to make local strain and deformation measurements in cracked material.
1996	**Helm, McNeill** *et al.*	Developed a robust stereo-vision system and demonstrated used on full-scale aero-structures as well as on laboratory-scale specimens.
2000	**Bay** *et al.*	Extended 2D and 3D methods to volumetric images and performs digital image correlation on volumetric elements on the interior of a material; Limited to those materials providing sufficient contrast during tomographic imaging.

1.5.2.3 The cross-correlation concept

The digital images (represented in greyscale to reduce computational time, augment contrast and sensibility) are divided into sub-matrices of MxN pixels called *facets*. For each step the algorithm provides the recognition of such surface portions by calculating the displacement and, by derivation, the deformation field. The principle of the operation is therefore based on the identification of the maximum correlation between the intensities of the pixels inside the facets of a reference image (i.e. represented by the undeformed object) with respect to another step (i.e. the deformed object image), assuming that the intensity of the pixels does not change during the deformation[109] (Fig.30). The degree of maximum correlation is evaluated by the normalized cross correlation function as in (1):

$$C(x, y, x^*, y^*) = (\Sigma\, F\,(x, y)\, G\,(x^*, y^*)) \,/\, \sqrt{(\Sigma\, F\,(x, y)^2\, G\,(x^*, y^*)^2)} \qquad (1)$$

where F (x, y) and G (x *, y *) indicates the grey values of the pixels into the facet at the coordinates (x, y) of the undeformed state image and coordinates (x *, y *) referred to the deformed state. The sum at the numerator and denominator indicates the number of pixels within the *facet*. Once maximized the correlation coefficient (C (x, y, x *, y *)) for each facet, the best match is found, and the global displacement field is automatically assessed (Fig.35). The software interface generally shows the coordinates, the displacement and the strain maps on the related surfaces in colour scale (Fig.36).
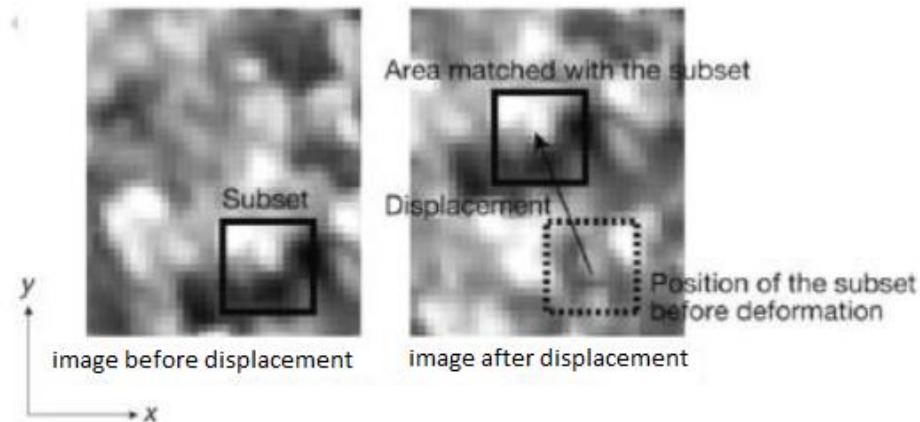
Fig.35: Best matching for pixels in a facet.

a.   b.
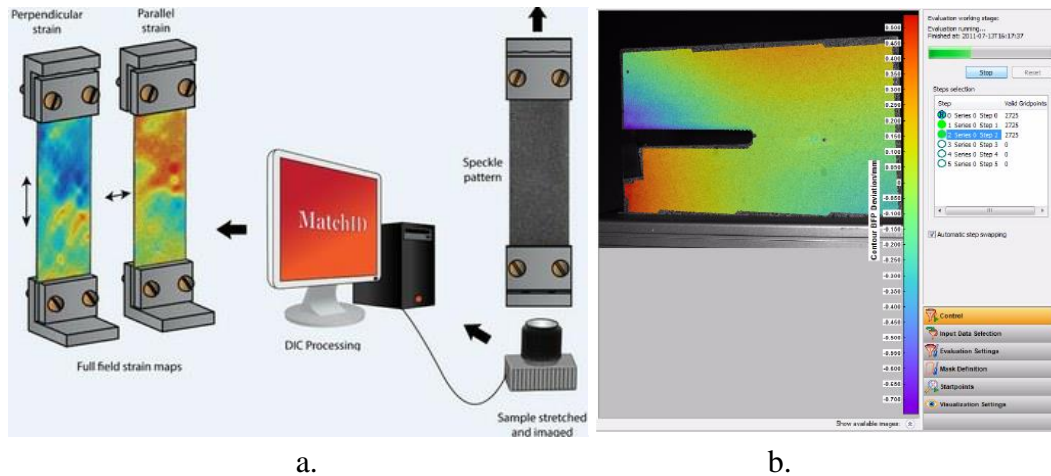
Fig.36: a diagram of DIC steps for a simplified specimen surface evaluation is shown. b. focus on the random surface object colour map about the object contour to the best fit plane (mm) is shown, observed on the typical graphic window of a DIC Software (Istra 4d DIC, Dantec Dynamic) during the correlation evaluation.

1.5.2.4 The map of deformation

Because of the specimen may be subjected to deformation and not only to displacement, the algorithm on which the DIC calculate the maps of deformation of the loaded specimen is based on the following theory[110]:

- Two points of an object are considered: P(x,y,x) and Q(x+dx,y+dy,z+dz), determining the PQ segment (Fig.37).
- After deformation, the points P and Q move to points P* and Q* with positions (1) and (2):

$$P^* = (x^*, y^*, z^*) = [x + u(P), y + v(P), z + w(P)] \qquad (1)$$

$$Q^* = (x^* + dx^*, y^* + dy^*, z^* + dz^*) = [x+u(Q)+dx^*, y+v(Q)+dy^*, z+w(Q)+dz^*] \quad (2)$$

Where: u, v and w are respectively the displacements along x, y and z.

- To detect deformations, it is convenient to assess the PQ and the P*Q* length, given by ds and ds* respectively, in (3) and (4)):

$$Sqrt(|PQ|^2) = dx^2+dy^2+dz^2=sqrt(\mathbf{ds^2}) \qquad (3)$$
$$Sqrt(|P^*Q^*|^2) = dx^{*2}+dy^{*2}+dz^{*2}=sqrt(\mathbf{ds^{*2}}) \qquad (4)$$

- Then, it is possible to explain dx*, dy* and dz* like in (5):

$$dx^* = u(Q)-u(P)+dx$$
$$dy^* = v(Q)-v(P)+dy$$
$$dz^* = w(Q)-w(P)+dz; \qquad (5)$$

and so |PQ*| as (6):
$$|P^*Q^*|= [u(Q) - u(P) +dx] + [v(Q)-v(P) +dy] + [w(Q) -w(P) +dz] \quad (6)$$

- Finally, the strain is determined. For use in digital-correlation works, it is observed that the intensity pattern is a two-dimensional projection of the object onto a plane[110]. Therefore, the form of the strain equation that one would employ to compute the strain is given by:

$$\varepsilon_{xx} = (|P^*Q^*|- |PQ|) / |PQ| = (\partial u/\partial x) +1/2 [(\partial u^2/\partial x) + (\partial v^2/\partial x) + (\partial w^2/\partial x)]$$
$$\varepsilon_{yy} = (\partial v/\partial x) +1/2 [(\partial u/\partial y)^2 + (\partial v/\partial y)^2]$$
$$\varepsilon_{xy} = 1/2 ((\partial u/\partial y) + (\partial v/\partial x)) + 1/2 [(\partial u/\partial x)(\partial u/\partial y) + (\partial v/\partial x)(\partial v/\partial y)] \qquad (7)$$

which relies on displacements derivates.
This is a simplified case because:

    a. the out-of plane displacement does not affect the in-plane deformation or displacement of characteristic intensity surfaces. This is typically true for low transverse magnifications or when the object deformation is predominately in plane; but it is not generally true.

    b. the derivatives of out-of-plane displacement (i.e. dw/dv) are much less than terms like du/dx so that this effect may be excluded from equations in (7).
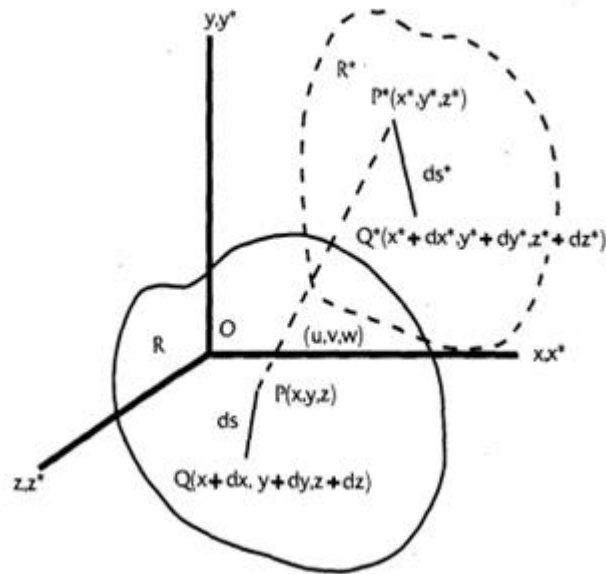
Fig.37: PQ segment before and under bodies deformation.

These considerations are extended to the entire *facet,* following the intensity of the point, which is detected by the DIC system through the cross-correlation method discussed in Par. 5.1.3 (Fig.38).

However, in order to find the six deformation parameters (u, v, $\partial u/\partial x$, $\partial u/\partial y$, $\partial v/\partial x$ and $\partial v/\partial y$) and match the facet, an approximate-solution method is adopted. Usually, the Newton–Raphson algorithm is used because of its computational economy [111].
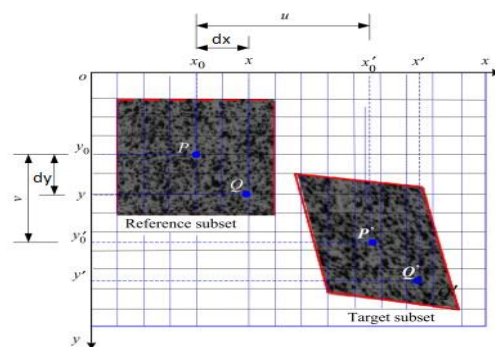
Fig.38: 2D facet (here called subset), from undeformed (reference subset) stage to deformed one (target subset) on a speckle pattern image discretized in pixels (squares).

1.5.2.5 Analysis/processing parameters
Facet size and grid spacing

Into every facet discrete pixels values are considered, so an interpolation (the most common used is a bi-cubic spline interpolation[111], [110]) is usually done, obtaining a continuous trend (Fig.39).
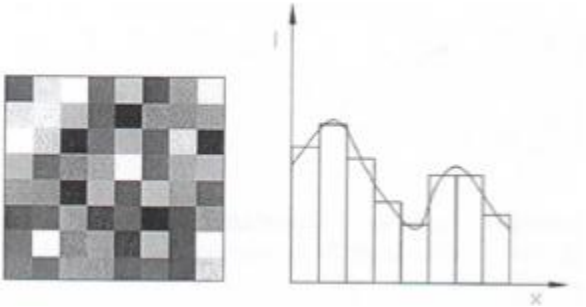
Fig.39: at left a facet is shown; at right the spline interpolation of the second row of the facet into its histogram.

Every *facet* is set side by side with an overlapping region that can be set by the operator. This parameter is called *grid spacing* (distance between two consecutive *facets*) and by its size, it is possible to augment computational time performancesFig.40):
The *facet size* is significant because:

- a large *facet* allows to reduce noise, but not to detect point-wise effects (loss of resolution): it is suitable for homogeneous strain fields;
- a small *facet* allows to assess local effects, but it doesn't work as noise filter. It is suitable for strong displacements gradients[112].

The facet size and the grid spacing are parameters that can be adjust directly on the software.
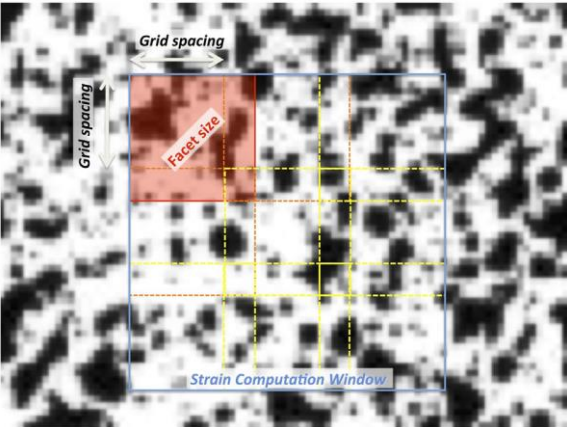
Fig.40: Detail of a speckle pattern digitized in pixels, with facet parameters highlighted.

Speckle pattern

This parameter is crucial for the optimal performance of the DIC. It must be characterized by:

- the *black and withe* colour *ratio* of approximately 50:50, to avoid regions that cannot be properly recognized;
- *roughness* which should be kept at minimum to avoid ashadows of the surface;
- specific speckle *dots size* in relation to the specimen size and geometry [113]. The dot size influences the accuracy of the measurement: dots smaller than pixels lead to the loss of movements smaller than the pixel size, because the dot, moving into the pixel, doesn't modify the pixel intensity. Conversely, dots that are bigger than the facet may lead to decorrelation. Thus, smaller speckles cause poor contrast, and larger speckles cause poor spatial resolution. It has been studied that the ideal speckle dot size should be of 3-5 pixels[114].

  It is possible to define the average of the speckle pattern by mean of the measurement window and the optical sensor resolution. Knowing these parameters and the magnification factor (M), which represents the ratio between the number of pixels on the long side of the sensor of the camera (sensor resolution) and the long side of the measurement window, the pixel size is defined by the ratio between the number of pixels that covers every speckle on the sensor of the camera and M. For example, using a camera-sensor of 5 Megapixels (2448 × 2050 pixels) on a field of view of 2 mm × 2 mm, gives an optimal dimension of the speckle pattern of about 0.003 mm [111].

The realization of the pattern is typically done through an airbrush, adjusting its pressure, airflow rate and dilution of the colour. The choice of these setup parameters depend on which kind of the pattern is being creating: if background or speckle dots.

Moreover, before starting the correlation it is necessary to calibrate the DIC system. This is possible by using a primary sample with a known geometry (Fig.41). During the calibration phase, the software determines all the geometrical and dimensional parameters of this object under the set-up conditions adopted for the specimen, for later assessing its displacements and strains[115].

Figure 55 Calibration Acquisition of images

Fig.41: DIC calibrator.

1.5.2.6 Measurement errors

The DIC outcomes, can be affected by errors due to different causes. They can be listed as:

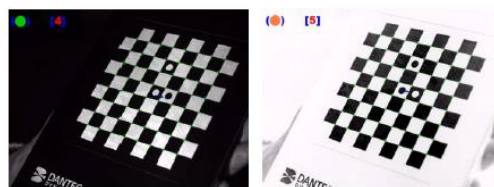- *3D reconstruction errors*. They are due to a not well calibrated system and are mainly problems related to distortion effects which not allow to catch the right *facets* positions. For 2D outcomes, the error is caused by out of plane acquisition that may occur during the mechanical test. Random errors are due to thermal noise (or dark noise), excess noise due to the sensor of the cameras (i.e. CCD) and electromagnetic noise of the relative measurement chain[106]. This is the most critical part, talking about errors, thus it is of outstanding importance to optimize all the parameters (hardware and software) to avoid errors, their propagation and to ensure accuracy in the measurement. In addition, the strain related error is more critical than the displacement one, because it is computed by the displacement derivation, which act an amplification of the error. Conversely the displacement measure is usually less problematic, because of the subpixel DIC system resolution (<0.,05 pixel)[116,107,111,105].

- *Correlation errors*. These represent the uncertainty in recognizing the *facets* into each frame of the images set. They can be divided in random and systematic errors: the systematic errors are due to local effects into the pixel like not proper illumination of the specimen (cold light illumination is preferable, i.e. LED), different illumination for each camera or a not correct speckle size or image contrast. They are the main limit about the accuracy of the results; random errors may occur for a limited number of pixels into the facet. To avoid this limit, it is necessary to increase the *facet* size. This second group of errors is less critical than reconstruction errors: to avoid problems correlation related, one can fix a threshold that may define the optimized setup which allows not to incur into correlation errors.

1.5.2.7 Digital Image Correlation in Biomechanics

Due to its strong power to:

- perform a simultaneous analysis of both soft and hard tissues,
- calculate full-field displacement (and strain) maps, overcoming the present limit of point-wise measurements with strain gauges and, even, for inhomogeneous geometry of surfaces,
- obtain contactless measurements (non-invasive) without acting directly on the specimen,

the digital image correlation has been started to be employed for biomechanical *in vitro* tests for about ten years[117].

However, until now, not many researches have been conducted on the acetabular cup. Everitt *et al.*[118] investigated acetabular cup deformation for various press-fit designs subjected to rim loading using DIC measurement and FE analysis. These studies show a good synergy between DIC and FE analysis. However, no satisfying information are given about relative movements at the cup-bone interface to assess the *primary stability*.

1.6 AIM OF THE STUDY

The overall aim of this study was to create an *in vitro* test method, able to assess the *primary stability* of a common acetabular component implanted into a synthetic hemipelvis specimen, using different approaches to detect micromovements: LVDT sensors and Digital Image Correlation (DIC). In this way, the study was able to measure the direction of the migration vector in 3D, hence retrieving richer information than the common techniques allow to get (2D); the aims of the study are to:

1. explore different measurement techniques for THA application:
   a. optimize measurements through the LVDTs
   b. optimize measurements through the DIC;

2. implement a reliable method for detecting the primary stability of the acetabular component:
   a. assessment of the permanent migration
   b. assessment of inducible micromotions

2. MATERIALS AND METHODS

The aim of the second chapter is to show the materials and the methods used to assess *in vitro* the behaviour of a synthetic hemipelvis specimen implanted by mean of an acetabular component and loaded. Through a customized mechanical test, the specimen underwent physiological load conditions to simulate the peak load of the cautious ambulation walking task (measured by Bergmann *et al.*[36]) related to the early post-operative period. Among all activities the patient is able to do, the cautious ambulation is the most reasonable motor task. The chapter illustrates the materials and the methods to perform the mechanical test and to calculate relative motions at the cup -bone interface, following a chronological order. In Fig.42, a flowchart summarizes the work.
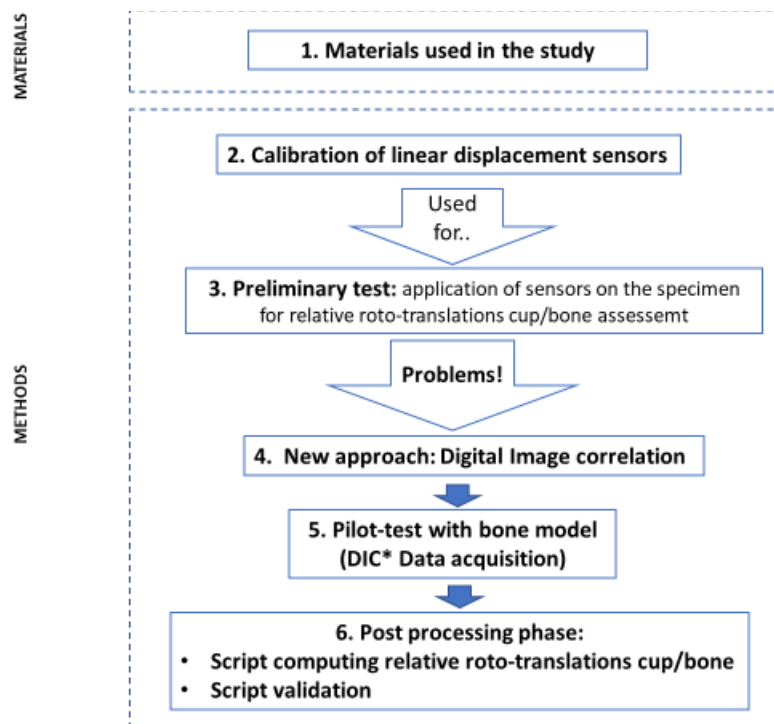

Fig.42 Flowchart summarizing the second chapter.
*DIC=Digital Image Correlation

2.1 COMMON MATERIALS

This *in vitro* study has been conducted at the laboratory of Biomechanics of the Department of Industrial Engineering (University of Bologna).
The experimental setup for the mechanical test on the synthetic hemipelvis was composed of:

- **LVDTs:** two linear variable differential transformers (Micro Epsilon): LVDT Mod. DTA1D3SAW, 1002 and 1004; each one equipped with its C701-3 wire and Mod. MSC 710-U conditioning unit.
- **DIC system**: A commercial 3D-DIC system (Q400, Dantec Dynamics, Denmark) was used:
    - two cameras (5 MegaPixels, 2440 ×2050 pixels, 8-bit) equipped with high- quality metrology-standard 17mm lens (Apo-Xenoplan 1.8/17, Schneider −Kreuznach, Germany; 65 mm equivalent) for a stereo-scopic view.
    - LED system (10000 lm).
    - 2 Airbrushes (AZ3 HTE 2, nozzle 1.8 mm, Antes Iwata, Italy)
    - Water based paint (Q250201 Bianco Opaco, Chrèon, Italy and Q250201 Nero, Chrèon, Italy)
    - Calibration target (Mod. Al4-BMB-9 ×9, Dantec Dynamics)
    - calibrator bearing system

- **Specimen**: one left male hemipelvis in polyurethane material (Sawbones) implanted with a commercial acetabular component (60 mm dimeter, Aesculap AG) and the suitable ceramic liner (Aesculap AG);

- **Testing machine**: uniaxial servo-hydraulic testing machine (8032, Instron, UK), equipped with a 25kN load cell.
- **Other tools:** all the other tools which were necessary for the specimen and the setup preparation:
    - Caliper
    - Set Square
    - Goniometer
    - Level
    - Specimen pot (connected with a wedge set)

2.2 LINEAR DISPLACEMENT SENSORS: CALIBRATION

At the beginning, the idea of this study was to measure the displacements of the cup by means of the linear displacement sensors as unique measurement tool.
Before making them work, a calibration was required to check their proper functioning. An internal standard procedure was created for linear variable differential transformers (LVDTs) and similar displacement transducers (see Appendix I).
It is important to underline that the created procedure does not replace in any way calibrations performed by calibration centres in Italy (SIT). In fact, as LVDTs available in the laboratory are characterized by a so high accuracy (0.1 class), it's impossible to assess it by a similar internal calibration (more accurate, sophisticated (and expansive!) tools are required). Into the Biomechanics laboratory conditions, a reliable LVDT is represented by a sensor able to assess

measurements with an error of about 20 micro meters, due to the games, environmental factors, the presence of dirt, temperature variations, etc…

The internal calibration was performed by using a primary standard (Fig. 43), with a micrometric head, characterized by a 5-micron resolution. Every LVDT was inserted axially into the plexiglass structure indicated in the figure (Fig.49), in order to contact the little peripherical surface of the primary standard with the probe of the LVDT. Thus, by rotating the micrometric head, the core of the LVDT was moved as:

- if the core of the LVDT was completely set into the sensor, the nominal position was acquired (translated in 1V),
- if the core of the LVDT was completely outside the sensor, the end of the stroke was
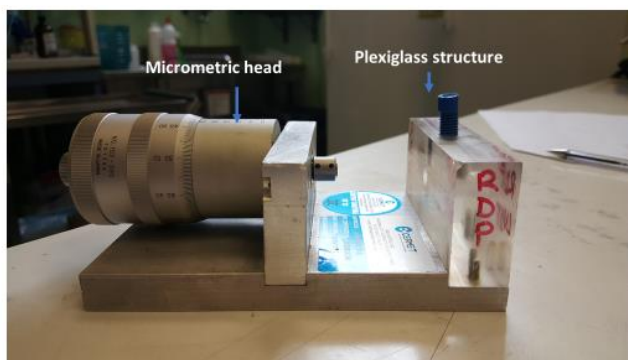
Fig. 43 Primary standard used to calibrate linear displacement transducers

detected with a translated electrical signal of 9V, as the sensor parameters given, are: an input full-scale of 2mm and an output full scale of 9V with a sensitivity (gain) of about 4 V/mm.

The micrometric head was rotated every 200 micro meters for eleven readouts, nominally imposing displacements from 0 mm to 2 mm on every LVDT. In addition, this procedure was repeated for three times for each LVDT. Every sensor was

connected to the PXIe terminal block (National Instrument) with its own conditioning system, to convert the measure in electrical signal and to monitor it on the PC (Fig. 44). By the collected data, it was possible to study the average deviation from the nominal position imposed, evaluating it the "answer" of the device was close enough to the nominal value.

If the dataset was not satisfying, the gain of the transducer would have been modified.

The LVDTs calibrated for this work were:

- LVDT_DTA1D3SAW_1002 called: LVDT_ML (ML=mediolateral, see also 2.4.2.2),
- LVDT_DTA1D3SAW_1004, called: LVDT_AP (AP=anteroposterior, see also 2.4.2.2).
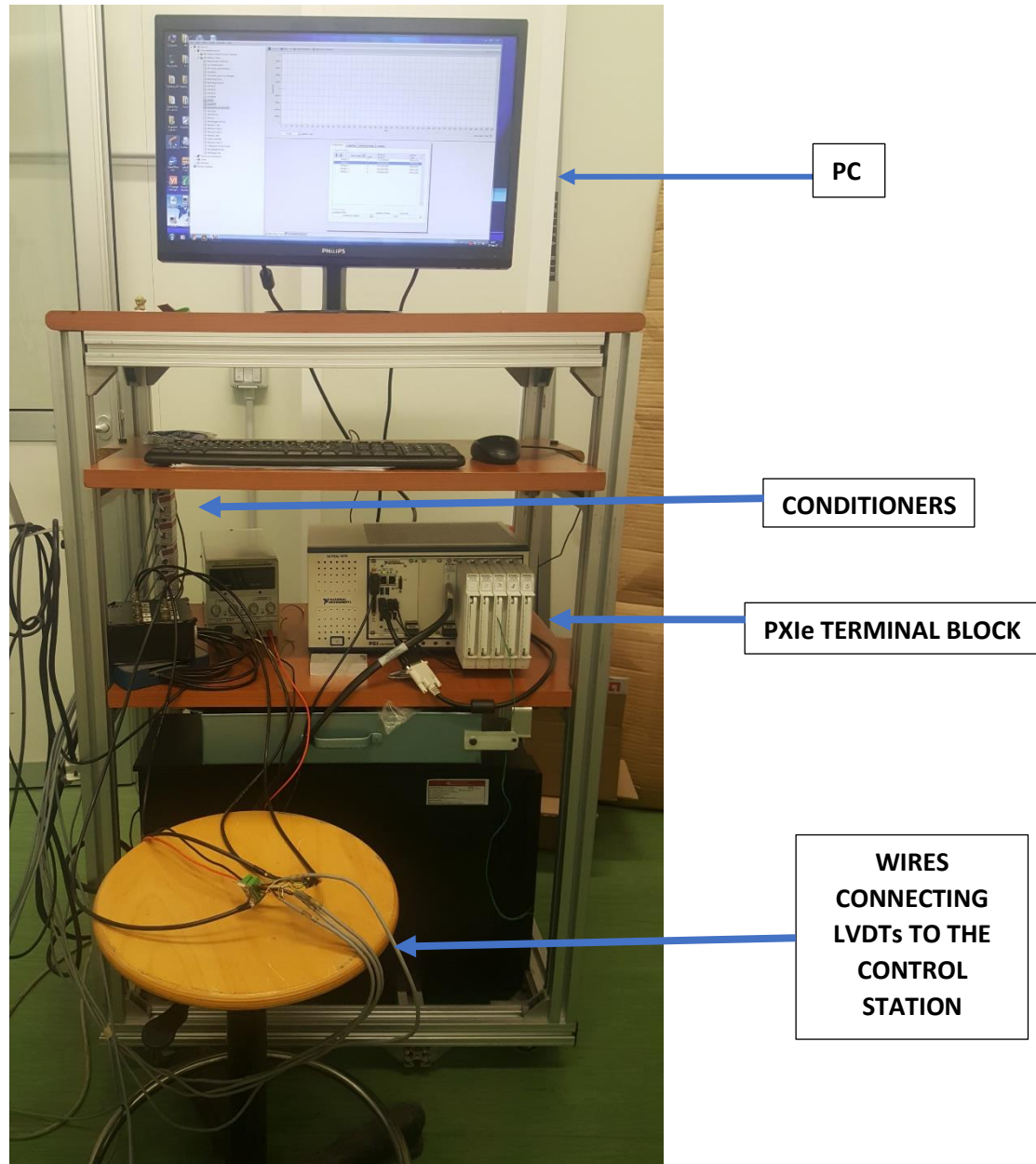
Fig.44: Control station for the LVDT signal

2.3 MEASUREMENT OF CUP STUBILITY WITH LVDTs

Before starting to test the specimen, it was aligned following the laboratory internal procedure about the Standard Acetabular Plane (SAP), into a cemented pot which constrained the hemipelvis only in the sacroiliac joint (Fig.45).

The specimen was, then, implanted with a press-fit acetabular primary cup following the surgical procedure. It consisted in performing a 1mm under reaming of the bone cavity, to create a suitable

seat for the acetabular component, and the manual implant (by surgeon) hitting the cup throughout the surgical impactor in the reamed acetabulum (Fig.45).
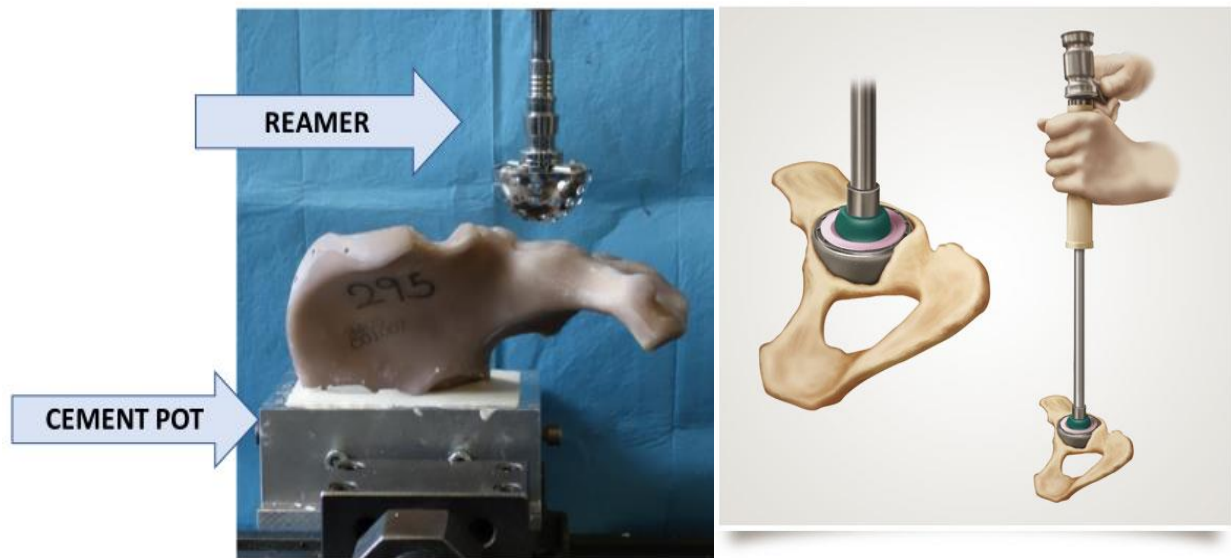
Fig. 45: Left: Hemipelvis aligned into the pot and surgical reamer perpendicular to the acetabulum. Right: press-fit fixation.

Once the pot was done, the specimen was ready to be mounted under the testing machine grabbing it through its pot bowl.

As mentioned in 2.1, the preliminary approach, used for measuring relative roto-translations at the cup-bone interface, was that by mean of four LVDTs. They were set vertically to the cup plane in four points diametrically opposed each other (Fig.46A), measuring perpendicular displacements with respect to the acetabular plane. A customized setup was created, which provided to attach metallic rods on the bone as LVDTs supports (Fig.46.B).

A cyclical axial load was applied to the cup by mean of a femur simulator, which passed across the LVDTs setup, directed to the centre of the cup (Fig.46.B).
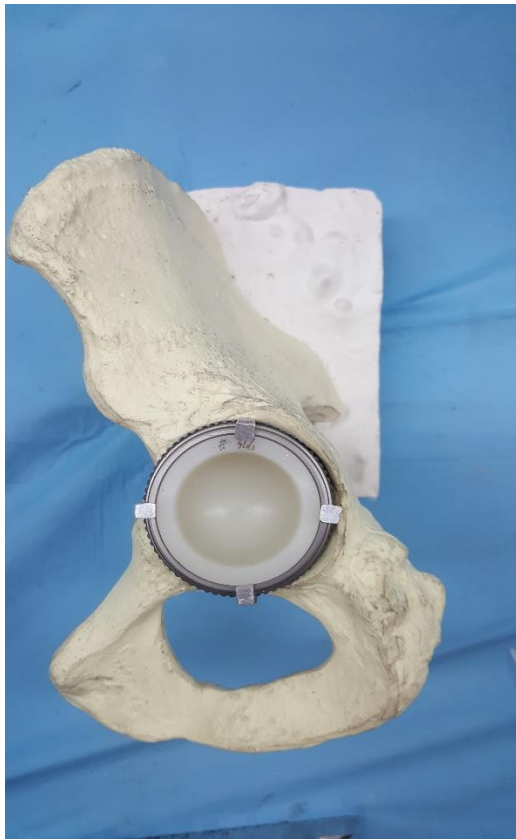
A.

B.

Fig.46 A: Synthetic hemipelvis implanted with a common acetabular cup. Four little raised surfaces indicate the LVDTs positions for detecting displacements. B: Final setup for displacements detection through four LVDTs mounted on the bone. The direction of the loader is represented in red dotted line.

Due to results obtained from measurements of the cup stability with LVDTs (see also Par 3.2 In Results), it was time to change mind about the use of LVDTs as reliable measurement technique for relative roto-translations cup-bone. For this reason, a good idea was to use the Digital Image Correlation (DIC) as reliable tool for displacements (and strains) measure and the LVDTs to monitor the mechanical test, identifying critical events in long mechanical tests (gross measure).

2.4 MEASUREMENTS WITH DIGITAL IMAGE CORRELATION

The DIC was already used in the Biomechanics field, for obtaining measurements about other anatomical districts (as spine), but it was never applied to an hemipelvis specimen. It was the best moment to try it!
The DIC approach involved several tests for optimizing both the software and the hardware DIC tools. The optimization steps are discussed as follows.

2.4.1 Speckle pattern

To guarantee the efficiency of the correlation algorithm, the pattern preparation phase was extremely important. Firstly, the background was prepared: the overall specimen surface was covered by the water based white paint. To do it the airbrush (Fig.47) for white paint was used, setting the following parameters:

- The dilution of the white paint: 30%
- The air pressure: 5 bar
- The airflow: 1,5 turns of the knob (bigger knob Fig.48)
- The round jet (fan): 2 turns of the knob (smaller knob Fig.48)
- The spraying distance: 450 mm

Then, the realization of the black speckle pattern was performed throughout the appropriate airbrush for black paint and the following parameters:

- The dilution of the black paint: 40%
- The air pressure: 1,5 bar
- The airflow: 3 turns of the knob
- The round jet (fan): knob totally turned for fan completely opened (right direction)
- The spraying distance: 450 mm

Fig.47: Airbrush used to paint the specimen
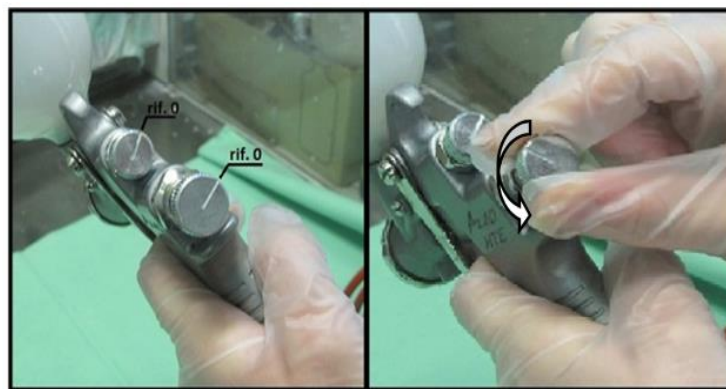
Fig. 48: Left: the two knobs (the upper knob is related to the fan; the lower knob is related to the airflow). Right: the knob is rotated countercloskwise (white arrow) to set the airflow parameters.

For optimizing the DIC outcomes and being sure the correlation between the frames would correctly be computed by the software, the ideal dot of the speckle pattern size should be of 3-5 pixels (as already described in *1.5.1.5*) with a low standard deviation. Following a laboratory internal procedure, the size of the speckle dots was measured in the 2D digital images of the field of view acquired by the two cameras of the DIC system.

The optimized pattern resulting, is shown in figure below (Fig.49):
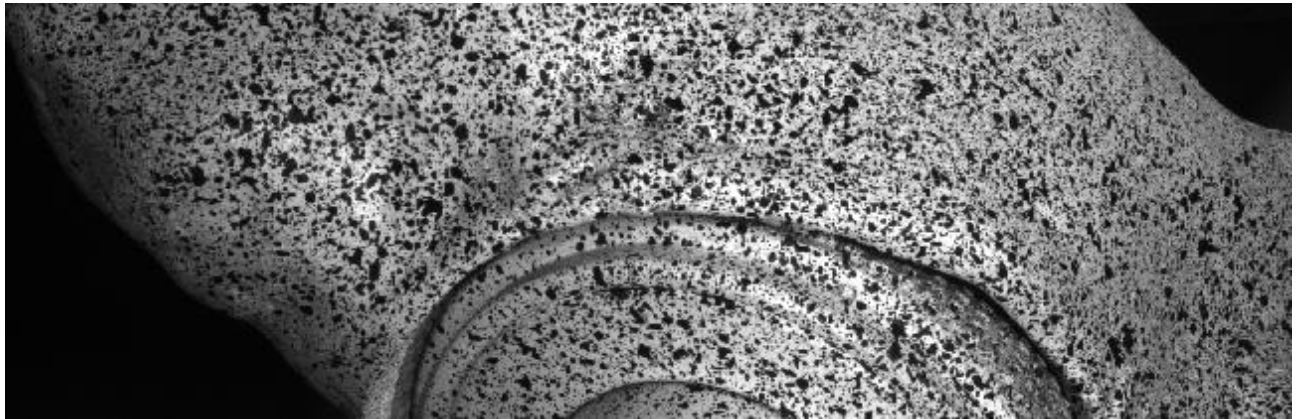
Fig.49: Speckle random pattern optimized for the DIC system acquisition of an implanted hemipelvis.

2.4.2 Alignment of the specimen under the testing machine

The alignment of the specimen under the testing machine was performed taking in account that it was necessary to:

- simulate the peak load direction during walking,
- achieve the best focus on a reasonable area of both the acetabular component and the bone (see Par.2.4.3).

Based on above, the specimen resulted mounted in lateral view under the testing machine (Fig.50). More details are discussed as follows.

2.4.2.1 Pelvic constrains

The specimen was connected to a wedge set (through its pot bowl), which was linked to the load cell (set at the top part of the Instron) throughout a connection platform (Fig.51).

The wedge set (Fig.50) was composed of 3 wedges respectively rotated of below listed angles:

- First wedge (bottom of the wedge set): rotated of 20° in anteversion;
- Second wedge: rotated of 45° in inclination;

- Third wedge (top of the wedge set): because of the limit of having an axial load (along y, vertical axis) applied to the specimen during the mechanical test and, because of the impossibility to direct the actuator of the machine at will, the last wedge (also called "walking wedge") was calculated to direct the specimen along the joint reaction force.

This last wedge contains two kinds of information: the first is the transformation from the Anterior Pelvic Plane to the ISB reference plane and the second is the change in inclination and anteversion about the peak load direction during walking. Through this device, it was possible to simulate the resultant vector of the peak load across the femur and to apply it into the acetabular component.

Moreover, it is possible to remove the third wedge to bring the specimen in physiological pose again (with the acetabulum oriented about 20° anteversion and 45° inclination).
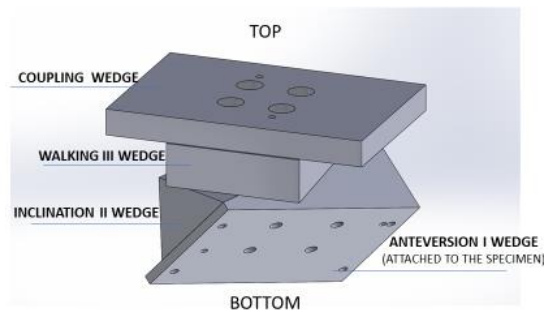
Fig.50: The wedges set (STL model).
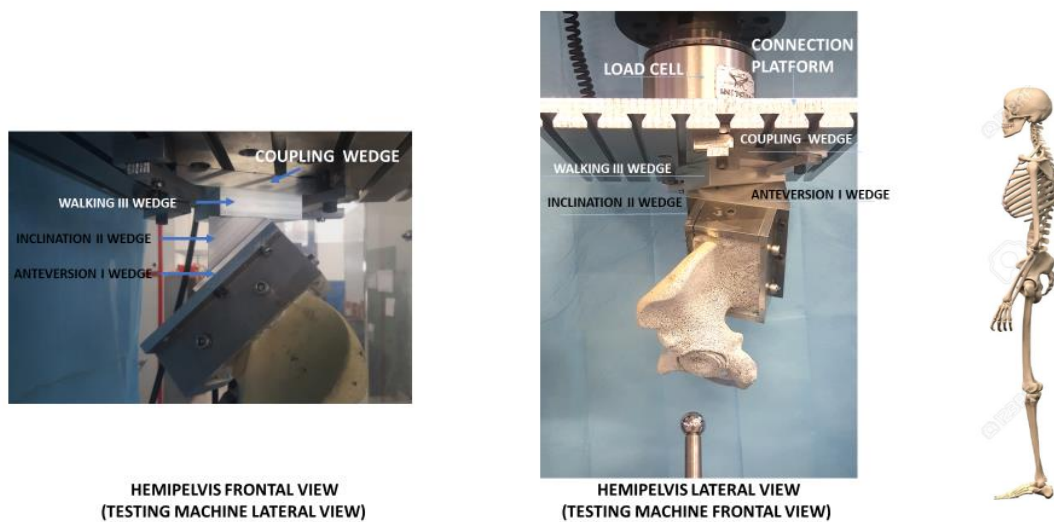
Fig. 51: Left: set wedges mounted under the testing machine (frontal view of hemipelvis); middle: entire specimen attached to the connection platform through the wedges set (lateral view of hemipelvis); right: skeleton in lateral view.

2.4.2.2 Actuator side: measurement of gross displacements

During the test, the load was applied to the specimen by means of an "actuator block", set in the actuator side (bottom part of the setup). The block is formed by the femur simulator mounted on two slides, connected to the actuator of testing machine actuator (Fig. 52). The two slides allowed the actuator to follow the movements of the specimen under loading. Applying linear displacement sensors in contact with the two slides and combining the extracted measurements with the measurement of the actuator LVDT, it was possible to have a measure of the total migration vector of the cup after the loading.

HEMIPELVIS QUASI- FRONTAL VIEW

WEDGES SET

SPECIMEN
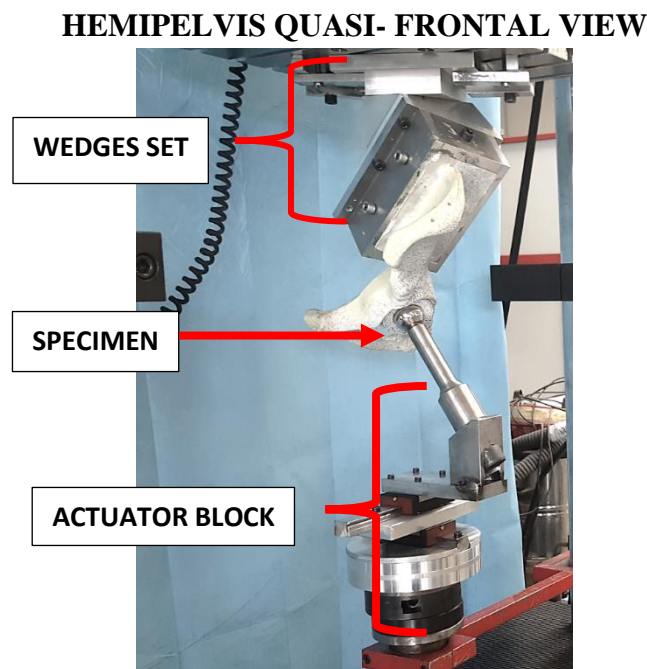
ACTUATOR BLOCK

Fig. 52: *Overview of wedges, specimen and actuator block set-up, assembled under the testing machine (quasi frontal view of hemipelvis).*

By this side it was decided to use two LVDTs (previously calibrated) for detecting displacements relative to the two slides of the actuator block. With the actuator sensor of the testing machine, they formed the spot-check system (independent from the DIC system). Since the DIC outcomes need to be elaborated before being assessed, the spot-check measure allowed to quickly and easily detect eventual drifts of the specimen throughout the entire test. In this way two approaches for the same measure were used: after all, results that agree across different methodologies are less likely to be artefacts![119]

LVDTs were set directly in contact with the slides by mean of two customized LVDTs plastic bearings and connected to the conditioning system throughout two BNC wires (Fig.52.b). Moreover, throughout two cables, a "safety system" was created tying LVDTs to the connection

platform, to avoid making them drop in case of excessive displacements. LVDTs were placed with their internal core at mid-run.

Due to the alignment of the specimen under the testing machine, the spot-check reference frame (XYZ) was defined as follows:

- the z-axis (displacement in z measured by LVDT_ML) is parallel to the mediolateral APP axis (ML);
- the x-axis (displacement in x measured by LVDT_AP) is parallel to the anteroposterior APP axis (AP), less than an angle of 5.6°: x=AP*cos (5.6°);
- the y-axis (displacement in y measured by the LVDT of the testing machine) is parallel to the antero-posterior APP axis (AP), less than an angle of 5.6°: y=CD*cos (5.6°);

The entire setup is shown in Fig.53. b.
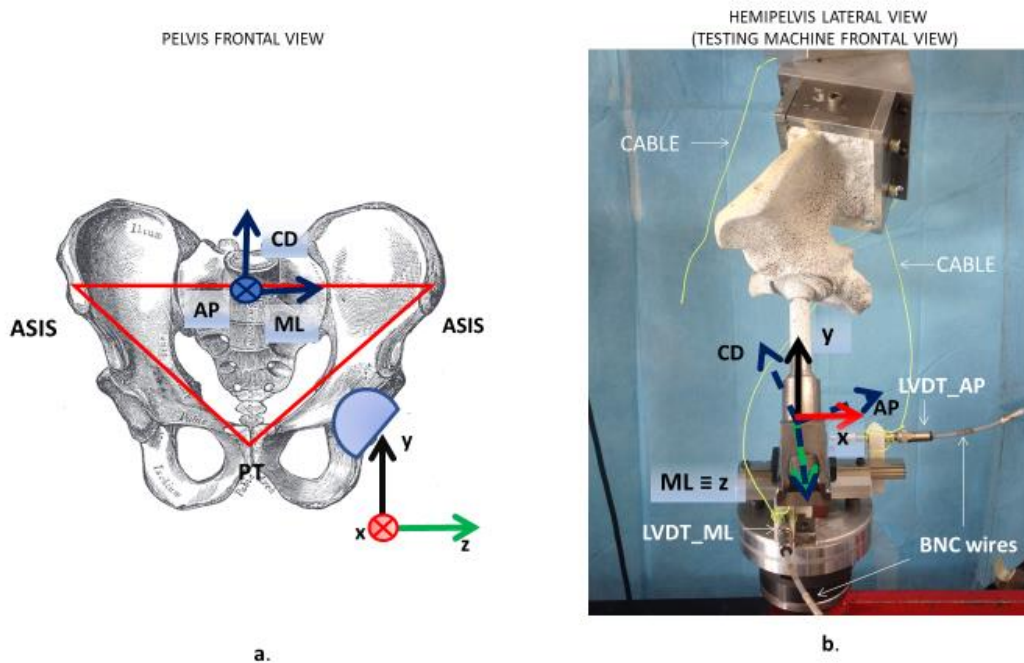
Fig.53: a.: Representation of the two reference frames adopted in the study: the APP reference frame (indicate by AP-, CD-, ML- axis) and the spot-check reference frame (indicated by x-, y-, z- axis), defined by the slides plane (XZ) and the actuator displacement direction (y). Frontal view of pelvis(a); lateral view of hemipelvis (b).

2.4.3 Optimization of Region of Interest (ROI)

For acquiring the best Region of interest (ROI), during the mechanical test, some important aspects have been taken in account, such as that:

- the cup-bone interface must be acquired for assessing the primary stability of the acetabular cup by mean of relative roto-translations;
- critical regions of the bone more subjected to high stress should be monitored underload, assessing its deformation (especially in view of next studies about cadaveric specimens with bone defects reconstructions in these critical areas);
- setting a large field of view causes a higher computational cost than a more contained field of view (even though it would be advantageous to see all the specimen in the frames acquired by the cameras);
- the smaller is the field of view the higher is the acquisition frequency that can be set on the software before the acquisition;

For aspects 1 and 2 listed above, the best compromise was found choosing the region of interest which involved: the posterior column of the acetabulum, the superior aspect of the acetabular rim and the liner.

After several trials, the optimized settlement of the cameras, which allowed to acquire the chosen ROI, was given by positioning them:

- in front of the cup (thus, acquiring a *quasi*-posterior view of the hemipelvis mounted under the testing machine);
- close to the specimen (about 30 cm lens-specimen distance);
- tilted with respect to the ground of approximately 20° in order to frame the ROI from the bottom of the specimen (Fig. 54);
- in order to focus the image in the middle of the depth of field, thus between the bone and the cup. (depth of field of 70 mm, lens aperture f22).

Moreover, 17mm lens were adopted for the two cameras.

The specimen illumination in the considered regions of interest, had to be homogeneous.

To assure the best images correlation, avoiding shadows on the specimen surface and finding the right compromise between too much saturation and too much darkness was of outstanding importance. Thus, after different light tests, the best choice was achieved by using three LEDs, positioned as Fig.55 shows.
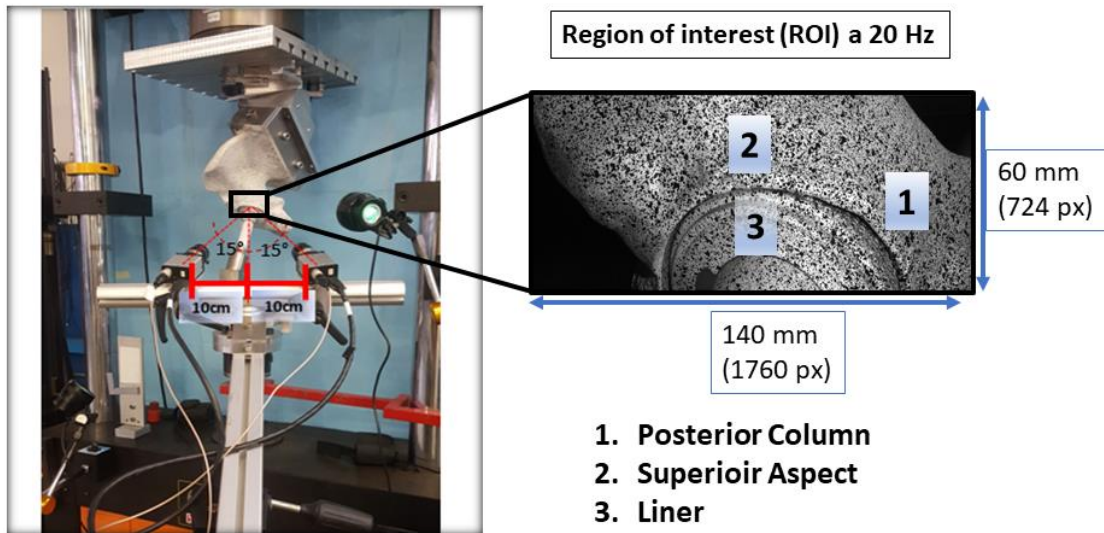
Fig.54.Left: Cameras inclination and settlement on the tripod; right: the correspondent ROI acquired as in left picture.
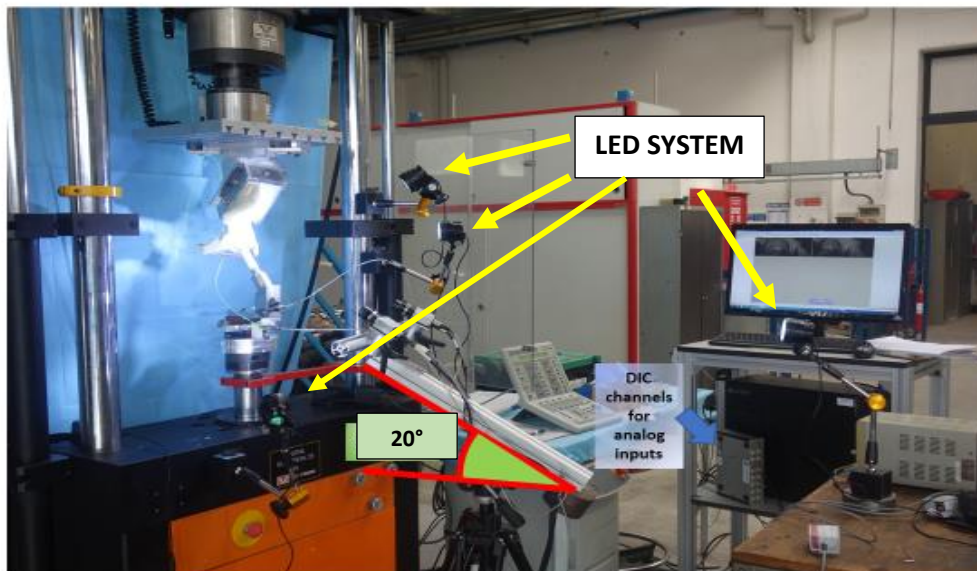
Fig. 55: Complete mechanical test setup (specimen+LVDTs+DIC components).

In order to synchronize all the sensors, LVDTs and outputs of the testing machine signals, they were connected to the virtual channels of the DIC system, designed for analogue inputs, through four BNC cables. All measurements were sampled, displayed and stored synchronously during and after the mechanical test. This fact allowed easily to compare spot-check and DIC outcomes. To sample all data at a reasonable frequency (allowing to acquire data with high accuracy during peaks and valleys of the cyclical test, see Par. 2.5), a 20 Hz acquisition frequency was selected on

the software. Thus, the corresponded field of view compatible with such frequency and with the chosen regions of interest was set as follows:

- the field of view size was: 140mm x 60mm,
- the pixel size was: 0.08 mm (calculated with the ratio between the longest side of the field of view and the longest size of the sensor: 140mm/1760 px) (Fig. 53),

In this way, the best compromise was found also for the aspects 3 and 4 listed above.

2.4.4 Digital Image Correlation Calibration

The DIC analysis is a versatile tool. Before to perform the images registration the DIC system needs to be calibrated for being adapted to the specimen framing and the environment in which it will be tested.

The calibration phase consists in acquiring 8 frames of the calibration target, in different orientations performed by the operator and at the same distance of the specimen set. In this way it is possible to verify if the software is able to recognise all markers on the calibrator in the same specimen's conditions and to make the calibration algorithm evaluate the projection parameters. The first snapshot of the calibration process set a reference frame, all the others adjust the calibration parameters. Typically, if the value of the residuum of pixels, detected by the algorithm, is less than 0.300 px, the calibration was conducted successfully (conversely, the calibration should be performed again, in order to avoid errors in the correlation).

The DIC system gives the possibility to choose a favourite reference frame, between three possibilities:

- Sensor system, reference frame. This is defined with the origin set at the centre point of the connecting line of the two sensor cameras. The z-direction points towards the line of site of the two cameras and is defined by the mean direction of the corresponding optical axes. The x-direction is along the connecting line of the two sensor cameras, pointing from the coordinates origin towards camera 2 (Fig.56). Due to the cameras alignment, it is affected by an operator-dependent uncertainty.

Sensor system
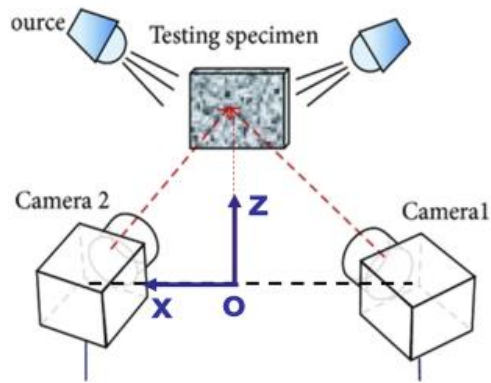
Fig. 56: Representation of Sensor System reference frame

- User system reference frame. This reference frame is directly chosen by the user, which can create it on the acquired picture, pointing the x and the y axes through software markers. Its limit is that markers can be applied only on correlated images.
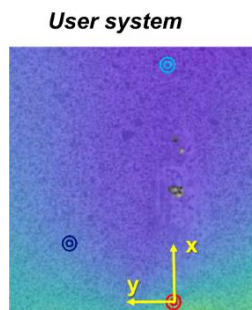
User system

Fig. 57: Example of user system reference frame: the light blue and the red points define the x-axis; with the blue point the XY plane is defined.

- Calibration system reference frame. This is defined with respect to the calibration target surface, which the software recognises in the first frame acquired during the calibration phase. The coordinate origin is set to the centre of the calibration target, defined by the centre of the circle in the central square. The x-direction is in the plane of the calibration target and points from the central circle to the closest circle. The y direction is in the plane of the calibration target and points from the central circle to furthest circle. The z axis is normal to the XY plane and points towards the cameras (Fig.58).

Calibration system
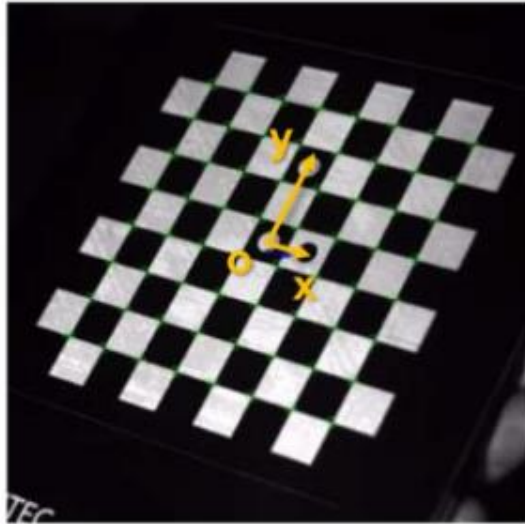
Fig. 58: Calibration target and the calibration XY plane related.

Its limit is that it could be hard to exactly set the calibrator in the same position of the surface of the specimen, which the operator would like to set as reference frame.

The calibration system was chosen, since it was possible to create the APP reference frame with the DIC system positioning the properly with a custom tool. the origin was set in the centre of the acetabular cup. Having the measures related to this plane, it was possible to obtain data with clinical relevance. (Fig. 59):
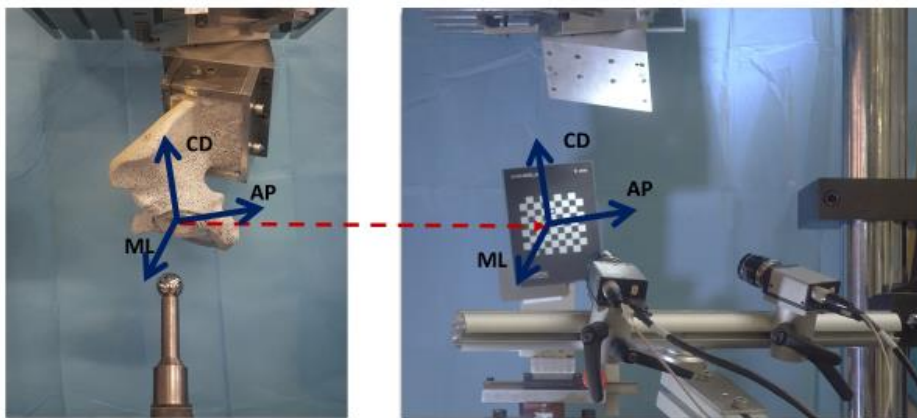
Fig. 59: left: The APP reference frame is centred in the middle of the acetabular component; right: the calibration target is centred and aligned as the same acetabular component under the testing machine allowing the Istra Software to acquire images into the APP reference frame.

After the calibration, the hemipelvis was set again in the preparatory setup alignment, ready for testing. To avoid plays between the cup and the femur simulator, the femoral head was placed into the acetabular component with pre-compression load of -100 N.

2.4.5 Digital Image Correlation calibration repeatability test

Conducting the DIC calibration repeatability test was a delicate and an essential phase of the procedure. In fact, the efficiency of the anatomical reference frame, thus all measures obtained with respect to it, belong to the DIC calibration. the outcome of the calibration repeatability test will introduce an error in positioning the calibration target: an offset about the origin of the anatomical reference frame, which will be propagate in measurements.

To test the repeatability in setting the origin of the reference frame in the centre of the acetabulum, the calibration was performed three times. Every time the calibrator was removed and remounted, by different operators. For each acquisition the specimen was remounted on the setup and acquired by mean of the new calibration. Then the images were correlated. After the correlation, three points were selected univocally on the specimen surface, assessing if their position was the same during the five acquisitions. This procedure allowed to determine the systematic error operator-dependent in setting the origin of the reference frame.

2.5 PILOT TEST WITH BONE MODEL

Once mounted the specimen, set the LVDTs and optimized the complete DIC setup *ad hoc* to frame the ROI throughout the mechanical test, at last the pilot test could start.

Before starting with the cyclical load, a preconditioning ramp was performed on the specimen in displacement control at 0.05 mm/s., reaching -1500 N in compression (about 2BW). This allowed to fix the limit of the actuator stroke for the cyclical test to 1.3 mm. Moreover, the choice to conduct the test in displacement control was due to the synthetic nature of the specimen: it is subjected to bending under high loads. Thus, the parameter to use was the displacement. It is important to underline that, in this experimental phase, the use of a polyurethane specimen was the more reasonable than the cadaveric (for ethical reasons) and the composite (for a higher cost) specimen.

The cyclical mechanical test was divided in three steps in displacement control, changing amplitude and number of cycles each time. An haversine wave form was imposed, in which:

- peaks represented the actuator maximum displacement in compression;
- valleys represented the load when the actuator stroke back in the starting position.

For each test parameters are shown below:

- haversine amplitude (A), number of samples (N), number of cycles imposed (CYC), test timespan (t) (Tab.5):

Tab.5: Pilot-test parameters indicated for the three steps in each column

First step	Second step	Third step
A= 0.25 mm	A= 0.50mm	A= 0.65 mm
N= 1100	N= 2200	N=500
CYC= 50	CYC= 100	CYC=22
t= 55 seconds	t=110 seconds	t=25 seconds

- time exposure or brightness: 250 Hz;
- acquisition frequency: 20Hz (frames/second and samples/second)
- Haversine frequency (1/T): 1 Hz (Fig.60);
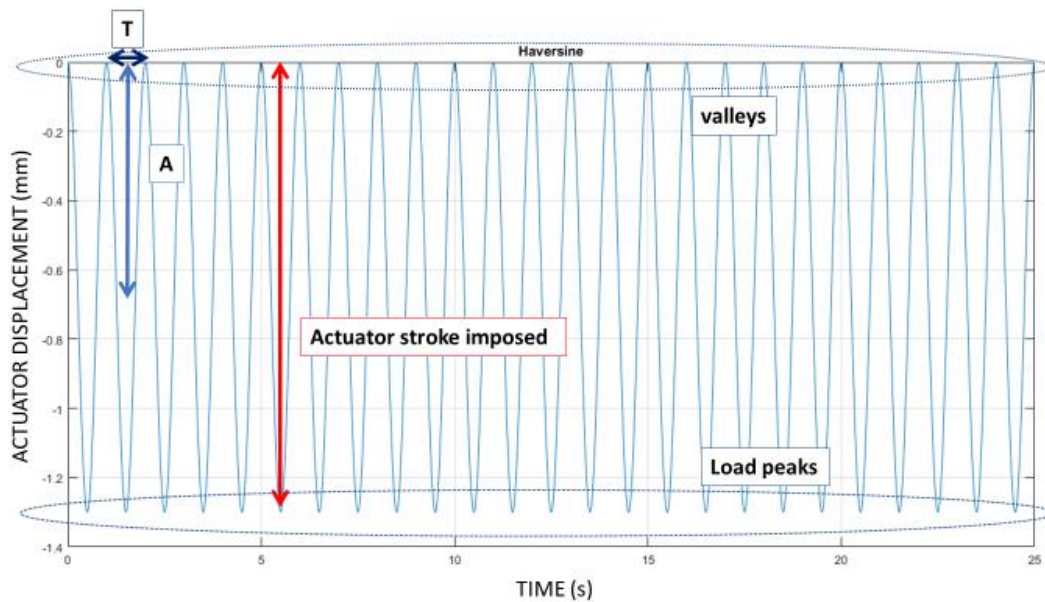
Fig. 60: Example of an haversine wave form, imposed on the specimen in displacement control through the testing machine actuator; A is the Haversine amplitude and T its period; the peak-peak amplitude is the actuator stroke set on the testing machine; peaks represented the actuator maximum displacement in compression; valleys represented the load when the actuator stroke back in the starting position: this means that the peaks are in the bottom and the valleys on the top.

Due to synchronization between DIC and analogue signals (LVDTs and outputs of the testing machine), the same number of images from DIC and samples from analogue signals, were acquired throughout the test.

2.6 CORRELATION ANALYSIS AND POST PROCESSING

The entire procedure of correlation analysis and post processing summarized in figure Fig.61.
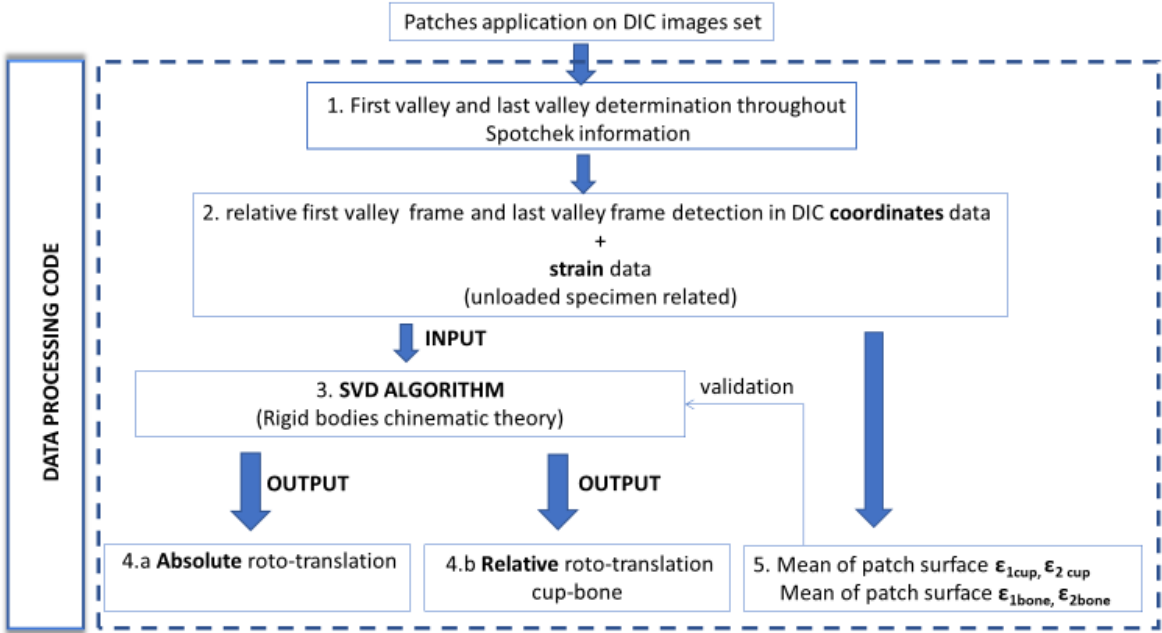
Fig.61: Work-flow of the post-processing analysis.

2.6.1 Correlation phase

After the mechanical test and the synchronized images acquisition due to the DIC system, the set of images recorded could be evaluated by the software through the correlation algorithm.

In this phase two masks were drawn on regions of interest of the acquired frames, this allowed to make the software elaborate not the whole, reducing the computational cost. Once these areas were outlined, a starting point for each one was selected. The starting point was essential to give to the software both a first easy recognizable point for starting the evaluation and the information that the assessing region was inside the outlined area and not outside it.

This process made the software able to compute the correlation of all the images set (made of N number of samples). The outlined areas are shown in Fig. 62.
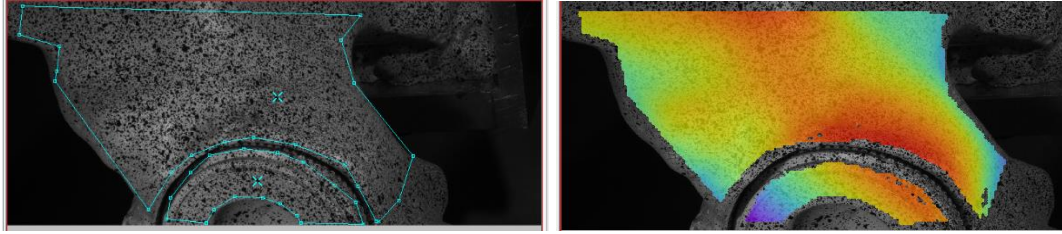
Fig. 62: Left: The areas outlined by the user and the starting points are shown. The upper region represents the bone area of interest, the lower region is the cup area of interest in the field of view acquired by the DIC cameras. Right: Once outlined, the image is correlated inside the chosen masks.

To perform the correlation, the software was set in each step as:

- facet size was: 19 pixels;
- grid spacing was: 15 pixels;
- smoothing: local regression (5x5).

After the correlation, the position, the displacement, and the strain maps were displatyed and extracted from each frame acquired during every machanical test.

2.6.2 Measurements uncertainty of the Digital Image Correlation

Two images of the same region of the specimen in zero-strain condition were acquired. A comparison of the two images allowed to evaluate measures uncertainty of the DIC. To evaluate the difference between the first and the second image, one patch (a virtual tool of the software, Fig.63) was applied on the desired area, defining a smaller region. Displacements and strains different to zero represented the error introduced by the DIC analysis.
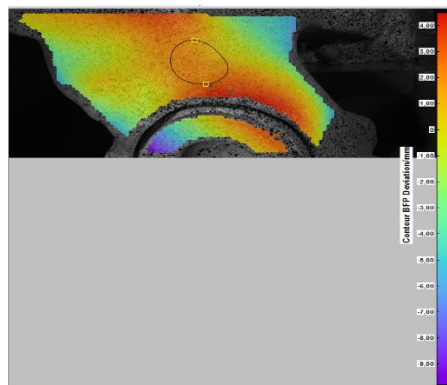
Fig.63: The patch used for the zero-strain error assessment is shown on the correlated area of the hemipelvis bone. In this image, the correlated area represents the contour map, thus the coordinates position into the chosen reference frame.

2.6.3 Relative cup-bone roto-translations

For the cup-bone roto-translations assessment, two patches were applied on correlated areas on the rim of the cup and the periacetabular bone (Fig.64).
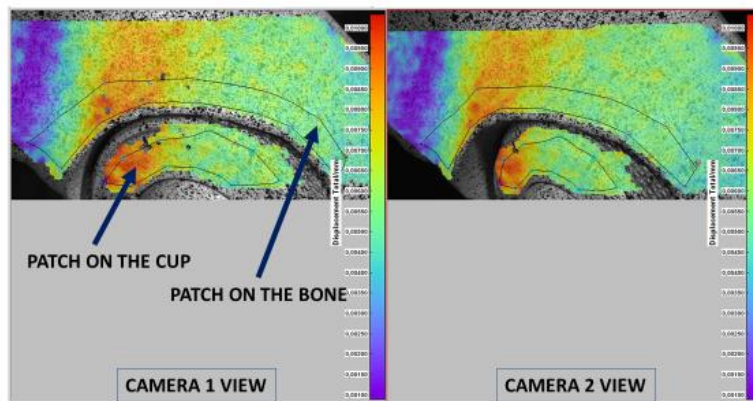
Fig.64: The images acquired by the the two cameras are shown. One patch for each region of interest is inicated by dark blue arrows. Each selected patch containes a defined number (M) of facets, stored in a 1xM vector which is possible to export in different formats. On this image the displacement map is reported on the correlated area.

Under the assumption that the cup and the bone were rigid bodies, the absolute and relative roto-translations between the cup and the bone were calculated through Singular Value Decomposition (see paragrapg 2.6.4). The assessment of the relative roto-translation was made comparing the valleys of the first and the last cycle. Assessing the first and the last valley allowed to verify if the cup significantly moved during the test. This kind of evaluation is called *permanent migration* assessment.

Later, to assess the cup behaviour also during peaks, it was thought to monitor the behaviour during a single cycle, in a period, between valley and peak (*inducible micromotion* assessemnt)

2.6.3.1 Singular Value Decomposition algorithm

The Singular Value Decomposition algorithm allows to calculate the optimal rigid roto-translations between two bodies knowing their position in two different configurations.
It is known that if:

- P_2 is the 1xN vector cointaining points of the second, rototranslated reference frame;
- R_{21} is the rotational matrix
- P_1 is the 1xN vector cointaining points of the first reference frame,

the best alignment of P_2 vector is ideally due to: $\mathbf{P}_2 = \mathbf{R}_{21}\mathbf{P}_1 + \mathbf{T}_{21}$.

The computation of the optimal roto-translation matrix was assessed by mean of the Singular Value Decomposition algorithm. This is a factorization of a real or complex matrix, of the form $\mathbf{M}=\mathbf{U\Sigma V^*}$, where:

- $\mathbf{U}$ is mxm square matrix
- $\mathbf{\Sigma}$ is a mxn rectangular diagonal matrix with non-negative real number on the diagonal
- $\mathbf{V}$ is a nxn square matrix.

The diagonal entries σ_i of Σ, are the singular value of M.
The SVD is applied to the product between $P_2'P1'^T$, where:

- P_1' is given by P_1-C_1, where C_1 is the centroid of the first frame point set,
- P_2' is given by P_2-C_2, where C_2 is the centroid of the rototranslated frame point set,

obtaining M= $\mathbf{U\Sigma V^*}$= $P_2'P_1'^T$ [120,121].
It is proven that the optimal rotational matrix is given by $\mathbf{R_{21opt}}=\mathbf{UV^T}$ and the optimal translation by $\mathbf{T_{21opt}}= C_2-\mathbf{R_{21opt}}\,C_1$.

2.6.3.2 Permanent migration

The procedure reported in paragraph 2.6.3.1 was extended to the facets inside the patches. By mean of the coordinataes in the two patches, the optimal absolute and relative cup-bone roto-translation matrix was assessed.

Every patch contained N vectors (number of frames) of 1xM (M = number of facets into each patched area) coordinate elements, which were exported in ASCII format with the spot-check analogue data (LVDT_ML displacement, LVDT_AP displacement and actuator displacement), all recorded simultaneously. These were the input data for a Matlab script implemented for this study. Operative steps are listed below:

1. *detecting the first and the last valley of the cyclical waveform, assessed on displacement plots of spot-check measures*. The first and the last valley were identified to retrieve the DIC frames to analyse (Fig.65).
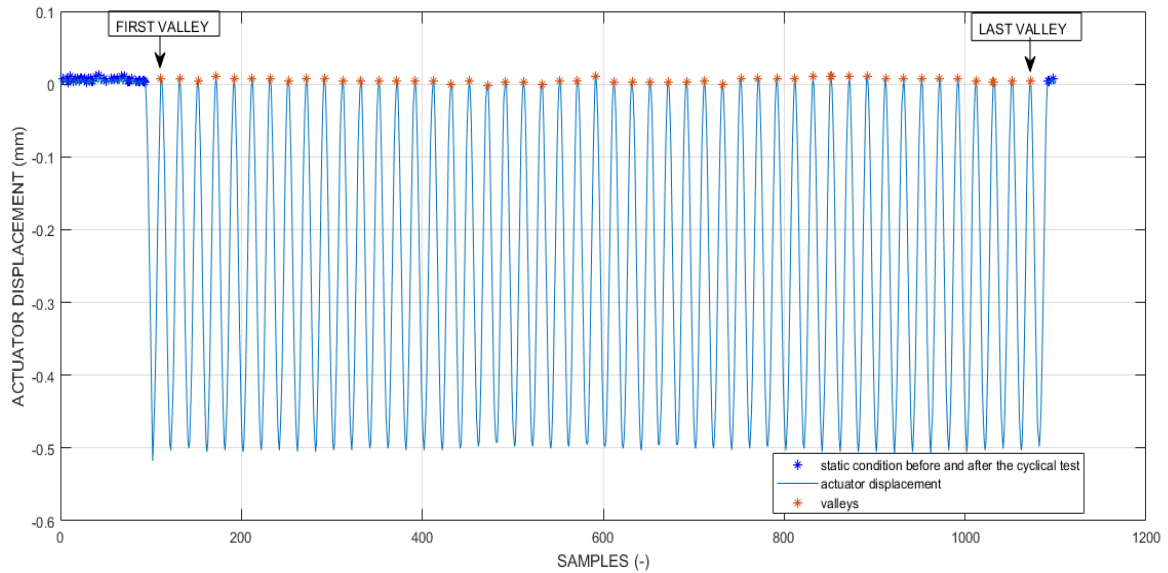
Fig.65: The picture shows the plot of the actuator displacement taken by playing the Matlab script. The Matlab code first step requires to recognize the cyclical wave form start and its end, differentiating it from the first samples before and after the dynamic test, acquired in static condition (blue stars in the plot). The samples related to haversine valleys are highlighted throughout red stars because, in those DIC equivalent frames the specimen is captured into its own unloaded condition, on which the permanent migration study relies on.

2. *Identifying the frames of the DIC patches related to detected valleys:* the coordinates vectors, relative to bone and cup, were selected in the frames corresponded to the first and the last valley (**P1** and **P2**). **P1** represented the first reference frame for cup and bone (**P1_cup**, **P1_bone**), **P2** represented the roto-translated reference frame (**P2_cup**, **P2_bone**).

3. *SVD algorithm for cup and bone.*
   Giving coordinates as input data in the Matlab script (SVD algorithm), following measures were obtained:

   - absolute rotational matrix (3x3) of cup $\mathbf{R}_{opt\_cup}$, from which extracting rotations about anatomical axes: [**r_AP_CUP, r_ML_CUP, r_CD_CUP**]
   - absolute rotational matrix (3x3) of bone (Fig.66) $\mathbf{R}_{opt\_bone}$, from which extracting rotations about anatomical axes: [**r_AP_BONE, r_ML_BONE, r_CD_BONE**]

Hence:

$$P_{2\_cup} = R_{opt\_cup} \, P_{1\_cup} + T_{opt\_cup}$$

- absolute translation vector (3x1) of cup:
  T_{opt_cup} = [ΔML_CUP, ΔAP_CUP, ΔCD_CUP]
  absolute translation vector (3x1) of bone:
- T_{opt_bone} = [ΔML_BONE, ΔAP_BONE, ΔCD_BONE]

Hence:

$$P_{2\_bone} = R_{opt\_bone} \, P_{1\_bone} + T_{opt\_bone}$$
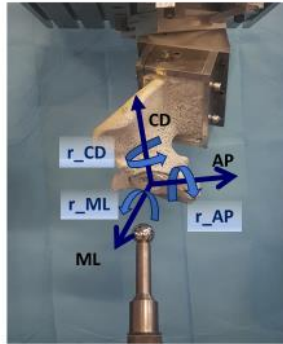
Fig.66: Representation of rotations about the anatomical reference frame.

4. *Computation of relative roto-translation*.

- relative rotational matrix (3x3): $R_{cup/bone} = (R_{opt\_cup})^{-1}(R_{opt\_bone})$, from which extracting relative rotations about anatomical axes: **[r_AP', r_ML', r_CD']**
- relative translation vector (3x1): $T_{cup/bone} = (T_{opt\_cup})^{-1}(T_{opt\_bone})$
  $T_{cup/bone}$ = [ΔML', ΔAP', ΔCD']

2.6.3.3 *Inducible micromotion*

The *inducible micromotion* is the relative motion between the cup and the bone induced by the transition from the valley to the following peak in a singular period of the cyclical load. This kind of motion should be elastic (if there is stability): even if a micromotion is induced at the peak, it will reset, restoring back to the starting position (next valley).

It was interesting to assess the *inducible migration* to monitor the behaviour of the cup not only during valleys (as required for the assessment of the permanent migration), but also during peaks (loading the specimen).

The evaluation of the *inducible migration* was performed by mean of the same Matlab script, adopted for the *permanent migration,* but choosing three periods in which relative roto-translations were calculated. Thus, in each test, three periods were selected:

- valley and peak at the starting point of the cyclical test;
- valley and peak at the middle of the test;
- valley and peak at the end of the test (Fig.67).

Then, the DIC data correspondent to frames of peaks and valleys listed above, were extracted and given as input to the script. Measurements of the relative displacement between the cup and bone were obtained, in terms of *inducible micromotion,* at the three states of the cyclical test.
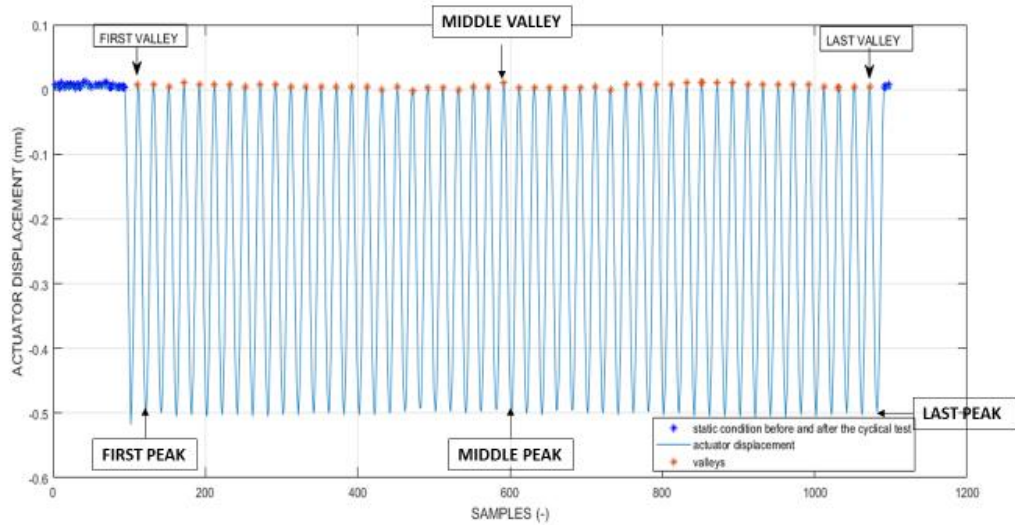
Fig. 67: Representation of selected valleys and following peaks for the assessment of the inducible micromotion.

2.6.3.4 Validation of roto-translations computation

To test the proper functioning of the DIC Matlab script, two aluminium bars (Fig.68) were painted with a speckle pattern and used as specimen for the DIC system (after imposing known rotations, translations and a combination of both). The DIC data were used as input for the Matlab script, whose outputs were compared to the known values of rotations and translations. Then, the uncertainty on the processed data was calculated.
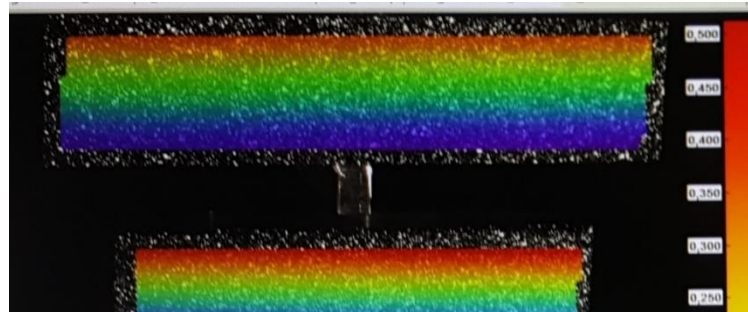
Fig.68:Correlation on two aluminium rods used as specimen to validate the Matlab script.

2.6.4 Strain distribution

In the last phase of the post-processing a strain evaluation has been conducted both for the *permanent migration* and *the inducible micromotion*.

To close the loop of validation of the flowchart in Fig.60 about the assumption of the rigid bodies to validate the SVD application to the cup and the bone patches, the point five was given as follows:

5. ***Extracting the mean of surfaces values of the two principal strains*** (ε_1, ε_2): they were assessed to validate the assumption about the rigid bodies motions.

Moreover, for the strain assessment, another patch was drawn on the posterior column, achieving information also about that critical bone region (Fig.69). Even for this area, the mean of the patch surface value of the strain was adopted.
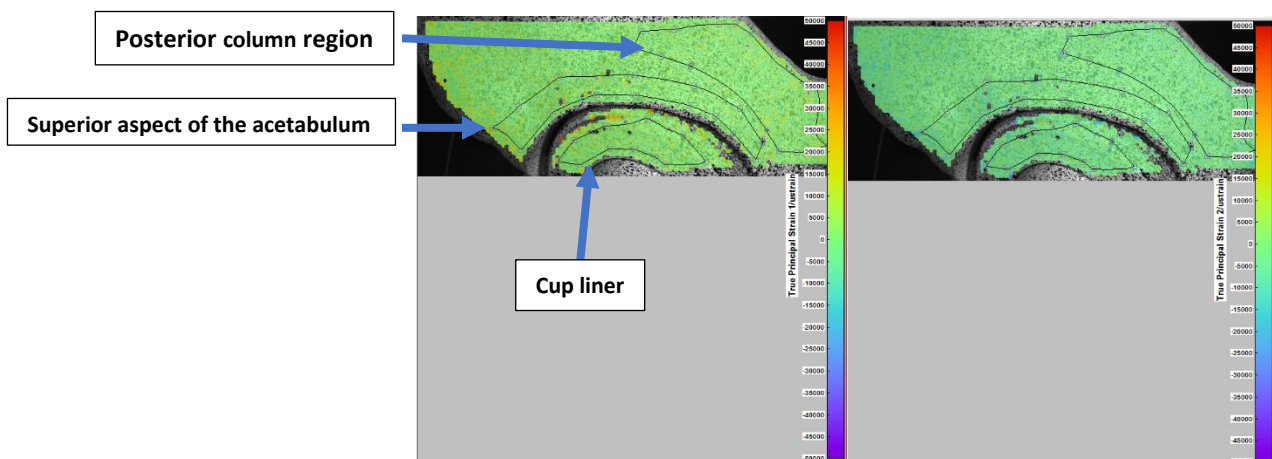
Fig. 69: Principal strain 1(left) and 2 (right)maps, evaluated for a peak frame in the middle of the test, with patches drwan on the liner, on the superior aspect of the acetabulum and on the poterior column region.

3. RESULTS

The third chapter shows all results obtained in the tests performed through the materials and methods described in chapter 2. The results are assembled into three macro topics: results about the LVDTs (calibration, preliminary test and spot-check outcomes), results about the DIC parameters optimization; finally results about mechanical tests and outputs of the Matlab script are reported.

3.1 LINEAR DISPLACEMENT SENSOR: CALIBRATION

From the LVDTs calibration performed, it resulted that:
•   LVDT_ML presented an average absolute deviation from the nominal position of 0.012 mm;
•   LVDT_AP presented an average absolute deviation from the nominal position of 0.011 mm;

3.2   MEASUREMENT OF CUP STABILITY WITH LVDTs

Using LVDTs do detect relative roto-translations at the cup-bone interface under cyclical load conditions, didn't result a good idea. In fact, many problems occurred, as:

1. The approach resulted invasive: the LVDTs were attached with to the bone;
2. Because of the point 1, the LVDTs measurements resulted relative to all the specimen motion underloading. The information about the relative micromotion of the cup with respect to the host bone was lost;
3. During the test the LVDTs were instable. They moved out from their own initial perpendicular to the acetabular plane position. This fact made data distorted;
4. Moreover, the customized setup for LVDTs wasn't easy to mount, especially with the view of a test campaign involving many specimens.

3.3 MEASUREMENTS WITH DIGITAL IMAGE CORRELATION

The innovative instrument chosen to detect the reliable measure of the cup-bone relative motion, was the Digital Image Correlation (replacing the LVDTs role involved in the non-performing preliminary test). It resulted to be the best way to obtain information about displacement and strain of the whole region of interest of the specimen.
The outcomes about the DIC parameters are following reported.

3.3.1 Speckle Pattern

The speckle dots resulted to be of 5-6 pixel in average with a low standard deviation (Fig.70).
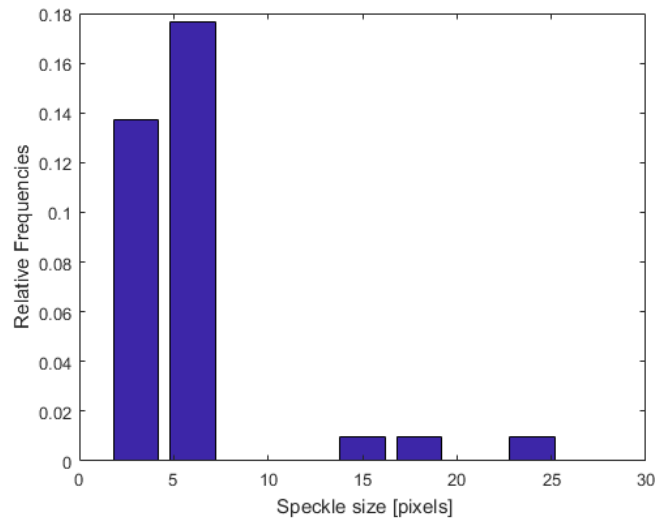
Fig.70: Histogram obtained through the scrip of the internal procedure to measure the speckle size and to quantify its dispersion.

3.3.2 Actuator side: outcomes of gross displacement

As LVDTs were not considered reliable measurements tools for the assessment of the relative motion cup-bone, they were involved in a more appropriate application: as spot-check system for gross measures.

The spot-check system monitored the mechanical tests through a different approach from the DIC system: acquiring samples on the actuator side. In each test, the spot-check system could successfully follow the specimen motions in all three directions of the space. In particular, the LVDT_ML and LVDT_AP remained attached to the setup during all the test. As example Fig.71 shows the plot of the anterior-posterior displacement (LVDT_AP) in the first mechanical test. Similar trends were found in each test, but the amplitude of the signal.

The spot-check system relieved succesfully all the valleys samples *in synchrono* with the DIC system and no drifts or anomalies were detected.

On the other hand, some problems resulted from the peaks: the more evident case resulted from the second test in wich the peaks were flat (Fig.72).
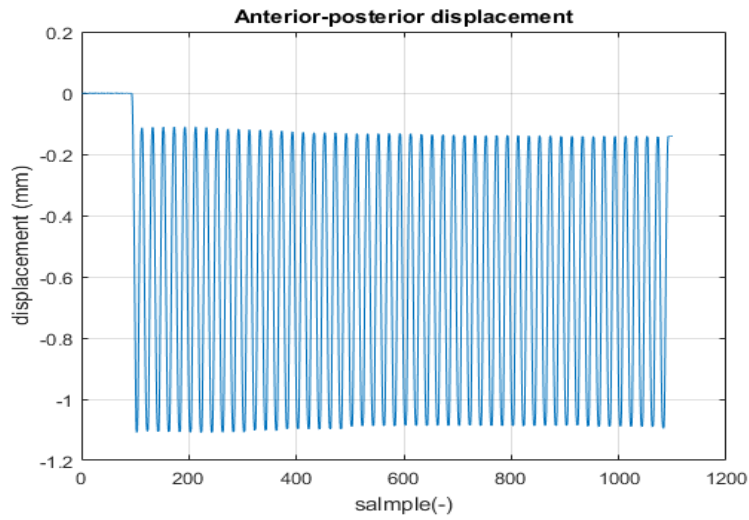
Fig.71: LVDT_AP signal acquired during the first mechanical test
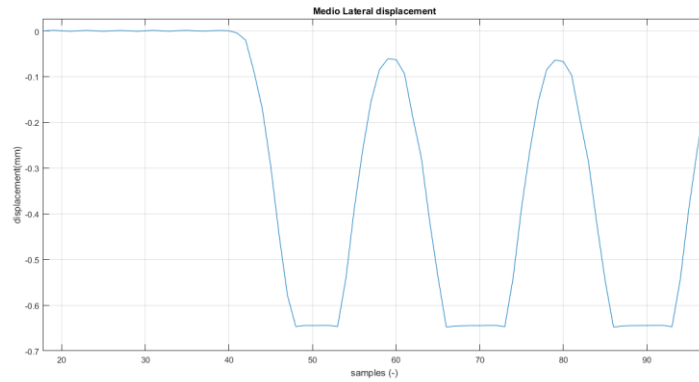
Fig.72: Focus on some flat peaks of the LVDT_ML signal acquired during the second mechanical test.

3.3.3 Optimization of the Region of Interest

Due to the DIC parameters optimization (ROI, speckle pattern, illumination, grid spacing, facet size and so on) the set of images acquired throughout every step of the mechanical test, resulted all correctly evaluated by the DIC software algorithm, resulting in successfully contour, displacement and strain map computations (Fig.73).
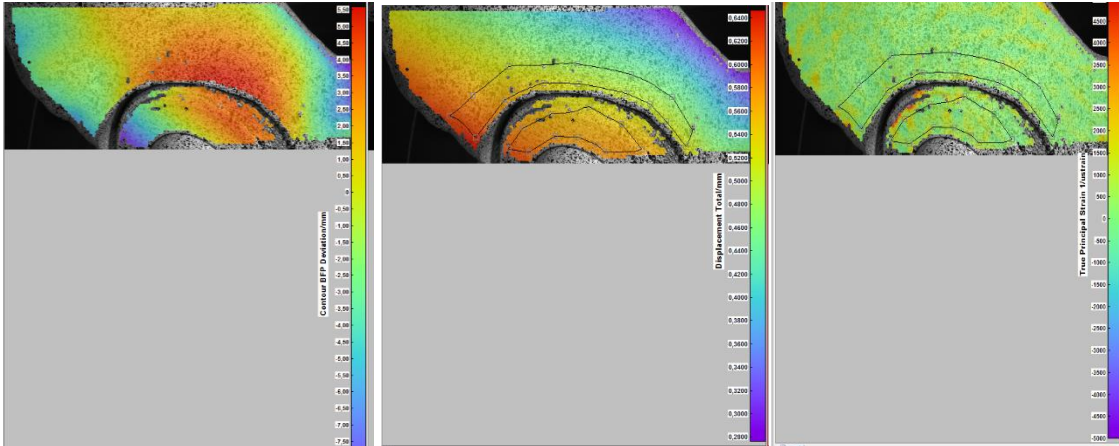
Fig.73: *A typical DIC image resulting after a successful correlation: contour map, displacement map and strain map (left to right). In the displacement and strain map images, the patches are drawn.*

3.3.4 Residuum in Digital Image Correlation calibration phase

The value of the residuum of pixels, detected by the algorithm was of:
- 0.127 pixels in the first and in the second test;
- 0.200 pixels in the third test.

3.3.5 Digital Image Correlation calibration repeatability test

The results of the calibration repeatability test are shown in Tab.6 and Tab.7. They represent an offset of the origin of the calibration reference frame. The repeatability test was better than 0,06 about the AP axis, better than 0.03mm about the CD axis and better than 0.15mm about the ML axis.

Tab. 6: I (a.), II (b.) and III (c.) test repetition average and standard deviation (AVERAGE and ST.DEV in last two columns) of coordinates (about AP-, CD-, ML- axes) of the same point extracted in the three times positioned reference frame.

I TEST				AVERAGE (mm)	ST.DEV (mm)
AP(mm)	-5.3374	-5.3926	-5.3113	-5.3471	0.0415
CD(mm)	8.7970	8.7871	8.7580	8.7807	0.0203
ML(mm)	10.8977	10.7188	10.6103	10.7423	0.1451

a.

II TEST				AVERAGE (mm)	ST.DEV (mm)
AP(mm)	-1.5609	-1.5648	-1.4661	-1.5306	0.0559
CD(mm)	9.1166	9.1124	9.0985	9.1092	0.0095
ML(mm)	13.4708	13.3280	13.2458	13.3482	0.1139

b.

III TEST				AVERAGE (mm)	ST.DEV (mm)
AP(mm)	-0.7198	-0.7624	-0.8327	-0.7716	0.0570
CD(mm)	8.1583	8.1608	8.1041	8.1411	0.0320
ML(mm)	13.7862	13.6788	13.5348	13.6666	0.1261

c.

Tab.7: Average of the three repetitions along AP-, CD- and ML-axes.

AVERAGE AP (mm)	0.0515
AVERAGE CD (mm)	0.0206
AVERAG. ML (mm)	0.1284

3.4 PILOT TEST WITH BONE MODEL

The mechanical test was successfully conducted. The cup resulted stable. The specimen was still integer, but in the last step showed little more compliance than the previous.

3.5 RESULTS OF THE POST PROCESSING

The DIC software recognized all the facets in each image of the set acquired. Because of this, the patches could be applied on the successfully correlated regions of interest.

3.5.1 Measurements uncertainty of the Digital Image Correlation

By the zero-strain condition test (discussed in Par. 2.6.2), the systematic and the random errors affecting the DIC measurements of displacement and strain, are shown in Tab.8 and Tab.9.

Tab.8: *Systematic error in DIC outcomes: total displacement (sqrt $(x+y^2+z^2)$) and true principal strains. The systematic error is in the last column, calculated as the difference between the first and the second frame in zero-strain.*

	FIRST FRAME	SECOND FRAME	SYSTEMATIC ERROR
TOTAL DISPLACEMENT (mm)	0.000	0.003	0.003
TRUE PRINCIPAL STRAIN1 (microstrain)	0.000	0.000	0.000
TRUE PRINCIPAL STRAIN2 (microstrain)	0.000	-100	-100

Tab.9: *Random Error in DIC outcomes: this error, is computed by the software and represents the noise affecting DIC data because of the measure chain. Here the random uncertainty is shown both in the first frame and in the second frame.*

	FIRST FRAME RANDOM ERROR	SECOND FRAME RANDOM ERROR
TOTAL DISPLACEMENT (mm)	0.000	0.000
TRUE PRINCIPAL STRAIN1 (microstrain)	±500	±500
TRUE PRINCIPAL STRAIN2 (microstrain)	±400	±500

3.5.2 Permanent Migration

Results reported in this paragraph are the measurements of *permanent migration* in terms of relative rotations and translations (displacement). The overall result shows that relative motion at the cup-bone interface was smaller than 20 mimrometers (for relative displacement) and smaller than 0.07° (for relative rotation). The measurements were calculated about the anatomical pelvic plane (APP), in each step of the pilot test, thanks to the calibration target position, studied for this work.

Tab.10: Relative cup - bone displacement about the three anatomical axes, computed by the SVD algorithm assessing the permanent migration in each step (1,2,3).

Relative CUP/BONE displacement (mm)	Step 1 (actuator stroke imposed= 0.50 mm; CYC=50)	Step 2 (actuator stroke imposed= 1 mm; CYC=100)	Step 3 (actuator stroke imposed= 1.3mm; CYC=100)
ΔAP'	-0.0012	-0.0070	-0.0007
ΔCD'	-0.0014	-0.0121	-0.0046
ΔML'	-0.0020	-0.0120	-0.0070

Tab.11: Relative cup - bone rotation about the three anatomical axes, computed by the SVD algorithm assessing the permanent migration in each step (1,2,3).

Relative CUP/BONE rotation (°)	Step 1 (actuator stroke imposed= 0.50 mm; CYC=50)	Step 2 (actuator stroke imposed= 1 mm; CYC=100)	Step 3 (actuator stroke imposed= 1.3mm; CYC=100)
r_AP'	0.0125	0.0605	0.0019
r_CD'	-0.0022	-0.0338	0.0013
r_ML'	0.0029	0.0011	-0.0015

3.5.3 Inducible micromotion

Results reported in this paragraph are the measurements of *inducible micromotion* in terms of relative rotations and translations (dispalcement). The overall result shows that relative motion at the cup-bone interface was smaller than 22 micrometers (for relative displacement) and smaller than 1.5° (for relative rotation) in each direction of each step. It is possible to note that the cup regitered a higher motion than in the permanent migration. This means that at the peak it moves but then the cup comes back to their origin settlment.

The measurements were calculated about the anatomical pelvic plane (APP), in each step of the pilot test, thanks to the calibration target position, studied for this work. In this case the measures were rassessed for three times with respect to three periods chosen on the haversine imposed to the specimen (see Par.2.6.3.3).

Tab.12: Relative cup - bone displacement about the three anatomical axes, computed by the SVD algorithm assessing the permanent migration in each step (1,2,3) at the first cycle of the haversine.

Relative CUP/BONE displacement At FIRST PEAK-VALLEY (mm)	Step 1 (actuator stroke imposed= 0.50 mm; CYC=50)	Step 2 (actuator stroke imposed= 1 mm; CYC=100)	Step 3 (actuator stroke imposed= 1.3mm; CYC=100)
ΔAP'	0.0029	0.0063	0.0094
ΔCD'	-0.0126	0.0261	-0.0057
ΔML'	-0.0013	-0.0001	-0.0189

Tab.13: Relative cup - bone rotation about the three anatomical axes, computed by the SVD algorithm assessing the permanent migration in each step (1,2,3) at the first cycle of the haversine.

Relative CUP/BONE rotation At FIRST PEAK-VALLEY (°)	Step 1 (actuator stroke imposed= 0.50 mm; CYC=50)	Step 2 (actuator stroke imposed= 1 mm; CYC=100)	Step 3 (actuator stroke imposed= 1.3mm; CYC=100)
r_AP'	0.0070	-0.0199	-0.0352
r_CD'	-0.004	-0.0165	-0.0133
r_ML'	-0.009	0.0039	-0.0204

Tab.14: Relative cup - bone displacement about the three anatomical axes, computed by the SVD algorithm assessing the permanent migration in each step (1,2,3) at the cycle of the haversine in the middle of the wave.

Relative CUP/BONE displacement At MIDDLE PEAK-VALLEY (mm)	Step 1 (actuator stroke imposed= 0.50 mm; CYC=50)	Step 2 (actuator stroke imposed= 1 mm; CYC=100)	Step 3 (actuator stroke imposed= 1.3mm; CYC=100)
ΔAP'	0.0040	-0.0050	-0.0099
ΔCD'	-0.0150	-0.0150	0.0087
ΔML'	-0.0030	0.0030	0.0238

Tab.15: Relative cup - bone rotation about the three anatomical axes, computed by the SVD algorithm assessing the permanent migration in each step (1,2,3) at the cycle of the haversine in the middle of the wave.

Relative CUP/BONE rotation At MIDDLE PEAK-VALLEY (°)	Step 1 (actuator stroke imposed= 0.50 mm; CYC=50)	Step 2 (actuator stroke imposed= 1 mm; CYC=100)	Step 3 (actuator stroke imposed= 1.3mm; CYC=100)
r_AP'	0.0159	0.0480	0.0444
r_CD'	0.0080	0.0119	0.0169
r_ML'	-0.007	0.0023	0.0207

Tab.16: Relative cup - bone displacement about the three anatomical axes, computed by the SVD algorithm assessing the permanent migration in each step (1,2,3) at the last cycle of the haversine.

Relative CUP/BONE displacement At LAST PEAK-VALLEY (mm)	Step 1 (actuator stroke imposed= 0.50 mm; CYC=50)	Step 2 (actuator stroke imposed= 1 mm; CYC=100)	Step 3 (actuator stroke imposed= 1.3mm; CYC=100)
ΔAP'	0.0042	0.0074	0.0083
ΔCD'	-0.0111	-0.0239	-0.0110
ΔML'	-0.0013	-0.0020	-0.0260

Tab.17: Relative cup - bone rotation about the three anatomical axes, computed by the SVD algorithm assessing the permanent migration in each step (1,2,3) at the last cycle of the haversine.

Relative CUP/BONE rotation At LAST PEAK-VALLEY (°)	Step 1 (actuator stroke imposed= 0.50 mm; CYC=50)	Step 2 (actuator stroke imposed= 1 mm; CYC=100)	Step 3 (actuator stroke imposed= 1.3mm; CYC=100)
r_AP'	0.0170	-0.0012	-0.0508
r_CD'	-0.0071	0.0199	-0.0186
r_ML'	-0.0028	0.0113	-0.0158

3.5.4 Validation of roto-translations computation

Checking the Matlab script functioning, which calculated the roto-translations of each district of interest (cup and bone), the uncertainty on the measures were smaller than 0.01 mm about the translations and of 0.02° about rotations.

3.5.5 Outcomes of the strain evaluation

The strain maps resulting from the DIC analysis were assessed both for the *permanent migration* (Par.3.5.5.1) and the *inducible micromotion* (3.5.5.2). In each evaluation (permanent migration and inducible micromotion) and for each step, the strain distribution resulted with small deformations because the strain value was smaller than the DIC strain uncertainty.

The most critical situation about noise, was observed in the *inducible micromotion* evaluation with the maximum noise oscillation range of ±500 microstrain. The region more affected to noise was the cup. Moreover, the cup registered a higher average strain than the bone differently than expected. Maybe, this fact was caused by too much noise introduced by the strain computation due to the small area correlated on the cup liner (the DIC analysis may requires more correlated facets to compute a reasonable evaluation about strain). Despite this, the bone and the liner in the outlined areas of each step, were considered subjected to small deformation because values were close to the DIC sensitivity. Thus, the assumption about the rigid bodies for the cup and the bone (superior aspect), was demonstrate and the SVD algorithm was validate.

For the sake of brevity only the results of *permanent migration* assessment are here reported, about the validation of the two rigid bodies. Thus, principal strains (ε_1, ε_2) mean values over the patch surface drawn on the cup and on the superior aspect were evaluated in the first, last and between the first and the last valley ($\Delta\varepsilon$), assessing the strain variation between the start and the end of the cyclical test.

Tab.18: Principal strains mean values over the patch surface drawn on the cup (1) and on the bone (2) evaluated in the first (a), last (c) and between the first and the last (b) valley.

First step CUP	Cup Principal Strain (microstrain) first valley	Cup Principal Strain (microstrain) last valley	Cup Principal Strain (microstrain) variation ($\Delta\varepsilon$)
True Principal Strain1 (Mean over surface), ε_1	-43	16	-60
True Principal Strain2 (Mean over surface), ε_2	-92	-129	-36

a.1

First step BONE	Bone Principal Strain first valley (microstrain)	Bone Principal Strain last valley (microstrain)	Bone Principal Strain variation ($\Delta\varepsilon$) (microstrain)
True Principal Strain1 (Mean over surface), ε_{1f}	-47	18	-66
True Principal Strain2 (Mean over surface), ε_{2f}	-88	-60	-28

a.2

Second step CUP	Cup Principal Strain first valley (microstrain)	Cup Principal Strain last valley (microstrain)	Cup Principal Strain variation ($\Delta\varepsilon$) (microstrain)
True Principal Strain1 (Mean over surface), ε_1	140	10	37
True Principal Strain2 (Mean over surface), ε_2	-95	-41	48

b.1

Second Step BONE	Bone Principal Strain first valley (microstrain)	Bone Principal Strain last valley (microstrain)	Bone Principal Strain variation ($\Delta\varepsilon$) (microstrain)
True Principal Strain1 (Mean over surface), ε_{1f}	-36	-46	-46
True Principal Strain2 (Mean over surface), ε_{2f}	-55	-14	-14

b.2

Third step CUP	Cup Principal Strain first valley (microstrain)	Cup Principal Strain last valley (microstrain)	Cup Principal Strain variation (Δε) (microstrain)
True Principal Strain1 (Mean over surface), ε_1	42	29	22
True Principal Strain2 (Mean over surface), ε_2	29	5	-12

c.1

Third step BONE	Bone Principal Strain first valley (microstrain)	Bone Principal Strain last valley (microstrain)	Bone Principal Strain variation (Δε) (microstrain)
True Principal Strain1 (Mean over surface), ε_{1f}	61	16	44
True Principal Strain2 (Mean over surface), ε_{2f}	8	-13	22

c.2

4. DISCUSSION

4.1 DEVELOPMENT OF THE STUDY

Developing all the parameters of the study was the fundamental phase to optimize and set the pilot test.

4.1.1 Linear displacement sensor: calibration

All the LVDTs calibrated for this work, showed a good behaviour and it was not necessary to change the gain in their conditioning system. The LVDTs were in good conditions with high accuracy.

Due to the good accuracy the LVDTs were considered optimized for measuring the slides displacements as the measures related to the uncertainty were below the conventional threshold of 20 micrometers.

Even though, the LVDTs brand reported a resolution equal to 1 micron, by the impossibility to recreate the same environment of the device internal calibration like in SIT centres, it was a more than reliable result.

4.1.2 measurement of cup stability with LVDTs

Due to the problems found throughout the preliminary test (see 3.2), a better measure instrument was requested. This new approach could have been less invasive avoiding any morphology alteration and easily repeatable. Moreover, a different method was needed to measure independently the bone and cup displacements throughout the mechanical test, thus, to assess their relative motions.

The Digital Image Correlation, resulted to be the best candidate for meeting these needs.

4.1.3 Measurements with Digital Image Correlation

Using the DIC system as reliable measurement tool allowed to overcome all the problems observed using LVDTs in the preliminary test. In fact, while the DIC method allowed to measure full-field displacement and strain maps through a contact-less method, the LVDTs performed a pointwise measure through an invasive method.

Using the DIC as a measurement tool for assessing the stability of the acetabular component has never been done before. Thus, it was necessary to study its parameters optimization to take fully advantages of their great potential and versatility. This is the reason why a large period of this work was focused on the *ad hoc* optimization of DIC parameters for the application on implanted hemipelvis (pre-acquisition parameters: dot size of speckle pattern, region of interest focus,

exposure, brightness, DIC reference frame definition etc. and post- acquisition parameters: facet size, grid-spacing, smoothing filter).

4.1.3.1 Speckle Pattern

Being the first time, the speckle pattern was adopted for a synthetic hemipelvis study, it was seen that the region of interest was too extended to use the parameters for the speckle patterns adopted in previous studies on different bone specimens. For this reason, it was required a little bit bigger dot size than usually (also depended on the use of 17mm lens, see Par 4.4.4).

After several attempts, the 5-6 px dot size was chosen adopted for the images correlation during the test. Having a low dispersion and a similar dot size favoured the high contrast black and white and the homogeneous distribution of the paint, optimizing the DIC system to correctly recognize every single facet in each step of registration.

4.1.3.2 Actuator side: outcomes of gross displacement

The spot-check system was useful both for the valleys detection, also used into the post - processing code analysis, and for monitoring the trend of all the tests. Because of the preliminary test outcomes, it was thought to set them in a more useful and accessible place: into the slides plane. This set could follow the actuator and so the specimen absolute motion, but the relative motion cup-bone or strain assessment couldn't be evaluated. For this reason, the DIC method was chosen as reliable measurement tool and the LVDTs system as spot-check. In fact, DIC power in detecting displacements and strain distribution all over the specimen surface and in being a contactless method, overcame issues about the troublesome setting of sensors and the results analysis, which was easy to do both visually through the displacement /strain maps and exporting data from the software.

In each test the spot-check plot (related to LVDT_ML and LVDT_AP, slides sensors) shows a gap at the starting point, passing from the zero-strain condition to the dynamic one (at the cyclical load application) (Fig.72). Moreover, at the end of the test, the LVDT didn't restore its initial position. This fact may depend on the viscoelastic nature of the synthetic specimen which seemed to slightly yield or because of friction due to the slides.

A problem found out in some plots (Fig. 73), was the LVTD saturation at the peaks. The expected displacement of sensors during the tests was lower and for this reason the internal core was set at mid-run: it was evidently not enough. It is recommended for next tests to put the LVDTs completely in compression, being free to move along their total stroke.

4.1.3.3 Optimization of the Region of Interest

The success of images correlation is due to the experimental study about DIC parameters optimization:

1. ***Optimization of field of view.*** Before using the 17mm lens, many acquisitions were conducted by mean of 35 mm lens mounted on both the cameras. In this, the depth of field

was not sufficient, hence the 17mm lens were chosen. In this phase the speckle pattern dot size was adapted to the windows of measure resulting from the 17mm lens use.

2. *Optimization of acquisition frequency.* With the purpose to follow the specimen motion during the entire the test, the signal was sampled at 20 Hz. This meant to acquire 20 images per second (in a period of the haversine), being able to capture peaks and valleys with high accuracy. The compromise to use this frequency was transduced in a smaller field of view: increasing the acquisition frequency, the height one of the field of view decreased. The use of 17mm allowed to acquire a reasonable area on the specimen at 20 Hz.

3. *Position configuration t of the cameras and ROI.* The Region of interest resulting from the settlement of the cameras, was functional to focus the specimen from the bottom. This was the best compromise to display the cup, which was tilted, and to observe a reasonable part of the bone, including both the superior aspect of the acetabulum and the posterior column. The periacetabular region of the bone directly interested the study because it was fundamental in computing the relative roto-translations; the posterior column was acquired to monitor a critical area of hemipelvises underloading. In fact, for the late test campaign, it will be important to monitor the behaviour and the strain distribution for this region in composite, cadaveric and in reconstructed broken cadaveric bones. Even though other focuses were experimented changing the cameras inclination, for example acquiring the specimen frontally, the result obtained from the bottom shot was the most satisfactory, also in terms of images correlation (Fig.74).
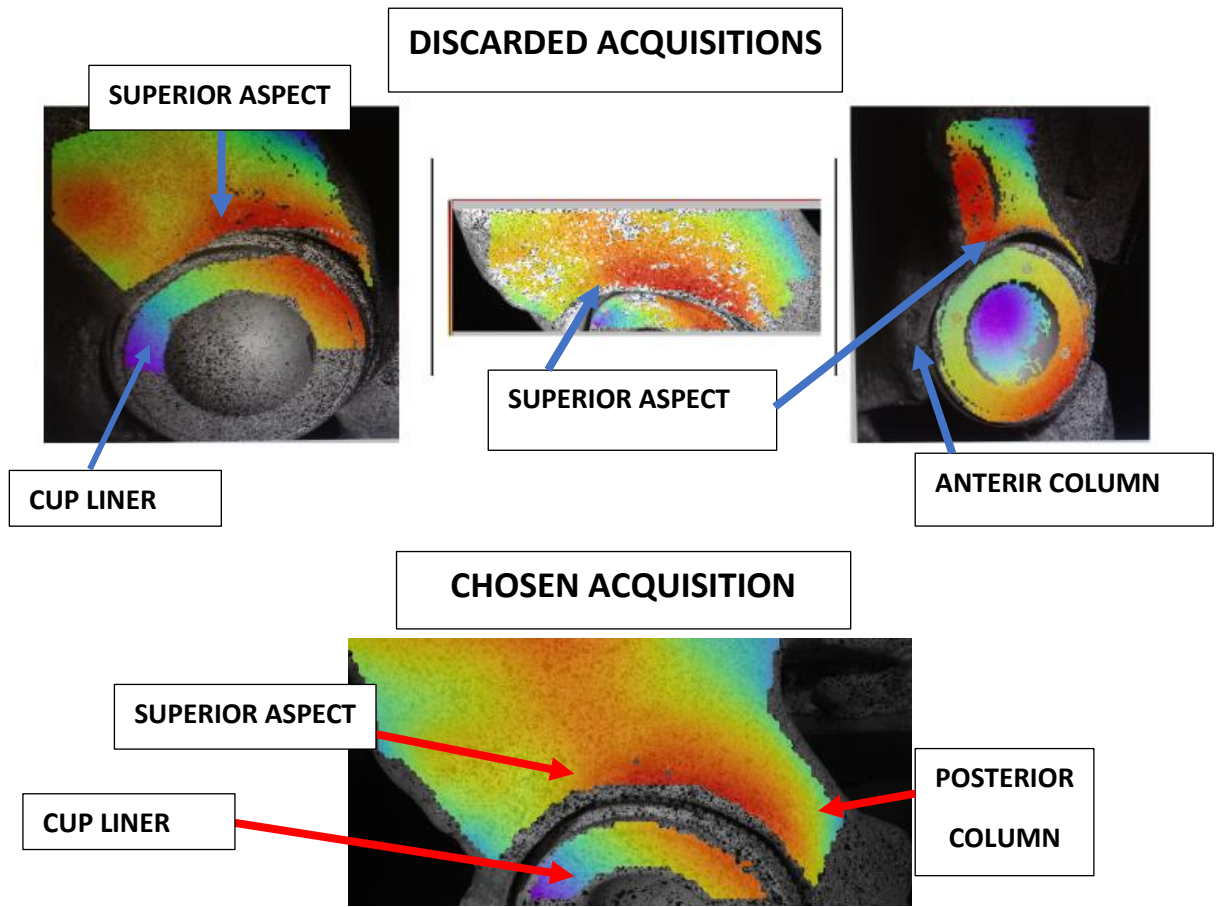
Fig.74: This illustration summarizes some examples of experimented focuses: above three discarded acquisitions, which were acquired by mean of 35 mm lens. Left: the cup was totally acquired with its upper bone region, but the posterior column was lost. Middle: it was tried to go closer to the specimen and acquiring more bone including the posterior column, but the correlation was not satisfying. Right: the cameras were tilted of 90 degrees: the cup was totally well evaluated but not the bone. Below: the chosen acquisition, done by mean of the 17mm lens, is shown.

4.1.3.4 Residuum in Digital Image Correlation calibration phase

The calibration was conducted successfully in each step with the first time. However, because the calibration was not always guaranteed, the most common problem, was due to the illumination. At last, the reasonable residuum value was reached. It is interesting to report that the best calibration was performed during the morning. It was thought the oscillatory nature of the neon light could interfere with the DIC illumination system.

4.1.3.5 Digital Image Correlation calibration repeatability test

The repeatability test conducted to quantify the offset in reaching the centre of the cup by mean of the calibration target, showed good results despite the procedure was very delicate. Accomplishing carefully the action of mounting the calibrator target instead of the specimen, it was possible to reach the origin of the anatomical axes with high accuracy.

4.2 PILOT TEST AND POST PROCESSING

The mechanical test phase was a delicate moment. To make the test be going right, it was important that all components of the setup were not moved during the test (or that no one passed through the setup location), avoiding changing focus or any kind of signal interference.
About the post processing, the Matlab implementation resulted to be an easy and reliable finding to assess the primary stability. By mean of the script it was possible to reach the aim of evaluate both the permanent migration and the inducible micromotion (fundamental for the primary stability assessment of the acetabular component).

4.2.1 Measurements uncertainty of the Digital Image Correlation

Displacement error. Thus, the uncertainty of the displacement, computed by the DIC system, was low and negligible (systematic deviation average of 0.03 mm and random deviation average less than 10 micron for the total displacement (as shown in Tab.9 and in Tab.10)).
Strain error. The strain introduced a major error, as the software algorithm is used to compute it by mean of the displacement derivation (which produces error amplification).

4.2.2 Permanent Migration

Displacement. The three tests were conducted increasing the stroke value step by step until reaching the stroke correspondent to the displacement of 1.3 mm (in which 2BW was reached). Through the first test, because of the 0.25mm of amplitude (actuator run: 0.50mm), the maximum load reached was almost -500 N; through the second test the maximum load measured by the load cell was of almost -800N, finally with the third one of almost -1000 N (approximately 1.5BW). Even thought it was seen through the preconditioning ramp (holding stressed the specimen in a static condition) that at 1.3 mm of actuator run corresponded a 2BW, it was not completely reached (-1000 N in the third test) because under cyclical conditions the polyurethane specimen changes its behaviour due to its viscoelastic nature and because the specimen was already stressed many time before, leading to major compliance.

Roto-translations. This study work represents a pilot test to prepare basis for the next test campaign on composite and cadaveric specimens. For this reason, it was essential to gradually investigate different parameters to load the specimen and to monitor its behaviour. In fact, the first mechanical test was conducted applying 50 cycles imposing low actuator displacement; then it was decided to augment both the number of cycles and the actuator displacement with the second test and finally, the 1.3mm displacement control was imposed, even if with a limited number of cycles.
Since now, the literature has shown that the most significative directions for cup migration, in clinical studies were clinical translation and change in inclination (Tab.19).

Tab.19: The first column of the table contains the typical directions of cup migration as results of many clinical studies. In the second column, the equivalent parameters in this study are shown.

LITERATURE	THIS STUDY
Cranial transaltion	Relative cup-bone displacement: ΔCD'
Change in inclination	Relative cup-bone rotation: r_AP'

Moreover, through this study it was possible to go further, measuring roto-translations about all anatomical axes and not only in the two directions showed in Tab.20.

Data outcoming from the post processing analysis, resulted in each test below 20 micrometers (threshold conventionally used for the possible fibrous tissue formation) both in cranial translation and better than 0.05° in change in inclination. However, being possible to exploit all the displacements in 3D, the total relative displacement is calculated $(sqrt(\Delta AP'^2+\Delta CD'^2+\Delta ML'^2))$.

Tab.20: Relative cup – bone displacement in each step and respective relative total displacement

Relative Cup-Bone Displacement (mm)	I step	II step	III step
ΔAP'	-0.0012	0.0007	0.0007
ΔCD'	-0.0014	0.0121	0.0046
ΔML'	-0.0020	0.0120	0.0075
TOTAL	**0.0027**	**0.0184**	**0.0084**

Tab. 43 shows that the second test achieves the worst result: 18 micrometers of total relative displacement at the end of the cyclical test (permanent migration). Conversely the first test shows the lowest total relative displacement (2.7 micrometers). Even though the cup is almost stable in each case, this pilot test gives some interesting information:

- as the cycles increase, the relative displacement also increases;
- augmenting the actuator run, the relative cup-bone displacement increases despite the minor number of cycles (the third test achieved a higher relative total displacement than the first one, 8.4micrometers vs 2.7micrometers (see Tab.15, Tab.23, Tab.31));

- for each test the higher relative cup-bone rotation is about the anterior-posterior axis, but as they are equal or lower than the uncertainty of rotation measurements, such rotations can be considered absent for the permanent migration.

4.2.3 Inducible micromotion

Calculating the average value of the inducible micromotion measurements of the three chosen periods, the *inducible micromotion* resulted:
- smaller than 22 micrometers (slightly over the threshold conventionally used for the possible fibrous tissue formation) in cranial translation ($\Delta CD'$)
- better than 20 microns about the other two anatomical axes.
- Better than 0.02° both in change in inclination (r_AP') and about the other anatomical axes.

Despite the craniocaudal displacement, close to the clinical threshold, it was reasonable to consider stable the cup under *inducible micromotion* conditions.

The inducible micromotion is a critical parameter because it causes the permanent migration after the load peak. It is important to assess this kind of micromovement to ensure the primary stability of the cup underloading (if the cup moves from peak to next valley at every load cycle, the osteointegration is not guaranteed). Moreover, the inducible micromotion it is hard to monitor through radiographs or other techniques (follow-up) because they are static analysis and not assessed in a preclinical scenario. By the DIC method it was possible to overcome this problem, having a complete scenario about the primary stability of cup.

4.2.4 Validation of roto-translations computation

By mean of the validity test about the roto-translation measurament uncertainty, the results about the displacement and rotation computation, lead to assure the high realibility and accuracy of the Matlab script outputs, which are discussed in Par. 4.2.1 and 4.2.2.

4.2.5 Strain Evaluation

Evaluation of permanent deformation and assumption of Rigid Bodies in permanent migration.
Observing strain results data (Tab.18) it was reasonable to assume the two considered patched areas belonged to approximated rigid bodies (with small deformation) and to validate the two rigid bodies theory applied to them. This result was hoped because the two patches selected two supposed rigid bodies. The strain values remained below the error introduced by the DIC on strain measurements, so, the bodies outlined by patches were rightly considered rigid (no plastic deformation).

Generally, looking at the strain maps (Fig.75 and Fig.76), the entire hemipelvis acquired in the adopted field of view of the last valley, appeared undeformed less than some points at edges (which are typically characterized by major noise in DIC computations).
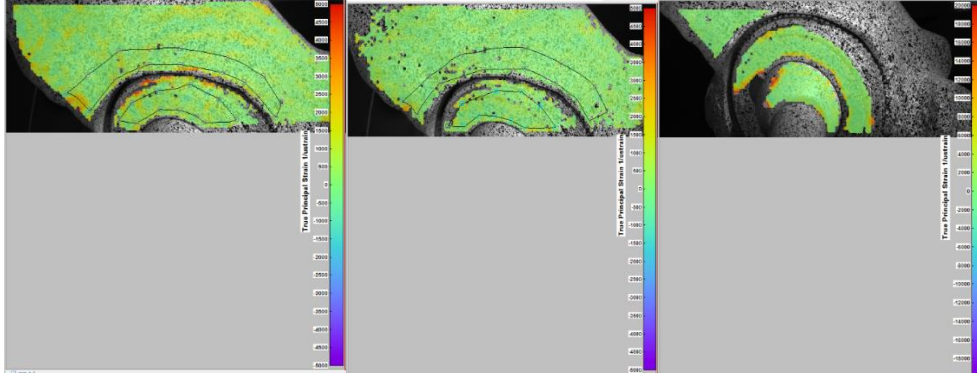

Fig. 75: True Principal strain1 (ε_1), in the last frame of the first, the second and the third mechanical test (left to righ).
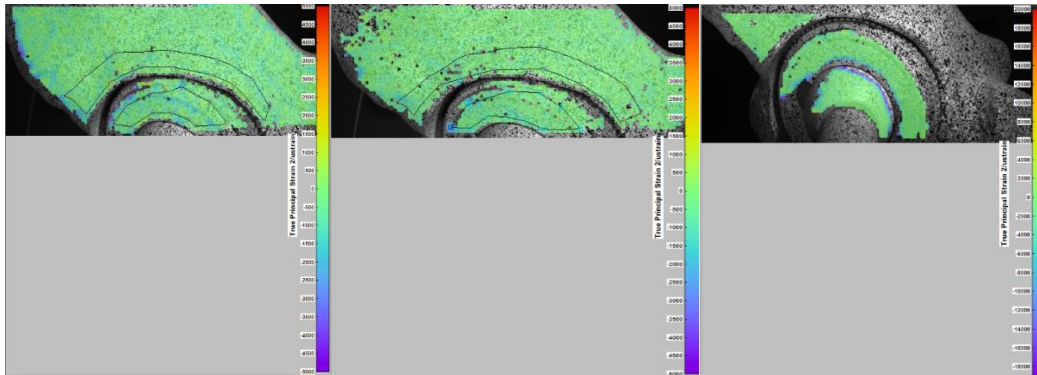

Fig. 76: True Principal strain2 (ε_2), in the last frame of the first, the second and the third mechanical test (left to right).

Evaluation of inducible deformation. Due to the low load reached in the three tests, both the superior acetabular aspect and the posterior column of the bone didn't show relevant strain measurements during peaks and following valleys, chosen for the assessment of the *inducible micromotions*.

Differently than expected, the bone in each state of performed steps, resulted small deformed, even if assessed during the inducible micromotion periods (underloading the bone was expected to deform more than results shows). The mean strain variations, resulting over the patches surfaces, were smaller than the DIC sensitivity about strain computation (both for the superior aspect and the posterior column), which was not better then about ± 500 microstrain. For this, a deeper study to optimaize the evaluation of the strains is requested. Thus, one of the future works will focus on this topic.

6. CONCLUSION

The overall goal, set for this study, was achieved: a reliable and innovative *in vitro* procedure for the *primary stability* assessment of a commercial acetabular component was created.

For the first time an *in vitro* method (pilot-test) to evaluate cup absolute and relative roto-translations in 3D was studied:

1. Two different methods have been explored simultaneously for the THA application: The Digital Image Correlation (DIC) and the use of linear displacement transducers. The DIC was the "reliable measure" and sensors were adopted as a monitor system and gross measure.

   While the reliable measure detected information on the specimen surface under load, the spot-check system detected information monitoring a custom mechanical setup mounted on the actuator block of the testing machine actuator (thus, from "another point of view"). The DIC system was found to be a strong measurement tool for the three-dimensional assessment of the cup motions as its information of displacement and strain in 3D space. An advantageous method for linking DIC output measures to anatomical axis was found. Collecting information about the anterior-posterior, cranio-caudal and medio-lateral axes was useful for a comparison with clinical parameters (the radiographic reference frame was used).

   a. As the DIC power in detecting displacement and strain in 3D depends on *ad hoc* adaptations of every DIC parameter for the specimen of interest, The DIC hardware and software optimization for the hemipelvis application was studied. It has been the first time that the DIC system was optimized for assessing the *primary stability* of a cup, implanted into the hemipelvis specimen, during a cyclical mechanical test. The optimization allowed to acquire the specimen at 20Hz evaluating a reasonable field of view including: the cup liner, the superior aspect of the acetabulum and the posterior column (critical bone regions). Moreover, thanks to the speckle pattern optimization, the homogeneous illumination and the right set of grid spacing and facet size, the correlation algorithm reached the evaluation of every images set (achieving the correlation of 2200 frames, during the 100 cycles of the second test).

   b. A calibration procedure for LVDTs sensor was created.

2. A reliable method for detecting both the permanent migration and the inducible micromotion of the acetabular component was implemented.

a. An algorithm in Matlab was created; it was able to compute roto-translation values assessing the permanent migration of the acetabular component after the performance of a cyclical mechanical test. As the permanent migration is defined by the evaluation of cup-bone micromotions under unloaded conditions (at valleys of the cyclical wave form imposed), the algorithm could select the initial cyclical test and the final cyclical test frames, elaborating the relative roto-translations matrices between cup and bone.

b. The same Matlab script, created for the assessment of the permanent migration, was modified *ad hoc* for the evaluation of the inducible micromotion. The script was able to select valleys and their following peaks, computing between them the relative roto-translations at the cup-bone interface. The inducible micromotion was assessed in three periods of each cyclical test: at the initial, the middle and the last period. This procedure allowed to monitor the cup even underloading.

Reaching successfully the aims defined in 1.6, this work gives guidelines for the next test campaign, which is going to test specimens in composite material and cadaveric specimens. Until now, similar specimens were not used because of ethical reasons (about cadaveric specimens) and because of a higher cost (about composite specimens). Thus, the future work aims to use the same *modus operandi* of the pilot-test defined in this work but testing the specimen with much more load cycles (packages of 100 cycles). Moreover, every 100 cycles the haversine amplitude will be increased of 1% until 2-3BW. The permanent migration and the inducible migration we'll be monitored during the test, also assessing the strain distribution.

APPENDIX I

		Codice	Pag 107 / 12
GRUPPO DI BIOMECCANICA	TARATURA INTERNA DI LVDT E SIMILI TRASDUTTORI DI SPOSTAMENTO	**MPP/03/rev2**	21/09/2017

TARATURA INTERNA DI LVDT E SIMILI TRASDUTTORI DI SPOSTAMENTO

SOMMARIO

		Codice	Pag 110 / 12
	TARATURA INTERNA DI LVDT E SIMILI TRASDUTTORI DI SPOSTAMENTO	**MPP/03/rev2**	21/09/2017

GRUPPO DI
BIOMECCANICA

MODIFICHE

Rev.	Data	Modifiche	Autori
IOR-LTM	2009	Nata come procedura Rizzoli LTM (MPP/15/01)	L. Cristofolini – M. Baleani
IOR-LTM	2010	Revisione come procedura Rizzoli LTM (MPP/15/01)	L. Cristofolini – M. Baleani
01	6 July 2016	Riscritta per UniBo PXIe	M. Palanca – L. Cristofolini
02	21 Sept. 2017	Revisione	M.Linsalata – K. Morellato

SCOPO /OBIETTIVI

Scopo della presente procedura è quello di fornire una guida per verificare il buon funzionamento degli LVDT e altri trasduttori di spostamento di struttura analoga.

CAMPO DI APPLICAZIONE

Questa procedura è applicabile esclusivamente a sensori di spostamento LVDT:

Sezione I: LVDT#1 (SPM/31), LVDT#2 (SPM/32), LVDT#3 (SPM/33), LVDT#4 (SPM/34), LVDT#5 (SPM/35), costruiti da microepsilon, Mod. DTA1D3SAW, con relativo cavo C701-3 e condizionatore Mod. MSC 710-U.

È possibile estendere la procedura ad altri trasduttori di spostamento di struttura analoga (in precedenza la procedura è stata usata su RDP), prevedendo nuove Parti della presente procedura.

Questa procedura è applicabile esclusivamente a sensori di spostamento _____:

Sezione II: _____

INDICAZIONI GENERALI DI PROCEDURA

Questa procedura descrive i metodi per la verifica di buon funzionamento degli LVDT sopra elencati. Dal momento che tali sensori hanno un'accuratezza migliore del micron, non è possibile eseguirne internamente una taratura accurata. La presente procedura ha solo la funzione di verificare il buon funzionamento del sistema, e tipicamente applicata quando l'operatore ne senta la necessità (a seguito d'incidenti, all'inizio di una campagna di prove importante, quando vengano modificati in qualsiasi modo i settaggi dal condizionatore o la catena di misura).

Questa verifica di buon funzionamento NON sostituisce in alcun modo tarature eseguite da centri SIT. Gli LVDT in oggetto vengono utilizzati in collegamento con gli input analogici della terminaliera National Instruments 6341 del PXIe e pertanto verificati per la specifica catena di misura.

SICUREZZA

Per l'utilizzo dell'LVDT, non è necessaria nessuna specifica guida di sicurezza.

DEFINIZIONI

Definizioni	
Messa a punto:	Insieme di operazioni compiute su un dispositivo per misurazione per imporgli di fornire determinati segnali di lettura in corrispondenza a particolari valori del misurando.

Abbreviazioni	

SEZIONE I: VERIFICA DI LVDT (Mod. DTA1D3SAW, microepsilon, *0-2 mm*) CON IL SUO CONDIZIONATORE COLLEGATO ALLA TERMINALIERA DEL PXIe

MODALITA' OPERATIVE

MATERIALI

Campione di riferimento: testina micrometrica Mitutoyo, Mod. 152-389, N° serie: 701384 (SPM/2). Esso è il campione primario. Ha una risoluzione di 5 micron.

Telaio in alluminio e plexiglas, su cui normalmente si trova già montata la testina micrometrica (Fig. 1).

Testina sferica da avvitare in cima allo stelo degli LVDT, se l'LVDT lo richiede (**M** in Fig. 1)

Alcool

Carta assorbente

Olio di vasellina

		Codice	Pag 114 / 12
	TARATURA INTERNA DI LVDT E SIMILI TRASDUTTORI DI SPOSTAMENTO	**MPP/03/rev2**	21/09/2017

GRUPPO DI
BIOMECCANICA
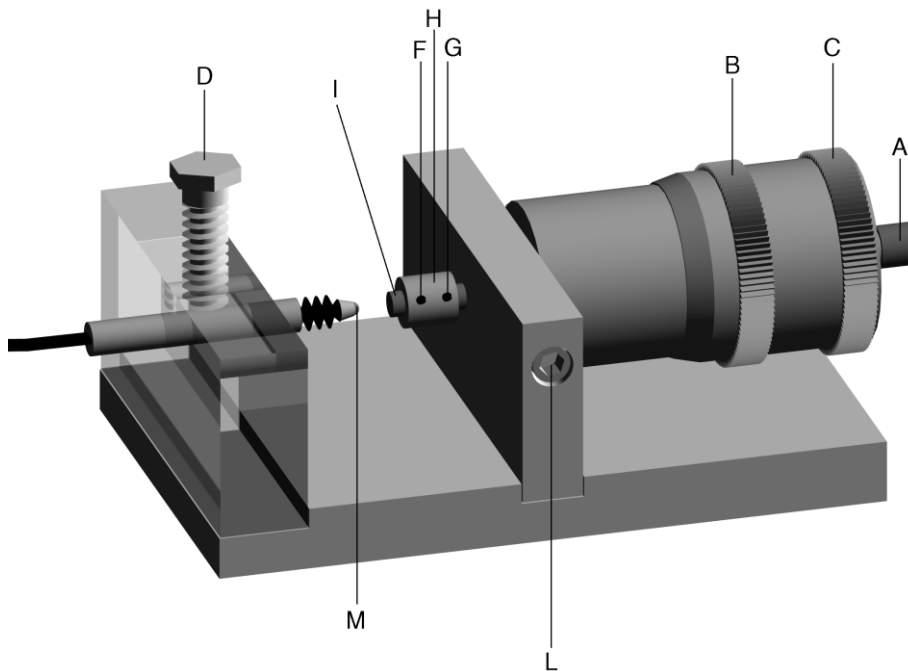
Fig. 1 – Telaio d'alluminio e plexiglas con la testina micrometrica ed un LVDT montati.

Sono indicati i vari azionamenti, e il dettaglio della punta sferica da montare sulla punta dello stelo dell'LVDT.

OPERAZIONI INIZIALI

Descrizione della testina micrometrica (Fig. 1)

La testina micrometrica ha una corsa di 25 millimetri e divisioni ogni 5 micron.

Le due ghiere **A** e **C** servono rispettivamente per fare avanzare velocemente e lentamente la testina.

La ghiera **B** può ruotare rispetto a **C**, per portare a zero la scala di lettura.

Le due scale graduate in nero e rosso servono rispettivamente per misurare spostamenti in fuori e in dentro dello stelo dell'LVDT.

Quando la vite **F** è allentata, la punta **I** può ruotare liberamente (**_e sfilarsi!_**) rispetto allo stelo. Se non ruota bene, si può pulire e ungere con olio di vaselina l'interno, dove si poggia sullo stelo.

1.   **Preparazione**.

NOTA: Non smontare per nessun motivo i pezzi che costituiscono il telaio di supporto, per non perdere l'allineamento.

Collegare l'LVDT al suo condizionatore e l'uscita del condizionatore alla terminaliera del PXIe.

Verificare che la testina micrometrica sia montata e serrata correttamente nel telaio. Se necessario, agire sulla vite a brugola **L**.

Verificare che la vite **G** in Fig. 1 sia ben serrata, perché il manicotto **H** non balli, e che la vite **F** sia sufficientemente lenta da consentire alla punta **I** di ruotare liberamente.

NOTA: Quando la vite F è lenta, la punta I si può sfilare. Fare attenzione a non perderla e a chiudere sempre la vite F finite le operazioni di verifica.

Inserire l'LVDT da verificare nel telaio come in Fig. 1. Lasciare lenta la vite **D** (Fig. 1), per consentire il posizionamento.

Pulire con carta imbevuta d'alcool le due punte.

Ungere le due punte con carta imbevuta d'olio di vaselina.

Ruotando la manopola **A** (regolazione grossolana), portare la testina micrometrica quasi completamente dentro (in modo da avere a disposizione tutta la corsa ad uscire).

2.   **Preparazione alle letture**

2.1   Verificare che l'LVDT da verificare sia correttamente collegato alla terminaliera del PXIe e avviare NImax dal PXIe;

2.3   Preparare un foglio di carta volante o direttamente il foglio di calcolo Excel presente in allegato, se l'operatore ritiene più comodo e utile visualizzare direttamente i risultati, su cui annotare le letture dall'LVDT (si guardino le prime colonne della tabella in Allegato A).

3 Posizionamento LVDT

3.1 Avvicinare manualmente l'LVDT alla punta della testina micrometrica (facendo scorrere la carcassa nel suo supporto di plexiglas), ponendone la punta in contatto e fissare l'LVDT. Serrare **a mano** la vite di nylon **D** (Fig. 1), in modo che l'LVDT non si possa muovere, ma senza eccedere, altrimenti si può danneggiare irreversibilmente l'LVDT.

3.2 Muovere in senso monotono crescente la ruota B fino a quando non è circa all'inizio della corsa del sensore, parte mobile dell'LVDT (stantuffo) tutto fuori e lettura di 1V (*ES: per LVDT con una corsa di 0-2 mm il PXIe indicherà circa 1-9 V; la corsa è più ampia di 0-2mm)*.

. **3.3** Con la regolazione fine della testina micrometrica (impugnare la ghiera **C**, Fig. 1) registrare la posizione iniziale dell'LVDT. Tenendo fissa la ghiera **C**, ruotare la ghiera **B** fino a portare la tacca dello zero in asse (ciò rende più facili tutte le operazioni seguenti). Iterare fino a che l'LVDT non è a un paio di micron dalla posizione desiderata, corrispondente a 0mm (1.0V).

NOTA: Fare attenzione mentre si ruota il micrometro a non forzare lo stelo dell'LVDT oltre il fine corsa, per non danneggiarlo.

NOTA: Per come vengono elaborati i dati, un piccolo offset iniziale non crea grossi

problemi, dato che viene sottratto nel foglio Excel automaticamente; per comodità di lettura, però, è bene essere più vicini possibile al valore nominale iniziale.

4. Esecuzione letture.

NOTA**:** impostare la posizione con la massima precisione, lentamente ed in maniera monotona crescente (evitando aggiustamenti avanti e indietro in modo da minimizzarne il gioco), facendo attenzione agli errori di parallasse. Se si dovesse comunque andare oltre la posizione desiderata si consiglia di tornare sula posizione dell'incremento precedente e riprendere da lì la misura.

Si eseguirà la lettura a 11 punti con incrementi del 10% della corsa (step da 200 micrometri):

Se l'LVDT ha 2.0 mm di corsa a: **+0.0; +0.2, +0.4; +0.6; +0.8; +1.0; +1.2; +1.4; +1.6; +1.8; +2.0 mm** come indicato in Tabella.1;

N° LETTURA	POSIZIONE NOMINALE (mm)	TENSIONE NOMINALE (V)	POSIZIONE PARTE MOBILE LVDT (STANTUFFO)
1	0.0	1	**Totalmente dentro (INIZIO CORSA)**
2	0.2	1.8	
3	0.4	2.6	
4	0.6	3.4	
5	0.8	4.2	
6	1.0	5	
7	1.2	5.8	
8	1.4	6.6	
9	1.6	7.4	
10	1.8	8.2	
11	2.0	9	**Totalmente fuori (FINE CORSA)**

Tabella.1: nella prima colonna è indicato il numero di lettura (11 in totale), nella seconda la posizione nominale imposta dal primo campione, nella terza la tensione nominale calcolata con un gain nominale rappresentativo pari a 4 V/mm (vedere NOTA punto 4 di 5.2) e nella quarta la posizione attesa dello stantuffo dell'LVDT ad inizio corsa e a fine corsa.

4.1 Ruotare la ghiera **C** in modo da posizionare esattamente la testina micrometrica sullo zero iniziale;

4.2 Leggere il segnale in ingresso da NImax ed annotarlo fino al millesimo di volt, prendendo un valore medio se l'ultima cifra oscilla (1micrometro equivale a circa 4mV).

4.3 Ruotare la ghiera **C** in modo da fare entrare l'LVDT di un incremento pari a 0.2 mm secondo Tabella.1. È comodo leggere l'annotazione in rosso sulla ghiera essendo crescente coerentemente al verso di entrata dello stantuffo;

4.4 Leggere il segnale in ingresso da NImax, ed annotarlo fino al millesimo di volt, prendendo un valore medio se l'ultima cifra oscilla (1micrometro equivale a circa 4mV).

4.5 Ripetere le operazioni 4.3 e 4.4 fino a fine corsa (come viene indicato in Tabella.1).

4.6 Per ripetere la procedura, allentare la vite di Nylon D in modo da svincolare l'LVDT; ruotare l'LVDT di un angolo casuale e serrarre nuovamente;

NOTA: in questo modo si cambia la configurazione di partenza dell'LVDT e si tiene conto della variabilità della lettura dell'LVDT derivante dalla non coassialità tra la direzione dello spostamento imposto e l'asse dello stantuffo ferromagnetico dell'LVDT;

4.7 Ripetere la procedura dal punto 3.3 per altre due volte in modo da collezionare tre ripetizioni di letture derivanti dalla stessa rampa di spostamento.

BIBLIOGRAPHY

1. Cristofolini, L. Tessuti connettivi calcificati o tessuti ossei (ossa scheletriche, denti), lectures of Meccanica dei tessuti Biologici (2017)

2. Bone Tissue. Available at: https://en.wikipedia.org/wiki/Bone_tissue.

3. Downey, P. & Siegel, M. Bone Biology and the Clinical Implications for osteoporosis. *Phys. Ther.* **86,** 77–91 (2006).

4. Robling, A. G., Castillo, A. B. & Turner, C. H. Biomechanical and Molecular Regulation of Bone Remodeling. *Annu. Rev. Biomed. Eng.* **8,** 455–498 (2006).

5. Florencio-silva, R.; Sasso, G.; Sasso-cerri, E.; Simões, M. J. & Cerri, P. S. Biology of Bone Tissue: Structure, Function, and Factors That Influence Bone Cells. *Biomed Res. Int.* **2015,** 1–17 (2015).

6. Frederic H. Martini, J. N. *Fondamenti di Anatomia e Fisiologia. cellule dell'osso.* (2009).

7. Cowin S.C. Bone Mechanics Handbook. *CRC Press* **second edition,** (2009).

8. Öhman, C. *et al.* Mechanical testing of cancellous bone from the femoral head: Experimental errors due to off-axis measurements. *J. Biomech.* **40,** 2426–2433 (2007).

9. Anderson, A. E., Peters, C. L., Tuttle, B. D. & Weiss, J. A. Subject-Specific Finite Element Model of the Pelvis: Development, Validation and Sensitivity Studies. *J. Biomech. Eng.* **127,** 364 (2005).

10. Does a Broken Bone Become Stronger After It Heals? - The New York Times. Available at: http://www.nytimes.com/2010/10/19/health/19really.html?ref=science. (Accessed: 11th January 2018)

11. Herzog, W., Nigg, B. M. & Read, L. J. Quantifying the effects of spinal manipulations on gait using patients with low back pain. *J. Manipulative Physiol. Ther.* **11,** 151–7 (1988).

12. Clarke, B. Normal bone anatomy and physiology. *Clin. J. Am. Soc. Nephrol.* **3 Suppl 3,** 131–139 (2008).

13. Manolagas, S. C. Birth and Death of Bone Cells: Basic Regulatory Mechanisms and Implications for the Pathogenesis and Treatment of Osteoporosis . *Endocr. Rev.* **21,** 115–137 (2000).

14. The Hip Bone - Ilium - Ischium - Pubis - TeachMeAnatomy. Available at: http://teachmeanatomy.info/pelvis/bones/the-hip-bone/. (Accessed: 11th January 2018)

15. Crosnier, E. A., Keogh, P. S. & Miles, A. W. A novel method to assess primary

stability of press-fit acetabular cups. *Proc. Inst. Mech. Eng. Part H J. Eng. Med.* **228,** 1126–1134 (2014).

16. Field, R. E. & Rajakulendran, K. The labro-acetabular complex. *J. Bone Joint Surg. Am.* **93 Suppl 2,** 22–7 (2011).

17. Hip. Available at: https://en.wikipedia.org/wiki/Hip

18. Berardi, G. C., Picchetta, F., Nai Fovino, P. L. Studio biomeccanico della anatomia funzionale della articolazione coxo-femorale. Clinica Ortopedica "G. Gaslini" dell'Università di Genova. PDF available at: http://www.giomi.com/Portals/Giomi/Pubblicazioni/pdf/Acta%20n.91963%20articolo%2023.pdf

19. Lu, T. W. & Chang, C. F. Biomechanics of human movement and its clinical applications. *Kaohsiung J. Med. Sci.* **28,** (2012).

20. Muscles of the hip. Available at: https://en.wikipedia.org/wiki/Muscles_of_the_hip

21. Konstantinidis, E. I., Billis, A. S., Plotegher, L., Conti, G. & Bamidis, P. D. Indoor Location IoT Analytics 'in the wild': Active and Healthy Ageing Cases. in 1231–1236 (2016). doi:10.1007/978-3-319-32703-7_237

22. Baker, R., Esquenazi, A., Benedetti, M. G. & Desloovere, K. Gait analysis: clinical facts. *Eur. J. Phys. Rehabil. Med.* **52,** 560–74 (2016).

23. Dickinson, A. S., Taylor, A. C., Ozturk, H. & Browne, M. Experimental Validation of a Finite Element Model of the Proximal Femur Using Digital Image Correlation and a Composite Bone Model. *J. Biomech. Eng.* **133,** 14504 (2011).

24. Kadaba, M. P., Ramakrishnan, H. K. & Wootten, M. E. Measurement of lower extremity kinematics during level walking. *J. Orthop. Res.* **8,** 383–392 (1990).

25. Kluess, D. Finite Element Analysis in Orthopaedic Biomechanics, Finite Element Analysis, David Moratal (Ed.), InTech, (2010). Available at: https://www.intechopen.com/books/finite-element-analysis/finite-element-analysis-in-orthopaedic-biomechanics.

26. Jacofsky, D. J., McCamley, J. D., Jaczynski, A. M., Shrader, M. W. & Jacofsky, M. C. Improving initial acetabular component stability in revision total hip arthroplasty. Calcium phosphate cement vs reverse reamed cancellous allograft. *J. Arthroplasty* **27,** 305–309 (2012).

27. Cristofolini, L. Anatomical Reference Frames for Long Bones: Biomechanical Applications. in *Handbook of Anthropometry* 2971–2999 (Springer New York, 2012). doi:10.1007/978-1-4419-1788-1_184

28. Morosato, F., Traina, F. & Cristofolini, L. Standardization of hemipelvis alignment for *in vitro* biomechanical testing. *J. Orthop. Res.* 1–25 (2017). doi:10.1002/jor.23825

29. Van Arkel, R. J. & Jeffers, J. R. T. In vitro hip testing in the International Society of Biomechanics coordinate system. *J. Biomech.* **49,** 4154–4158 (2016).

30. Jóźwiak, M. *et al.* An accurate method of radiological assessment of acetabular volume and orientation in computed tomography spatial reconstruction. *BMC Musculoskelet. Disord.* **16,** 1–10 (2015).

31. Lee, C., Kim, Y., Kim, H. W., Kim, Y. S. & Jang, J. A robust method to extract the anterior pelvic plane from CT volume independent of pelvic pose. *Comput. Assist. Surg.* **22,** 20–26 (2017).

32. Dalstra, M., Huiskes, R. & Section, B. Load Transfer Across the Pelvic. *Biomechanics* **28,** (1995).

33. Lewton, K. L. In vitro bone strain distributions in a sample of primate pelves. *J. Anat.* **226,** 458–477 (2015).

34. Miles, A. W. & Gheduzzi, S. Basic biomechanics and biomaterials. *Surgery* **30,** 86–91 (2012).

35. Byrne, D., Mulhall, K. & Baker, J. Anatomy & Biomechanics of the Hip. *Open Sport. Med. J.* **4,** 51–57 (2010).

36. Bergmann, G. *et al.* Hip forces and gait patterns from rountine activities. *J. Biomech.* **34,** 859–871 (2001).

37. Houcke JV, Khanduja V, Pattyn C, A. E. The history of biomechanics in total hip arthroplasty. *Indian J Orthop* **51:359-67.,** (2017).

38. McLeish, R.D.Charnley, J. et al. Abduction forces in the one-legged stance. *J. Biomech.* **Volume 3,** 195–209 (1970).

39. Rydell, N. W. Forces Acting on the Femoral Head-Prosthesis: A Study on Strain Gauge Supplied Prostheses in Living Persons. *Acta Orthop. Scand.* **37,** 1–132 (1966).

40. Siopack, J. S. & Jergesen, H. E. Total hip arthroplasty. *West. J. Med.* **162,** 243–249 (1995).

41. Warre, M. Patients undergoing total hip arthroplasty : a perioperative pain experience. (2006).

42. Traina, F. & Faldini, C. Fracture of ceramic bearing surfaces following total hip replacement: a. *Emerg Med Pr.* **15,** 1–18 (2013).

43. Total Hip Replacement - OrthoInfo - AAOS. Available at: orthoinfo.aaos.org/en/treatment/total-hip-replacement.

44. Protesi all'anca in aumento I progressi degli ultimi anni - Scienze - Repubblica.it. Available at: www.repubblica.it/2009/11/sezioni/scienze/protesi-anca/protesi-anca/protesi-anca.html.

45. Hallan, G. *et al.* Medium- and long-term performance of 11 516 uncemented primary

femoral stems from the Norwegian arthroplasty register. *J. Bone Jt. Surg. - Br. Vol.* **89–B,** 1574–1580 (2007).

46. Registro dell'Implantologia Protesica Ortopedica dell'Emilia Romagna RIPO.

47. Klerken, T., Mohaddes, M., Nemes, S. & Kärrholm, J. High early migration of the revised acetabular component is a predictor of late cup loosening: 312 cup revisions followed with radiostereometric analysis for 2-20 years. *HIP Int.* **25,** 471–476 (2015).

48. Graves, S. E. *et al.* Hip and Knee Arthroplasty Annual Report- National Joint Registry. *Aust. Orthop. Assoc.* **180,** 217 (2011).

49. Amirouche, F. *et al.* Factors influencing initial cup stability in total hip arthroplasty. *Clin. Biomech.* **29,** 1177–1185 (2014).

50. Perona, P. G., Lawrence, J., Paprosky, W. G., Patwardhan, A. G. & Sartori, M. Acetabular micromotion as a measure of initial implant stability in primary hip arthroplasty. An in vitro comparison of different methods of initial acetabular component fixation. *J. Arthroplasty* **7,** 537–547 (1992).

51. Havelin, L. I. *et al.* The Norwegian Arthroplasty Register: 11 years and 73,000 arthroplasties. *Acta Orthop Scand* **71,** 337–353 (2000).

52. Baleani, M., Fognani, R. & Toni, A. Initial stability of a cementless acetabular cup design: Experimental investigation on the effect of adding fins to the rim of the cup. *Artif. Organs* **25,** 664–669 (2001).

53. Tabata, T., Kaku, N., Hara, K. & Tsumura, H. Initial stability of cementless acetabular cups: press-fit and screw fixation interaction???an in vitro biomechanical study. *Eur. J. Orthop. Surg. Traumatol.* **25,** 497–502 (2015).

54. Bobyn, J. D., Toh, K. K., Hacking, S. A., Tanzer, M. & Krygier, J. J. Tissue response to porous tantalum acetabular cups: A canine model. *J. Arthroplasty* **14,** 347–354 (1999).

55. Kwong, L. M. *et al.* A quantitative in vitro assessment of fit and screw fixation on the stability of a cementless hemispherical acetabular component. *J. Arthroplasty* **9,** 163–170 (1994).

56. Adler E, Stuchin S.A. Stability of press-fit acetabular cups. *J. Arthroplasty* **7,** 295–301 (1992).

57. Wilson-MacDonald J, Morscher E, M. Z. Cementless uncoated polyethylene acetabular component in total hip replacement. *J Bone Joimt Surg* **72(B),** 423 (1990).

58. Shon, W. Y., Santhanam, S. S. & Choi, J. W. Acetabular Reconstruction in Total Hip Arthroplasty. **28,** 1–14 (2016).

59. Illigen R. The Optimal Fixation of the Cementless Acetabular Component in Primary Total Hip Arthroplasty. *J. Am. Acad. Orthop. Surg.* **10,** 43–56 (2002).

60. Abdulkarim, A., Ellanti, P., Motterlini, N., Fahey, T. & O'Byrne, J. M. Cemented

versus uncemented fixation in total hip replacement: a systematic review and meta-analysis of randomized controlled trials. *Orthop. Rev. (Pavia).* **5,** 8 (2013).

61. Murray, D. W. The definition and measurement of acetabular orientation. *J. Bone Joint Surg. Br.* **75,** 228–232 (1993).

62. Seagrave, K. G., Troelsen, A., Malchau, H., Husted, H. & Gromov, K. Acetabular cup position and risk of dislocation in primary total hip arthroplasty: A systematic review of the literature. *Acta Orthop.* **88,** 10–17 (2017).

63. Lubovsky, O. *et al.* Acetabular orientation: Anatomical and functional measurement. *Int. J. Comput. Assist. Radiol. Surg.* **7,** 233–240 (2012).

64. Aitken, J. Anatomical factors in the stability of the hip joint in the newborn. *J. Pediatr. Surg.* **6,** 92–93 (1971).

65. Mothersill, C., Seymour, C. B. & O'Brien, A. Induction of c-myc oncoprotein and of cellular proliferation by radiation in normal human urothelial cultures. *Anticancer Res.* **11,** 1609–1612 (1991).

66. Grammatopoulos, G. *et al.* Optimal acetabular orientation for hip resurfacing. *J. Bone Jt. Surg. - Br. Vol.* **92–B,** 1072–1078 (2010).

67. Malik, A., Wan, Z., Jaramaz, B., Bowman, G. & Dorr, L. D. A Validation Model for Measurement of Acetabular Component Position. *J. Arthroplasty* **25,** 812–819 (2010).

68. Ulrich, S. D. *et al.* Total hip arthroplasties: What are the reasons for revision? *Int. Orthop.* **32,** 597–604 (2008).

69. Delaunay, C., Hamadouche, M., Girard, J. & Duhamel, A. What are the causes for failures of primary hip arthroplasties in France? *Clin. Orthop. Relat. Res.* **471,** 3863–3869 (2013).

70. Zant, N. P., Wong, C. K. Y. & Tong, J. Fatigue failure in the cement mantle of a simplified acetabular replacement model. *Int. J. Fatigue* **29,** 1245–1252 (2007).

71. Regional Register of Orthopedic Prosthetic Implantology (RIPO).

72. Maloney, W. J., Jasty, M., Rosenberg, A. & Harris, W. H. Bone lysis in well-fixed cemented femoral components. *J. Bone Joint Surg. Br.* **72,** 966–70 (1990).

73. Charnley J. Low friction arthroplasty, theory and practice. *Springer-Verlag,* (1979).

74. Sutherland, D. . The evolution of clinical gait analysis. *Gait Posture* **16,** 159–179 (2002).

75. Sinha RK, Shaubhag AS, Maloney WJ, Hasselman CT, R. H. Osteolysis: Cause and Effect, Instructional Course Lectures. *Am. Acad. Ortheopedic Surg. Press* **47,** pp 307-20 (1998).

76. Stocks G.W., Freeman M.A.R & Evans. S. J. W. Acetabular cup migration, prediction of aseptic loosening. *J Bone Jt. Surg [Br]* **77,** (1995).

77. Brånemark P. Osseointegration and its experimental background. *J. Prosthet. Dent.* **50 (3),** pp: 399-410 (1983).

78. Sennerby, L., Dasmah, A., Larsson, B. & Iverhed, M. Bone Tissue Responses to Surface-Modified Zirconia Implants: A Histomorphometric and Removal Torque Study in the Rabbit. *Clin. Implant Dent. Relat. Res.* **7 (Suppl 1,** S13–S20 (2005).

79. Søballe, K., Hansen, E. S., B.-Rasmussen, H., Jørgensen, P. H. & Bünger, C. Tissue ingrowth into titanium and hydroxyapatite-coated implants during stable and unstable mechanical conditions. *J. Orthop. Res.* **10,** 285–299 (1992).

80. Ramaglia L., Capece G., Di Spigna G., Esposito D., P. L. In vitro expression of osteoblastic phenotype on titanium surfaces. *Minerva Stomatol.* **59,** 259–270 (2010).

81. Pilliar RM, Lee JM, M. C. Observations on the effect of movement on bone into Porous-surfaced implants. *Biomater. Res.* **number 208,** (1986).

82. Jasty, M. *et al.* In vivo skeletal responses to porous-surfaced implants subjected to small induced motions. *J. Bone Jt. Surg. - Ser. A* **79,** 707–714 (1997).

83. Nieuwenhuijse, M. J., Valstar, E. R., Kaptein, B. L. & Nelissen, R. G. H. H. Good diagnostic performance of early migration as a predictor of late aseptic loosening of acetabular cups: Results from ten years of follow-up with Roentgen Stereophotogrammetric Analysis (RSA). *J. Bone Jt. Surg. - Ser. A* **94,** 874–880 (2012).

84. Ilchmann, T., Kesteris, U. & Wingstrand, H. EBRA improves the accuracy of radiographic analysis of acetabular cup migration. *Acta Orthop. Scand.* **69,** 119–124 (1998).

85. Selvik, G. Roentgen stereophotogrammetry: A method for the study of the kinematics of the skeletal system. *Acta Orthop.* **60,** 1–51 (1989).

86. Kim, Y. S. *et al.* Proximal translation of > 1 mm within the first two years of revision total hip arthroplasty correctly predicts whether or not an acetabular component is loose in 80% of cases. *Bone Joint J.* **99–B,** 465–474 (2017).

87. Pijls, B. G. *et al.* Early proximal migration of cups is associated with late revision in THA: A systematic review and meta-analysis of 26 RSA studies and 49 survival studies. *Acta Orthop.* **83,** 583–591 (2012).

88. Curtis, M. J., Jinnah, R. H., Wilson, V. D. & Hungerford, D. S. The initial stability of uncemented acetabular components. *J. Bone Joint Surg. Br.* **74,** 372–376 (1992).

89. Zietz C, Fritsche A, Kluess D, Mittelmeier W, B. R. Influence of acetabular cup design on the primary implant stability : an experimental and numerical analysis. *Orthopade* **38,** 1097–105 (2009).

90. Heaton-Adegbile, P., Zant, N. P. & Tong, J. In vitro fatigue behaviour of a cemented acetabular reconstruction. *J. Biomech.* **39,** 2882–2886 (2006).

91.   Pitto RP, Willmann G, S. M. Initial stability of modular acetabular components. Comparative in-vitro study with polyethylene and ceramic liners. *Biomed Tech (Berl). 2001 Apr;46(4)109-12.*

92.   Ghosh, R., Gupta, S., Dickinson, A. & Browne, M. *Experimental Validation of Finite Element Models of Intact and Implanted Composite Hemipelvises Using Digital Image Correlation. Journal of Biomechanical Engineering* **134,** (2012).

93.   Philippot, R. *et al.* Prevention of dislocation in total hip revision surgery using a dual mobility design. *Orthop. Traumatol. Surg. Res.* **95,** 407–413 (2009).

94.   Metodi di diagnosi e compicanze, protesi d'anca. Available at: http://fisiokinesiterapia-news.it/download/revisioni

95.   Abrahams, J. M. *et al.* The diagnostic performance of radiographic criteria to detect aseptic acetabular component loosening after revision total hip arthroplasty. *Bone Jt. J.* **99B,** 458–464 (2017).

96.   Wooley, P. H. & Schwarz, E. M. Aseptic loosening. *Gene Ther.* **11,** 402–407 (2004).

97.   Temmerman, O. P. P. et al. A comparison of radiographic and scintigraphic techniques to assess aseptic loosening of the acetabular component in a total hip replacement. The Journal of bone and joint surgery. American volume **86–A,** (2004).

98.   Linear variable differential transformer. Available at: https://en.wikipedia.org/wiki/Linear_variable_differential_transformer

99.   Measuring Position and Displacement with LVDTs - National Instruments. Available at: www.ni.com/white-paper/3638/en/.

100. Taratura interna di lvdt e simili trasduttori di spostamento. MPP/03/rev2. Internal Procedure: Lab. of Biomechanics, Department of Industrial Engineering, Bologna, (2017).

101.   Tartagni M. Fundamentals on robotics. Lectures of Sensor and Nanotechnology, (2017)

102. Factors to Consider When Selecting and Specifying LVDT Linear Position Sensors - Tech Briefs : Tech Briefs. Available at: https://www.techbriefs.com/component/content/article/15371?start=1&Itemid=690.

103.   Displacement Transducers and Accuracy Classification per ASTM E2309. MTS System Corporation, PDF (2005).

104. Gonzalez, M. H. & Amirouche, F. Cementless Acetabular Revision with Rim Acetabular Defects: Experimental and FEA Investigation. **3639588,** 121 (2014).

105. Siebert, T., Becker, T., Spiltthof, K., Neumann, I. & Krupka, R. Error Estimations in

Digital Image Correlation Technique. *Appl. Mech. Mater.* **7–8,** 265–270 (2007).

106. Palanca, M. Ottimizzazione dei parametri di acquisizione ed elaborazione per l'analisi di segmenti ossei tramite correlazione di immagini digitali. (2012).

107. Michael A. Sutton. Digital Image Correlation. *Univ. Illinois Urbana-Champaign* 7–10 (2008).

108. Digital image correlation. Available at: https://en.wikipedia.org/wiki/Digital_image_correlation#cite_note-3.

109. Yoneyama, S. & Murasawa, G. Digital Image Correlation, in Experimental Mechanics. *Encycl. Life Support Syst.* 7–10 (2009).

110. Chu, T. C., Ranson, W. F. & Sutton, M. A. Applications of digital-image-correlation techniques to experimental mechanics. *Exp. Mech.* **25,** 232–244 (1985).

111. Palanca, M., Tozzi, G. & Cristofolini, L. The use of digital image correlation in the biomechanical area: A review. *Int. Biomech.* **3,** 1–21 (2016).

112. Pan, B., Xie, H., Wang, Z., Qian, K. & Wang, Z. Study on subset size selection in digital image correlation for speckle patterns. *Opt. Express* **16,** 7037 (2008).

113. Lionello, G. & Cristofolini, L. A practical approach to optimizing the preparation of speckle patterns for digital-image correlation. *Meas. Sci. Technol.* **25,** (2014).

114. Estrada, J. B. & Franck, C. Intuitive Interface for the Quantitative Evaluation of Speckle Patterns for Use in Digital Image and Volume Correlation Techniques. *J. Appl. Mech.* **82,** 95001 (2015).

115. Software Manual. Istra 4d. Q-400 System, Dantec Dynamic, 2012

116. Hall, S. Full-field displacement/strain measurements and Digital Image Correlation – principles and methods. *Div. Solid Mech. Lund Univ. Sweden Eur. Spallation Source, Lund, ppt. Available at: http://alertgeomaterials.eu/data/school/2012/ALERT_DIC1_red.pdf*

117. Palanca, M., Brugo, T. M. & Cristofolini, L. Use of Digital Image Correlation To Investigate the Biomechanics of the Vertebra. *J. Mech. Med. Biol.* **15,** 1540004 (2015).

118. Everitt, H., Evans, S. L., Holt, C. A., Bigsby, R. . & Khan, I. . Acetabular component deformation under rim loading using Digital Image Correlation and finite element methods. *Appl. Mech. Mater.* **24–25,** 275–280 (2010).

119. Marcus R. Munafò & George Davey Smith, Repeating experiments is not enough. Nature, 399, Vol. 553, 25 January 2018

120. Soderkvist, I., Wedin, P.-Ã., 1993. Determining the movements of the skeleton using well-configured markers. Journal of Biomechanics. 26, 1473 - 1477.

121. Schonemann, P. H., 1966. A generalized solution of the orthogonal procrustes problem. Psychometrika. 31, 1–10

FIGURES

1. Cristofolini, L. Tessuti connettivi calcificati o tessuti ossei (ossa scheletriche , denti). Lectures of Meccanica dei tessuti Biologici (2017)

2. http://teachmeanatomy.info/pelvis/bones/the-hip-bone/

3. http://www.lawrencegaltman.com/Naugbio/Bio211/Lab/BONEvideos/PELVIC%20GIRDLE/OS%20COXAE/OsCOXAE.html;
   http://teachmeanatomy.info/pelvis/bones/the-hip-bone/

4. *https://upload.wikimedia.org/wikipedia/commons/c/c4/Gray342.png;* Crosnier, E. A., Keogh, P. S. & Miles, A. W. A novel method to assess primary stability of press-fit acetabular cups. *Proc. Inst. Mech. Eng. Part H J. Eng. Med.* **228,** 1126–1134 (2014).

5. *Grey's Anatomy- Gray, Henry. Anatomy of the Human Body. Philadelphia: Lea & Febiger, 1918; Bartleby.com, 2000. www.bartleby.com/107/*

6. http://people.unica.it/pau/files/2015/11/7-anca.pdf

7. https://www.google.it/search?q=http://en.wikipedia.org/wiki/Muscles_of_the_hip

8. Morosato, F. Alignment of hemipelvic specimens for *in vitro* testing. Internal Procedure, Lab. Of Biomechanics, (Department of Industrial Engineering, Bologna), 2016

9. Marek Jóźwiak *et al*, An accurate method of radiological assessment of acetabular volume and orientation in computed tomography spatial reconstruction , BMC Musculoskeletal Disorders (2015)

10. left: https://en.wikipedia.org/wiki/Greater_sciatic_notch; right: Dalstra M., Huiskes R., Load transfer across the pelvic bone. Journal of Biomechanics, 28:715-724, 1995

11. Miles, A. W. & Gheduzzi, S. Basic biomechanics and biomaterials. *Surgery* **30,** 86–91 (2012).

12. http://www.orthoload.com/main.php?act=info&bid=36&showres=con

13. Bergmann, G. *et al.* Hip forces and gait patterns from rountine activities. *J. Biomech.* **34,** 859–871 (2001).

14. https://orthoinfo.aaos.org/en/treatment/total-hip-replacement

15. Graves, S. E. *et al.* Hip and Knee Arthroplasty Annual Report- National Joint Registry. *Aust. Orthop. Assoc.* **180,** 217 (2011).

16. Aesculap® Plasmafit® Cementless Acetabular Cup Sys, Brochure

17. Data from The Norwegian Arthroplasty Register, 2005-2015.

18. Seagrave Kurt G. et al., Acetabular cup position and risk of dislocation in primary total hip arthroplasty. Acta Orthopaedica, 88 (1): 10 –17, 2017 (up right); http://www.radiologyassistant.nl/en/p431c8258e7ac3/hip-arthroplasty.html (up left); https://openi.nlm.nih.gov/detailedresult.php?img=PMC2739474_IJO-42-260-g004&req=4 (down)

19. Personal Picture

20. Delaunay, C., Hamadouche, M., Girard, J. & Duhamel, A. What are the causes for failures of primary hip arthroplasties in France? *Clin. Orthop. Relat. Res.* **471,** 3863–3869 (2013) (up); Regional Register of Orthopedic Prosthetic Implantology (RIPO) (down)

21. Mediators of the inflammatory response to joint replacement devices - Scientific Figure on ResearchGate. Available from: https://www.researchgate.net/Figure-3-Schematic-of-periprosthetic-inflammation-and-aseptic-osteolysisWear-particles-generated_51621725_fig3 [accessed 14 Jan, 2018]

22. Sinha RK, Shaubhag AS, Maloney WJ, Hasselman CT, R. H. Osteolysis: Cause and Effect, Instructional Course Lectures. *Am. Acad. Ortheopedic Surg. Press* **47,** pp 307-20 (1998).

23-24. Personal pics.

25. Perona, P. G., Lawrence, J., Paprosky, W. G., Patwardhan, A. G. & Sartori, M. Acetabular

   micromotion as a measure of initial implant stability in primary hip arthroplasty. An in vitro comparison of different methods of initial acetabular component fixation. *J. Arthroplasty* **7,** 537–547 (1992).

26. Kwong, L. M. *et al.* A quantitative in vitro assessment of fit and screw fixation on the stability of a cementless hemispherical acetabular component. *J. Arthroplasty* **9,** 163–170 (1994).

27. Kwong, L. M. *et al.* A quantitative in vitro assessment of fit and screw fixation on the stability of a cementless hemispherical acetabular component. *J. Arthroplasty* **9,** 163–170 (1994).

28. Biau, David J. Brand, Richard A.Robert Merle d'aubigné, 1900-1989. Clinical Orthopaedics and Related Research; 467(1): 2-6 (2009)

29. Measuring Position and Displacement with LVDTs - National Instruments. Available at: www.ni.com/white-paper/3638/en/.

30. http://www.ni.com/white-paper/3638/en/

31. Tartagni M. Fundamentals on robotics. Lectures of Sensor and Nanotechnology, (2017)

32. Taratura interna di lvdt e simili trasduttori di spostamento. Internal Procedure: Lab. of Biomechanics, Department of Industrial Engineering, Bologna, (2017).

33. Gonzalez, M. H. & Amirouche, F. Cementless Acetabular Revision with Rim Acetabular Defects: Experimental and FEA Investigation. 3639588, 121 (2014).

34. Validation of Shape Context Based Image Registration Method Using Digital Image Correlation Measurement on a Rat Stomach, Zhao J. et al. Volume 48, Issue 6, 13 April 2015, Pages 1075-1083.

35. Palanca, M. Ottimizzazione dei parametri di acquisizione ed elaborazione per l'analisi di segmenti ossei tramite correlazione di immagini digitali. (2012).

36. a: https://iiw.kuleuven.be/onderzoek/mem2p/research/dic; b: Software Manual. Istra 4d. Q-400 System, Dantec Dynamic, 2012

37. Chu T.C, *et al.*, *Applications of digital-image-correlation techniques to experimental mechanics*, in Experimental Mechanics, September 1985, DOI: 10.1007/BF02325092.

38. Zhang *et al., Measurement of mixed-mode stress intensity factors using digital image correlation method*, in Optics and Lasers in Engineering Volume 50, Issue 7, Pages 1001-1007 (2012)

39. Palanca, M., Tozzi, G. & Cristofolini, L. The use of digital image correlation in the biomechanical area: A review. *Int. Biomech.* **3,** 1–21 (2016)

40. Palanca, M. Ottimizzazione dei parametri di acquisizione ed elaborazione per l'analisi di segmenti ossei tramite correlazione di immagini digitali. (2012).

41. Software Manual. Istra 4d. Q-400 System, Dantec Dynamic, 2012

42-45(left). Personal Pic

45 (Right). http://www.corailpinnacle.net/pinnacle/surgical-steps/ceramic

43-55. Personal Pics

56-58. Software Manual. Istra 4d. Q-400 System, Dantec Dynamic, 2012

59-76. Personal pics

THANKS

Al Professor Cristofolini, a Federico, a Kavin, a Marco, a Toti, ad Alberto.

Al DIN*.

Grazie per avermi INSEGNATO con dedizione, amore e pazienza a scalare le montagne.

Ad aiutarmi quando la salita era più ripida del previsto.

Grazie per avermi spronata…. Per avermi fatta CRESCERE.

…

Grazie per avermi fatto notare la bellezza dei dettagli e coglierli da…. diversi sistemi di riferimento (nel vero senso della parola… e non!)

…

Grazie perché ho IMPARATO mestieri, il valore della CONOSCENZA e della CURIOSITA', che grazie a voi si è finalmente e felicemente sprigionata.

….

Grazie perché mi avete accolta nel luogo di istruzione più produttivo e più efficiente che io conosca,

grazie perché il DIN per me è scuola, ma è anche famiglia.

*Rettifico,

alla DIN family

Ringraziamento particolare, speciale e intimo, dal più profondo del mio DNA:

Grazie Mamma, Papà e Pinu per essere con me, per me e me SEMPRE.

Ringrazio te, per avermi fatto pedalare su quelle montagne… (Vitt, a te con amore).